Radiated Noise From a Three Dimensional Truss

by

Leo E. Chiasson Jr.

B.S. Aerospace Engineering
Boston University (1981)

Submitted in partial fulfillment of the requirements for the degrees of

MASTER OF SCIENCE IN OCEANOGRAPHIC ENGINEERING
at the
MASSACHUSETTS INSTITUTE OF TECHNOLOGY
and the
WOODS HOLE OCEANOGRAPHIC INSTITUTION

and

MASTER OF SCIENCE IN MECHANICAL ENGINEERING
at the
MASSACHUSETTS INSTITUTE OF TECHNOLOGY

September 1995.

Author: .....
Department of Ocean Engineering, MIT and the MIT-WHOI
Joint Program in Oceanographic Engineering, August 4, 1995

Certified by: .....
Assistant Professor J. Robert Fricke
Department of Ocean Engineering, MIT, Thesis Supervisor

Certified by: .....
Assistant Professor Zaichun Feng
Department of Mechanical Engineering, MIT, Thesis Reader

Accepted by: .....
Professor Arthur B. Baggeroer, Chair, Joint Committee
for Applied Ocean Science and Engineering, MIT-WHOI

RADIATED NOISE FROM A THREE DIMENSIONAL TRUSS

by
Leo E. Chiasson Jr.

Submitted to the Department of Ocean Engineering on August 4, 1995
in partial fulfillment of the requirements for the degrees of
Master of Science in Oceanographic Engineering and
Master of Science in Mechanical Engineering

Abstract:

The Massachusetts Institute of Technology Truss Damping Group continues to study the dynamic and vibrational characteristics of a three dimensional aluminum truss which is based on a repeating square pyramidal pattern. The truss is a notional model of the type of structure which will be considered for use in the future design of submersibles and Autonomous Underwater Vehicles (AUV's) to mount machinery. A current concern is in the ability to accurately predict the level of radiated noise which the truss will transmit to the environment inside the submersible due to an arbitrary vibrational loading.The noise produced could have unsatisfactory coupling effects with the fluid surrounding the submersible and could also produce unacceptable levels of noise inside.

The vibrational energy in the truss members as a result of arbitrary loading is predicted using a previously developed numerical analysis technique known as the Direct Global Stiffness Matrix (DGSM) method. These vibrational levels are then used to calculate the radiated sound power, with the struts modeled as finite length vibrating wires. The sound power with the addition of flat plates to the truss is also modeled.

A truss, which was previously constructed at MIT, is vibrated at one end and the sound power radiated, normalized to input power, is measured using an intensity probe. The measured sound power for the bare truss is within 3 dB of the DGSM prediction for a structural loss factor, η_s, of .003. The structural loss factor, η_s, is the most crucial entering argument to the DGSM prediction. A method of measuring the total loss factor, η_{TOT} to improve the DGSM input of structural loss factor reduces the difference between prediction and measurement to approximately 1 dB. The prediction of the sound power with plates attached to the truss exceeds the measurement by 20 dB. Further experimentation and analysis proves that the method of mounting the plates to the truss resulted in poor coupling of the plates to the struts; the DGSM method assumes strong coupling thereby leading to the erroneously high estimate.

The measured sound power for the bare truss peaks at 6 kHz, where 16 % of the input power is transmitted as sound. When $\frac{1}{2}$ meter square aluminum plates of 2 mm thickness are placed on the truss, the amount of input power which is radiated as sound increases to 28 % at the same 6 kHz peak.

Thesis Supervisor: Dr. J. Robert Fricke
Title: Assistant Professor

Acknowledgments

As in any endeavor in the field of Engineering, no one works alone. This thesis could not have been completed without the help and guidance of my thesis advisor Assistant Professor J. Robert Fricke and my thesis reader Assistant Professor Frank Feng. I also owe thanks to Professor Ira Dyer for his probing and often painful questions, which always got me back on the right path. In addition, I am grateful for the continuous help I received from all the members of the Acoustics and Vibration Laboratory, most notably Dr. Joe Bondaryk, and Mark Hayner. This thesis would also not have been possible without the pioneering work of Marcus Heath, who single-handedly designed and constructed the object of this study.

The greatest thanks go to my family. The support I received from my wife Mary and my sons Jeffrey and Gregory enabled me to concentrate on the completion of my graduate program, and made the whole process bearable.

Lastly, I would like to thank the United States Navy for giving me the opportunity and financial support to pursue this degree, and the Advanced Research Projects Agency (ARPA) and the Office of Naval Research (ONR) for providing the funding associated with this project. In particular, I am thankful for the support received from the Navy Academic Office, most notably their administrative assistant Jennifer Laible, who was probably the most helpful and friendly person I met during my entire time at MIT. Her competence and cheerful attitude made her a pleasure to work with.

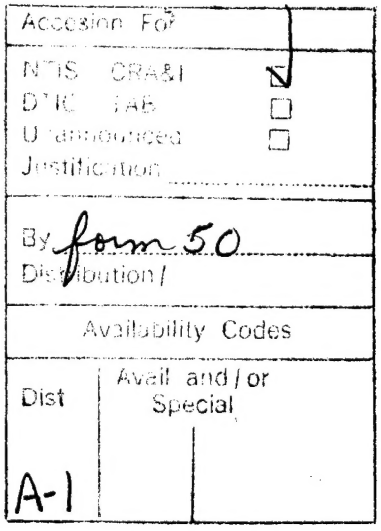

Table of Contents

List of FIGURES

List of Symbols

A	Cross-sectional area of the strut
C_a	Speed of sound in air
C_L	Longitudinal wave speed in the beams
C_T	Torsional wave speed in the beam
C_{By}	Bending wave speed for flexural waves about the y axis = $\sqrt{\omega\kappa_y C_L}$
C_{Bz}	Bending wave speed for flexural waves about the z axis = $\sqrt{\omega\kappa_z C_L}$
E	Modulus of elasticity
f	Applied force
f	Cyclic frequency
G	Shear modulus
H_1	Hankel function of the first kind
$\overline{H_1}$	Derivative of the Hankel function of the first kind with respect to the argument
I	Second moment of inertia
$\vec{I}$	Intensity
I_r	Intensity in the radial direction
J	Polar moment of inertia
J_1	First order Bessel function of the first kind
k_a	Acoustic wave number in air
k_L	Longitudinal wave number
k_T	Torsional wave number
k_{By}	Bending wavenumber for flexural waves about the y axis
k_{Bz}	Bending wavenumber for flexural waves about the z axis
L	Length of strut
p	Pressure field radiated by the vibration of the strut
p_∞	Pressure in the far field, far from the strut, in the radial direction
r	Mean radius of the strut
r_i	Inner radius of the strut
r_o	Outer radius of the strut
t_{wall}	Wall thickness of strut
T	Period
U_o	Spatially constant vibration amplitude of the strut
u^+	Compressional wave amplitude for wave travelling in $+x$ direction
u^-	Compressional wave amplitude for wave travelling in $-x$ direction
v^+	Harmonic flexural wave amplitude for wave travelling in + direction, associated with flexure in the y direction
v^-	Harmonic flexural wave amplitude for wave travelling in - direction, associated with flexure in the y direction

v_e^+	Evanescent flexural wave amplitude in + direction, associated with flexure in the y direction
v_e^-	Evanescent flexural wave amplitude in - direction, associated with flexure in the y direction
v	Velocity in air produced by the vibration of the strut
v_∞	Velocity in the far field, far from the strut, in the radial direction
w^+	Harmonic flexural wave amplitude for wave travelling in + direction, associated with flexure in the z direction
w^-	Harmonic flexural wave amplitude for wave travelling in - direction, associated with flexure in the z direction
w_e^+	Evanescent flexural wave amplitude in + direction, associated with flexure in the z direction
w_e^-	Evanescent flexural wave amplitude in - direction, associated with flexure in the z direction
Y_1	First order Bessel function of the second kind

η_{RAD}	Radiation loss factor
η_s	Structural loss factor
$\eta_{TOT\,DGSM}$	Total loss factor computed using the DGSM program
$\eta_{TOT\,MEAS}$	Total loss factor measured experimentally
θ	Coordinate angle defined from the plane of vibration
κ_y	Radius of gyration about the y axis = $\sqrt{\frac{I_y}{A}}$
κ_z	Radius of gyration about the z axis = $\sqrt{\frac{I_z}{A}}$
λ	Wavelength
ν	Poisson's ratio
Π_{RAD}	Radiated sound power
ρ_a	Density of air
σ_{RAD}	Radiation efficiency of the beam
ϕ^+	Torsional wave amplitude about x axis in + direction
ϕ^-	Torsional wave amplitude about x axis in - direction
ω	Radian frequency

$\Re$	Real part
$\Im$	Imaginary part
$*$	Complex conjugate
$\bar{}$	Spatial averaging
$\langle\rangle$	Temporal averaging

CHAPTER 1: Introduction

In the continuing evolution of submarine design the methods of mounting machinery have progressed from bolting attachments directly to the hull to mounting vibration sources on vibration damping bedplates. The next step, which is considered here, is mounting the machinery on a three dimensional truss type structure. One advantage which is sought is the ability to replace whole sections of the interior machinery by simply exchanging one loaded truss for another by making a transverse hull cut. The relative time savings envisioned in replacement and modernization programs is considerable. The secondary advantage lies in the ability to reduce the noise and vibration transmitted by the truss to the hull. Reduction of radiated noise is implemented in two ways. The design of the truss is such that there is a torturous path for the energy to follow in travelling from the source to the hull, and attachment points at the hull are minimized. Since there are few attachment points, it is conceivable that vibrational isolation mountings could be designed which could minimize the noise transmitted directly to the hull. Secondly, the truss has the capability to have distributed damping added to the members or discrete damping applied at the joints; both methods would reduce transmitted energy.

A: Objective

Since 1993, Massachusetts Institute of Technology has been participating in the study of three-dimensional trusses and in methods of damping them. As part of this ongoing study, a scale model of a square pyramidal based truss has been constructed [1] and is currently being analyzed. The transverse scale is based upon roughly on a 15:1 ratio with respect to the full scale. The cylindrical members that are the connecting legs of the truss lend themselves well to the radiation of energy. It has also been demonstrated that due to the complex geometrical nature of the truss and the many interactions at the joints, the energy

that travels down the truss very quickly reaches an equilibrium partitioning between flexural, compressional and torsional waves. The vibrational energy also shows considerable attenuation when measured at points along the truss as you move away from the drive point.

A current concern is in the amount of airborne radiated sound power produced by the truss. The truss is located in a large and semi-reverberant room and in initial experiments airborne noise production has not been considered. Since a truss will eventually be mounted in an enclosed cylindrical hull, the interactions with the surrounding environment must be considered. It is possible that the sound energy produced by the truss could couple well with the hull and cause undesirable noise transmission into the water. The objective of this research is to analyze the noise produced by the vibration of this complicated structure and to develop analytical tools to quantitatively predict the levels of radiated noise for any given excitation. Since the truss will also support horizontal deckplates, the radiation from a horizontally mounted plate is also considered.

B: Approach

In previous analysis of the truss by Fricke and Hayner [11], a method was formulated to predict the level of vibrational energy in the truss for a given excitation. This method is known as the Direct Global Stiffness Matrix (DGSM) Method. In chapter 2, analytically derived formulae for the radiated sound power are developed starting from the radiation efficiency of plates and beams and the spatially and temporally averaged mean square velocity, $\langle\overline{v^2}\rangle$. In chapter 3, the DGSM method is explained and then used to predict the spatially and temporally averaged mean square velocity, $\langle\overline{v^2}\rangle$, at any point in the truss. The mean square velocity is then utilized in the formulae of chapter 2 to predict the sound power radiated. The result is a method to predict the radiated sound power for an input excitation at any given joint of the truss. A prediction is calculated for an input of white noise at the extreme end of the truss, both

in the as-built condition, and with the addition of square aluminum plates to the horizontal surfaces of the truss. A big uncertainty in the DGSM prediction method is the level of structural damping in the truss. Initial simulations using the DGSM program showed that the structural loss factor η_s is the single most important variable to be input to the program. Added to that uncertainty is a lack of information in the literature on the frequency dependence of η_s, and uncertainty in the nature of the damping in the joints of the truss which was built. Therefore, in chapter 3, a parameterization is conducted to calculate the radiated sound power using various values of η_s.

In chapter 4, the truss is excited in the same manner as the prediction, again with and without plates mounted, and the total sound power radiated is measured using an intensity probe.

In chapter 5, initial comparison between the parameterization and the measured sound power for the bare truss case showed reasonable agreement but hinted that the form of η_s was more complicated than originally thought. Therefore, in chapter 6, an experiment was designed to measured the total loss factor of the bare truss η_{TOT}. The measured total loss factor $\eta_{TOT_{MEAS}}$ was compared to the predicted total loss factor from the DGSM program $\eta_{TOT_{DGSM}}$ and the comparison was used to refine the value of η_s which is an input to the DGSM program. In chapter 6, the DGSM program was then re-run and the result again compared to measured sound power. The refined value of η_s showed considerable improvement in predicting the radiated sound power.

For the truss with plates, initial comparison in chapter 5 finds that the DGSM prediction is approximately 20 dB higher than the measured value. The DGSM prediction was made assuming that the plates were hard mounted to the struts of the truss. In reality, they were mounted using a visco-elastic epoxy which may have prevented sufficient coupling between the struts and the plates to justify the assumption used in the DGSM program. The difference between the prediction and the measurement is explored in chapter 5.

CHAPTER 2: Radiated Noise From The Truss

A: Description of the Structure To Be Analyzed

The three-dimensional truss structure, which is being analyzed, was constructed by Marcus Heath, a previous graduate student at the Massachusetts Institute of Technology [1]. The structure consists of a repeated pattern of square based pyramidal cells, which are 54.8 cm on a side and 77.5 cm in height. Six of the cells are upright and the remaining five are inverted. The complete structure is pictured below as figure 2-1 and the global x, y, and z directions are shown:

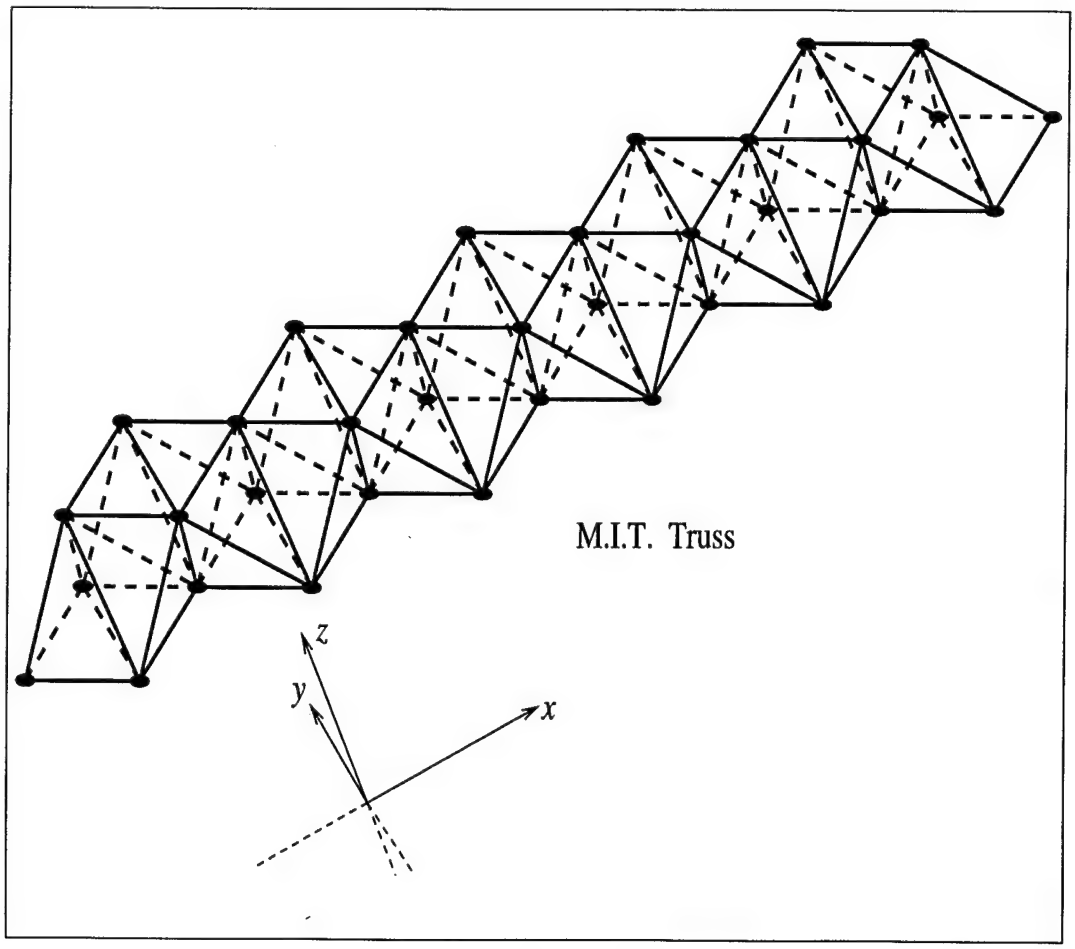

Figure 2-1: MIT Truss

The truss joints and struts are given a naming convention which allows each strut and joint to be uniquely defined. The joints are named with a letter and a number; the letter defines the position of the joint in the y direction and the number defines the position in the x direction. The letters a, b, and c indicate the bottom level of the truss, with b as the centerline and a as the negative y direction. The letters d, e, and f indicate the upper level of the truss and are similarly named. The numbers indicate the position of the joint along the truss with the number 1 indicating the x = 0 position. Figure 2-2 illustrates the convention used. The struts are named with the names of the two joints to which they are attached. For instance strut e8f9 shown in Figure 2-2 connects joints e8 and f9. This convention will be used for the remainder of this analysis.

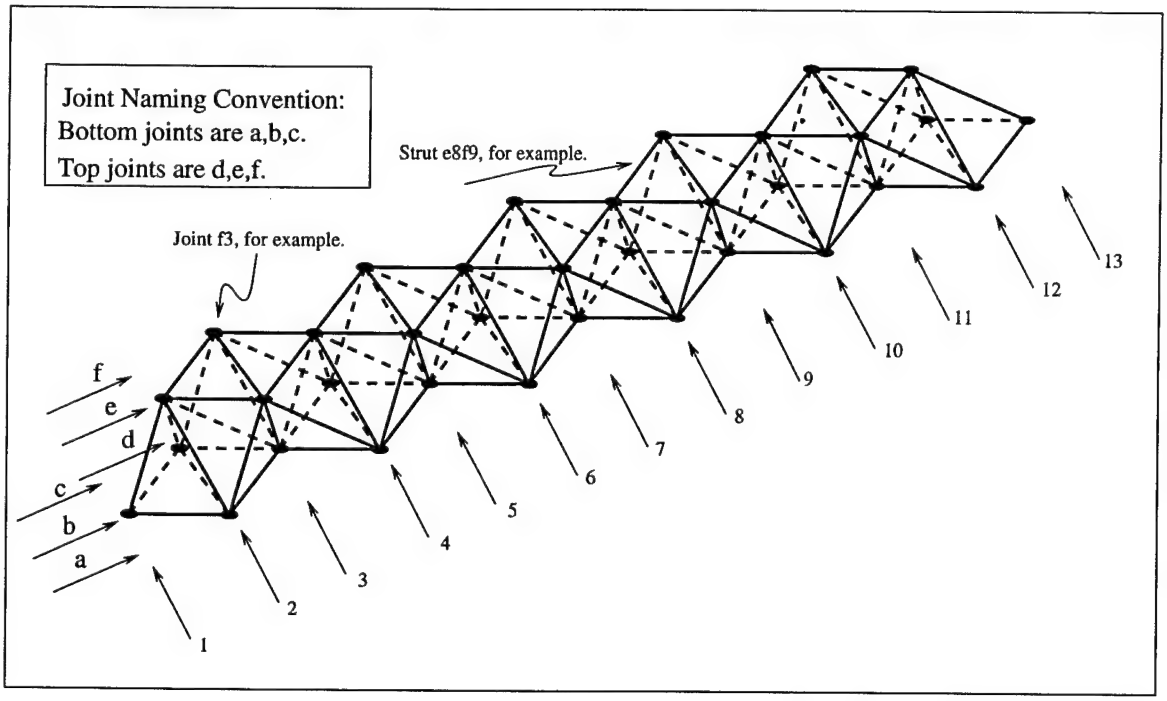

Figure 2-2: Truss joint and strut naming convention

The struts comprising the majority of the truss consist of stock aluminum tubing having the material characteristics shown in table 2-1. The plates which will be later placed on the truss have the characteristics shown in table 2-2.

Material:	6061 T6 Aluminum
Density ρ:	2700 $\frac{\text{kg}}{\text{m}^3}$
Young's Modulus E:	6.89 x 10^{10} $\frac{\text{N}}{\text{m}^2}$
Shear Modulus G:	2.59 x 10^{10} $\frac{\text{N}}{\text{m}^2}$
Poisson's ratio ν:	.33
Outside Radius r_o :	.00635 meters
Inside Radius r_i:	.0047 meters
Mean Radius r_m:	.005525 meters
Wall Thickness t_{wall}:	.00165 meters
Cross-Sectional Area A:	5.73 x10^{-5} meter^2
Mass/unit length:	.154 $\frac{\text{kg}}{\text{m}}$
Longitudinal Sound Speed C_L:	$\sqrt{\frac{E}{\rho}} = 5051.6$ $\frac{\text{m}}{\text{sec}}$
Radius of Gyration κ:	$\sqrt{\frac{\frac{\pi}{4}(r_o^4 - r_i^4)}{\pi(r_o^2 - r_i^2)}} = \frac{1}{2}\sqrt{r_o^2 + r_i^2} = .00395$ meters

Table 2-1: Material characteristics of the struts

Material:	6061 T6 Aluminum
Density ρ:	2700 $\frac{\text{kg}}{\text{m}^3}$
Young's Modulus E:	6.89 x 10^{10} $\frac{\text{N}}{\text{m}^2}$
Shear Modulus G:	2.59 x 10^{10} $\frac{\text{N}}{\text{m}^2}$
Poisson's ratio ν:	.33
Length :	.5 meters
Width :	.5 meters
Thickness :	.002 meters
Surface Area A:	.25 meter^2
Perimeter:	2 meters
Longitudinal Sound Speed C_L:	$\sqrt{\frac{E}{\rho(1-\nu^2)}} = 5351.4$ $\frac{\text{m}}{\text{sec}}$

Table 2-1: Material characteristics of the plates

B: The Radiated Noise From the Struts

A few preliminary points are made. The struts of the truss are considered to be Euler-Bernoulli beams. The commonly accepted criteria for neglecting the effects of shear and rotary inertia is that the wavelength of the flexural wave on the beam be greater than 6 times the height of the beam. Since in this case the beam is an annular cylinder with outer diameter of .0127 meters, the wavelength must be greater than .0762 meters. The wavelength is given by $\lambda_B = \frac{C_B}{f}$ or $\lambda_B = \frac{\sqrt{2\pi f \kappa C_L}}{f} = \sqrt{\frac{2\pi\kappa C_L}{f}}$; therefore,

$$f < \frac{2\pi(.00395 \text{ meters})5051.6 \frac{\text{meters}}{\text{sec}}}{[6(.0127\text{meters})]^2} \tag{2.1}$$

or $f < 21592$ Hz. The frequencies under consideration meet this criteria, and thus there is justification in treating the struts as Euler-Bernoulli beams. Additionally, it will be assumed that the struts and plates alone contribute to the radiated noise, and that the radiation from the joints can be neglected. This assumption was proven valid by Heath [1]. His thesis also supported the supposition that the vibrational energy in the truss was incoherent. This conclusion will be extended to the radiated sound power caused by the vibration of the struts. Thus it will also be assumed that the radiated sound power from the individual struts can be added incoherently.

First consider the radiated noise from a cylinder which is in rigid translation and is moving harmonically in a direction perpendicular to it's axis as shown in figure 2-3 below,
with a harmonic velocity given by the real part of

$$v(t) = U_o e^{-i2\pi ft} = \Re\left\{U_o e^{-i2\pi ft}\right\}. \tag{2.2}$$

In this equation U_o is a constant amplitude vibration of the beam. Later, this expression will be made more general by allowing U_o to be a mode shape superimposed on the rigid translation of the beam.

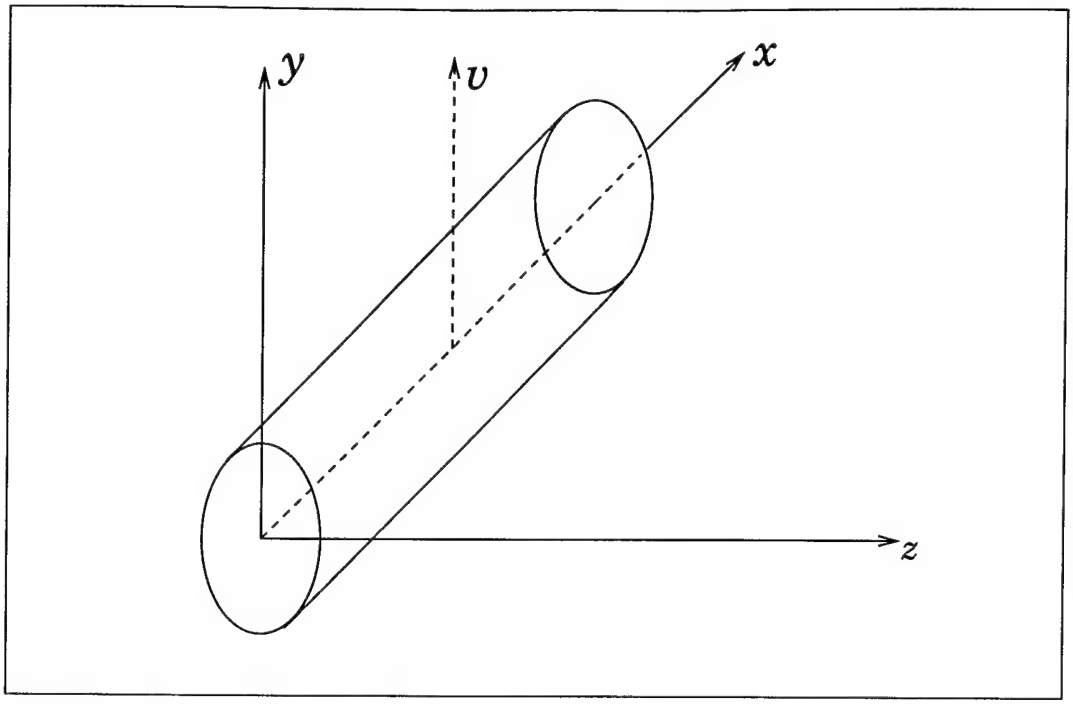

Figure 2-3: Local coordinates to be used in the struts

The wave equation in cylindrical coordinates is given by

$$\frac{\partial^2 \mathrm{p}}{\partial t^2} = C_a^2 \left[\frac{1}{r} \frac{\partial}{\partial r} \left(r \frac{\partial \mathrm{p}}{\partial r} \right) + \frac{1}{r^2} \frac{\partial^2 \mathrm{p}}{\partial \theta^2} + \frac{\partial^2 \mathrm{p}}{\partial z^2} \right]. \tag{2.3}$$

Assuming solutions of the type $\mathrm{p}(r, \theta, z, t) = R(r)\Theta(\theta)Z(z)T(t)$ leads to the solution

$$\mathrm{p} = A \left[\mathrm{J}_1(k_a r) + i \mathrm{Y}_1(k_a r) \right] \cos(\theta) e^{-i2\pi f t}, \quad \{r > a\}, \tag{2.4}$$

where A again is a constant amplitude of vibration, possibly complex. The functions J_1 and Y_1 are the first order Bessel functions of the first and second kind respectively. The angle θ is defined with respect to the plane of vibration.

The velocity for the above solution is given by

$$\vec{\mathrm{v}} = \frac{1}{i\omega\rho_a} \vec{\nabla} \mathrm{p}, \tag{2.5}$$

with a radial velocity component of

$$\mathrm{v}_r = \frac{1}{i\omega\rho_a}\left[\frac{\partial \mathrm{p}}{\partial r}\right]. \tag{2.6}$$

Substituting in the previous result of equation (2.4) gives

$$\mathrm{v}_r = \frac{A}{i\omega\rho_a}\frac{d}{dr}\left[\mathrm{J}_1(k_a r) + i\mathrm{Y}_1(k_a r)\right]\cos(\theta)e^{-i2\pi ft}, \tag{2.7}$$

or,

$$\mathrm{v}_r = \frac{A}{i\rho_a C_a}\left\{\frac{\mathrm{J}_1(k_a r)}{k_a r} - \mathrm{J}_2(k_a r) + i\left[\frac{\mathrm{Y}_1(k_a r)}{k_a r} - \mathrm{Y}_2(k_a r)\right]\right\}\cos(\theta)e^{-i2\pi ft}. \tag{2.8}$$

Next, the boundary conditions are used to find the amplitude of A. The boundary condition on the surface of the cylinder is used; radial velocity must equal $U_o e^{-i2\pi ft}$ when $r = a$. Therefore the value of A is

$$A = \frac{i\rho_a C_a}{\beta(a)}U_o, \tag{2.9}$$

with $\beta(a)$ given by,

$$\beta(a) = \frac{\mathrm{J}_1(k_a a)}{k_a a} - \mathrm{J}_2(k_a a) + i\left[\frac{\mathrm{Y}_1(k_a a)}{k_a a} - \mathrm{Y}_2(k_a a)\right]. \tag{2.10}$$

The interest is in the far-field effects, therefore the result at $k_a r \gg 1$ is important, and the near-field effects can be neglected. For the physical problem being studied this means that

$$k_a r = \frac{2\pi fr}{C_a} \gg 1, \tag{2.11}$$

or,

$$fr \gg \frac{C_a}{2\pi} \gg \frac{340.15}{2\pi}, \tag{2.12}$$

and since the lower limit of usable frequency will be shown later to be on the

order of 1000 Hz, the radius at which the sound radiated can be considered the far-field is when $k_a r > 10$, or

$$r > 10\frac{C_a}{2\pi f} = 10\frac{340.15}{2\pi 1000} \approx .5\text{meters.} \tag{2.13}$$

At large values of the argument, the Bessel functions can be approximated as sinusoidal waves with decreasing amplitude

$$\mathrm{J}_p(k_a r) \approx \sqrt{\frac{2}{\pi k_a r}} \cos\left(x - \frac{3\pi}{4} - \frac{p\pi}{2}\right). \tag{2.14}$$

This gives the following relations for the velocity and pressure far from the strut ($k_a r \gg 1$)

$$\mathrm{p}_\infty = \frac{i\rho_a C_a}{\beta(a)} U_o \sqrt{\frac{2}{\pi k_a r}} \cos(\theta) e^{i\left(k_a r - \frac{3\pi}{4} - 2\pi f t\right)}, \tag{2.15}$$

$$\mathrm{v}_\infty = \frac{U_o}{\beta(a)} \sqrt{\frac{2}{\pi k_a r}} \cos(\theta) e^{i\left(k_a r - \frac{3\pi}{4} - 2\pi f t\right)}. \tag{2.16}$$

The temporally averaged sound power intensity can be calculated from the relation

$$I_r = \frac{1}{2}\Re\left\{\mathrm{p}_\infty \mathrm{v}_\infty^*\right\}. \tag{2.17}$$

Substitution of equations (2.15) and (2.16) into equation (2.17) yields

$$I_r = \frac{1}{2}\Re\left\{\frac{i\rho_a C_a U_o U_o^*}{\beta(a)\beta(a)^*} \frac{2}{\pi k_a r} \cos^2(\theta)\right\}, \tag{2.18}$$

which reduces to

$$I_r = \frac{\rho_a C_a |U_o|^2}{|\beta(a)|^2} \frac{1}{\pi k_a r} \cos^2(\theta). \tag{2.19}$$

The subscript r indicates that this is intensity in the radial direction since the radial velocity was used. Clearly the radiated sound power can be calculated by integrating the above sound intensity over any surface enclosing each individual strut. For simplicity a cylindrical surface is chosen. It is also noted that there is no sound intensity coming out of the ends of the cylinder due to

the chosen geometry and the direction of the rod's motion. Integrating over a cylindrical surface yields the result

$$\Pi_{RAD} = \int_0^{2\pi} \int_0^L I_r r d\theta dx. \tag{2.20}$$

Evaluating the integral and treating $|U_o|^2$ as a constant yields

$$\Pi_{RAD} = \int_0^{2\pi} \int_0^L \frac{\rho_a C_a |U_o|^2}{\pi k_a r |\beta(a)|^2} \cos^2(\theta) r d\theta dx, \tag{2.21}$$

or

$$\Pi_{RAD} = \frac{\rho_a C_a |U_o|^2}{\pi k_a |\beta(a)|^2} \int_0^{2\pi} \int_0^L \cos^2(\theta) d\theta dx, \tag{2.22}$$

resulting in,

$$\Pi_{RAD} = \frac{\rho_a C_a |U_o|^2}{\pi k_a |\beta(a)|^2} L\pi = \frac{\rho_a C_a L |U_o|^2}{k_a |\beta(a)|^2}. \tag{2.23}$$

Equation (2.23) is recognized to be similar to the format which is standard for radiated power

$$\Pi_{RAD} = \rho_a C_a S \sigma_{RAD} \langle \overline{v^2} \rangle, \tag{2.24}$$

where S is defined to be the radiating surface area, which in this case is the area of $\frac{1}{2}$ of the cylinder (πaL), σ_{RAD} is the radiation efficiency of the cylinder and $\langle \overline{v^2} \rangle$ is the spatially and temporally averaged mean square velocity of the beam. Since in the standard formulation the velocity term is the mean square velocity, a factor of $\frac{1}{2}$ must be added to convert the amplitude to a mean square quantity. Equation (2.23) becomes

$$\Pi_{RAD} = \frac{\pi a 2 \frac{1}{2} \rho_a C_a L |U_o|^2}{\pi a k_a |\beta(a)|^2} = \frac{2}{\pi a k_a |\beta(a)|^2} \rho_a C_a S \langle \overline{v^2} \rangle. \tag{2.25}$$

This requires that σ_{RAD} must equal

$$\sigma_{RAD} = \left\{ \frac{2}{\pi k_a a} \right\} \left\{ \frac{1}{|\beta(a)|^2} \right\}. \tag{2.26}$$

The above expression can be simplified by recognizing that expression for β

in equation (2.10) is the same as the derivative of Hankel function of the first kind of order one. The Hankel function of the first kind of order one is the following

$$\mathrm{H}_1(k_a a) = \mathrm{J}_1(k_a a) + i\mathrm{Y}_1(k_a a). \tag{2.27}$$

It's derivative with respect to $k_a a$ is

$$\overline{\mathrm{H}_1}(k_a a) = \frac{d\mathrm{H}_1(k_a a)}{dk_a a} = -\mathrm{H}_2(k_a a) + \frac{1}{k_a a}\mathrm{H}_1(k_a a), \tag{2.28}$$

or,

$$\overline{\mathrm{H}_1}(k_a a) = \frac{\mathrm{J}_1(k_a a)}{k_a a} + i\frac{\mathrm{Y}_1(k_a a)}{k_a a} - \mathrm{J}_2(k_a a) - i\mathrm{Y}_2(k_a a), \tag{2.29}$$

which is recognized to be the same as $\beta(a)$ from equation (2.10). So therefore

$$|\beta(a)|^2 = |\overline{\mathrm{H}_1}(k_a a)|^2 = \overline{\mathrm{H}_1}(k_a a) \bullet (\overline{\mathrm{H}_1}(k_a a))^*, \tag{2.30}$$

and the radiation efficiency can be written as

$$\sigma_{RAD} = \left\{\frac{2}{\pi(k_a a)}\right\}\left\{\frac{1}{|\overline{\mathrm{H}_1}(k_a a)|^2}\right\}. \tag{2.31}$$

The curve of the radiation efficiency is plotted as figure 2-4. For frequencies below the coincidence frequency, where the flexural wave speed on the strut equals the acoustic wave speed in air, the struts are not very efficient radiators of sound, which is to be expected. Furthermore, at frequencies above the coincedence frequency, the radiation efficiency approaches unity. The coincidence frequency for the struts is

$$C_a = C_b = \sqrt{\omega\kappa C_L}, \tag{2.32}$$

or,

$$f = \frac{{C_a}^2}{2\pi\kappa C_L} = \frac{(340.15)^2 \frac{\text{meters}^2}{\text{seconds}^2}}{2\pi(.00395 \text{ meters})5052\frac{\text{meters}}{\text{seconds}}} = 923Hz. \tag{2.33}$$

Therefore, as long as the spatially and temporally averaged mean square

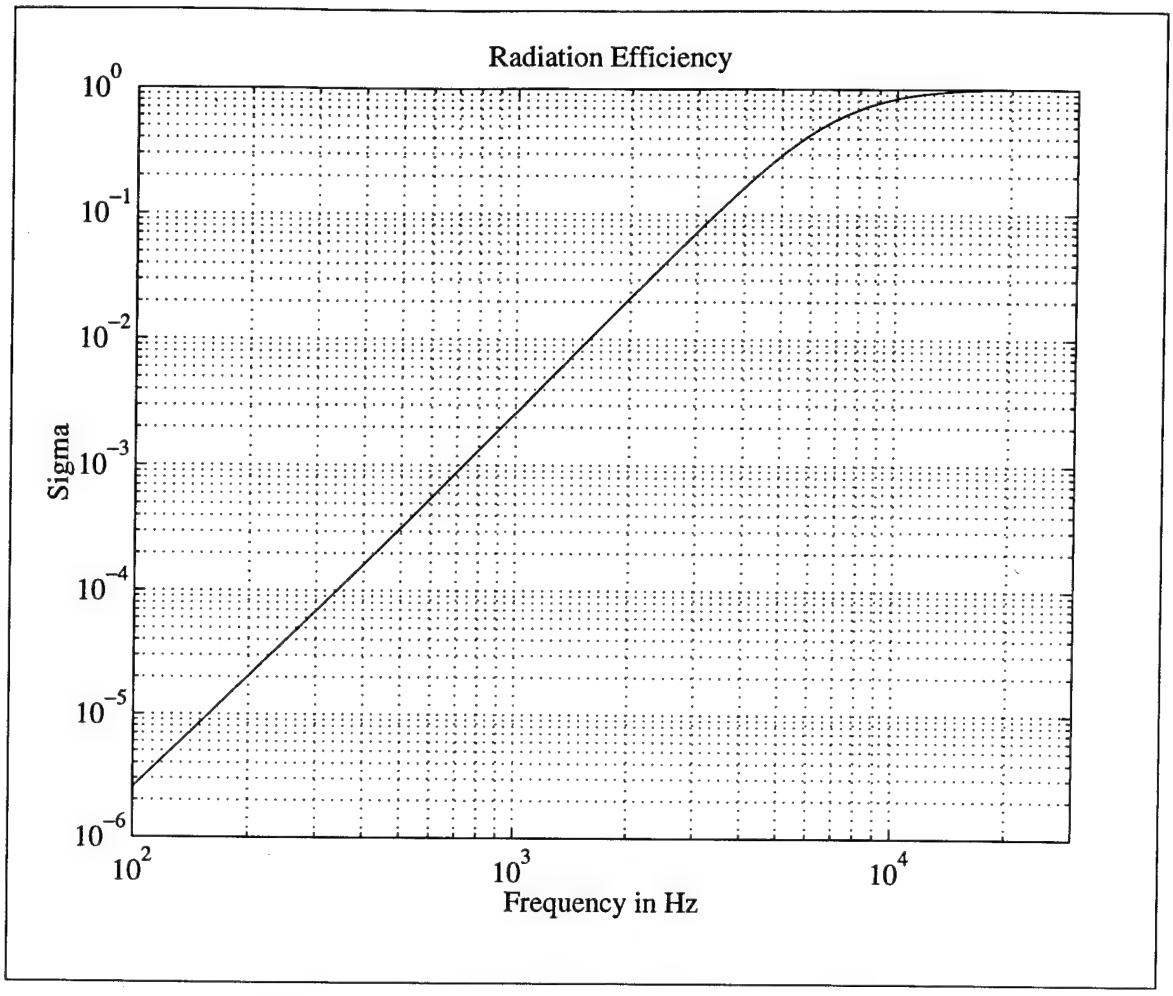

Figure 2-4: Radiation efficiency of the struts

velocity of a strut in the truss can be determined, the radiated power from that strut can thus be predicted. As discussed previously, it will be assumed, for the purposes of this analysis, that the radiated power from the individual struts can be added incoherently.

The next task is to determine a formulation of the spatially and temporally averaged mean square velocity of a beam undergoing flexural vibration. Consider the vibration of the strut in the direction perpendicular to it's longitudinal axis, about the y axis, so that the deflection is in the z direction. The governing equation of motion for the flexural vibration of the strut is the following

$$\frac{EI_y}{\rho A}\frac{\partial^4 w}{\partial x^4} = -\frac{\partial^2 w}{\partial t^2}, \tag{2.34}$$

which leads to the solution for the displacement of the beam in the z direction as a function of distance x along the beam as,

$$w(x,t) = \{w^+ e^{ik_{B_y}x} + w^- e^{-ik_{B_y}(x-L)} + w_e^+ e^{k_{B_y}(x-L)} + w_e^- e^{-k_{B_y}x}\} e^{-i\omega t}. \tag{2.35}$$

The above is recognized to be comprised of two harmonic travelling waves and two evanescent waves. The response is harmonic and the time averaged mean square velocity can be found by using the well-known relation

$$\langle \dot{w}^2 \rangle = \frac{1}{2} \Re \{ \dot{w} \dot{w}^* \}, \tag{2.36}$$

and where the dot notation indicates differentiation with respect to time which is necesary to convert from displacement to velocity. The spatial averaging can then be completed by integration over the length of the strut.

$$\langle \overline{\dot{w}^2} \rangle = \int_0^L \langle \dot{w}^2 \rangle = \int_0^L \frac{1}{2} \Re \{ \dot{w} \dot{w}^* \}. \tag{2.37}$$

Substitution of the result from equation (2.35) yields the following result for the temporally averaged mean square velocity

$$\langle \dot{w}(x,t)^2 \rangle = \frac{1}{2} \Re \left\{ \begin{array}{l} \left[w^+ e^{ik_{B_y}x} + w^- e^{-ik_{B_y}(x-L)} + w_e^+ e^{k_{B_y}(x-L)} + w_e^- e^{-k_{B_y}x} \right] (-i\omega) e^{-i\omega t} \bullet \\ \left[(w^+)^* e^{-ik_{B_y}x} + (w^-)^* e^{ik_{B_y}(x-L)} + (w_e^+)^* e^{k_{B_y}(x-L)} + (w_e^-)^* e^{-k_{B_y}x} \right] i\omega e^{i\omega t} \end{array} \right\}. \tag{2.38}$$

Simplifying yields

$$\langle \dot{w}(x,t)^2 \rangle = \frac{\omega^2}{2} \left\{ |w^+|^2 + |w^-|^2 + |w_e^+|^2 e^{2k_{B_y}(x-L)} + |w_e^-|^2 e^{-2k_{B_y}x} \right\} + \text{crossterms}. \tag{2.39}$$

The cross terms in the above equation are

$$\langle \dot{w}(x,t)^2 \rangle = \frac{\omega^2}{2} \Re \left\{ \begin{array}{c} (w^+)(w^-)^* e^{i2k_{B_y}(x-L)} + (w^+)(w_e^+)^* e^{ik_{B_y}x + k_{B_y}(x-L)} + \\ (w^+)(w_e^-)^* e^{(ik_{B_y} - k_{B_y})x} + (w^-)(w^+)^* e^{ik_{B_y}L - 2ik_{B_y}x} + \\ (w^-)(w_e^+)^* e^{-ik_{B_y}(x-L) + k_{B_y}(x-L)} + (w^-)(w_e^-)^* e^{-ik_{B_y}(x-L) - k_{B_y}x} + \\ (w_e^+)(w^+)^* e^{k_{B_y}(x-L) - ik_{B_y}x} + (w_e^+)(w^-)^* e^{k_{B_y}(x-L) + ik_{B_y}(x-L)} + \\ (w_e^+)(w_e^-)^* e^{-k_{B_y}L} + (w_e^-)(w^+)^* e^{-ik_{B_y}x - k_{B_y}x} + \\ (w_e^-)(w^-)^* e^{ik_{B_y}(x-L) - k_{B_y}x} + (w_e^-)(w_e^+)^* e^{-k_{B_y}L} \end{array} \right\}. \tag{2.40}$$

When the above cross terms are closely examined, two trends are noticed. Many terms contain exponential functions with purely real exponents. There are terms with exponents of $-k_{B_y}L$, $k_{B_y}(x-L)$, and $-k_{B_y}x$. Since the range of x is from 0 to L, these exponents must always be negative. In fact these exponential terms become very small even at very low frequencies. At a frequency as low as 1000 Hz, the bending wavenumber is

$$k_{B_y} = \frac{2\pi f}{C_B} = \frac{2\pi f}{\sqrt{2\pi f \kappa C_L}} = \sqrt{\frac{2\pi f}{\kappa C_L}} = \sqrt{\frac{2\pi 1000}{(.00395)(5052)}} = 17.7 \text{meters}^{-1}, \tag{2.41}$$

which means that the exponential term dies out very quickly and will contribute very little to the total mean square velocity. The second major trend to be noticed is that all terms which do not have an exponential term have a harmonic function dependence. There are also terms which have both a harmonic and exponential function; the exponential term will dominate. For the purely harmonic terms, when the real part is taken, the result will be a sinusoidal shape. Since it has been shown that the wavenumber is relatively high for all frequencies of interest, there will be many waves present on the strut. Thus when the spatial averaging is performed, there will be cancellation except at the very ends of the strut. When the non-cancelling portion is averaged across the strut the total contribution to mean square velocity will again be small. This discussion assumes that the wave amplitudes for all wave types is of the

same order of magnitude. Prior experimentation on the truss, and previous results from the DGSM method have shown this assumption to be a valid one [1]. To illustrate these points, consider the evaluation of the spatial averaging of the cross terms

$$\overline{\langle \dot{w}(x,t)^2 \rangle} = \frac{\omega^2}{2} \int_0^L \Re \left\{ \begin{array}{c} (w^+)(w^-)^* e^{i2k_{B_y}(x-L)} + (w^+)(w_e^+)^* e^{ik_{B_y}x + k_{B_y}(x-L)} + \\ (w^+)(w_e^-)^* e^{(ik_{B_y} - k_{B_y})x} + (w^-)(w^+)^* e^{ik_{B_y}L - 2ik_{B_y}x} + \\ (w^-)(w_e^+)^* e^{-ik_{B_y}(x-L) + k_{B_y}(x-L)} + (w^-)(w_e^-)^* e^{-ik_{B_y}(x-L) - k_{B_y}x} + \\ (w_e^+)(w^+)^* e^{k_{B_y}(x-L) - ik_{B_y}x} + (w_e^+)(w^-)^* e^{k_{B_y}(x-L) + ik_{B_y}(x-L)} + \\ (w_e^+)(w_e^-)^* e^{-k_{B_y}L} + (w_e^-)(w^+)^* e^{-ik_{B_y}x - k_{B_y}x} + \\ (w_e^-)(w^-)^* e^{ik_{B_y}(x-L) - k_{B_y}x} + (w_e^-)(w_e^+)^* e^{-k_{B_y}L} \end{array} \right\} dx, \tag{2.42}$$

which yields

$$\overline{\langle \dot{w}(x,t)^2 \rangle} = \frac{\omega^2}{2} \left[\begin{array}{c} \Re\{(w^+)(w^-)^*\} \Re\left\{e^{-ik_{B_y}L}\right\} \Re\left\{\frac{e^{i2k_{B_y}L}-1}{2ik_{B_y}L}\right\} + \\ \Re\{(w^+)(w_e^+)^*\} \left\{e^{-k_{B_y}L}\right\} \Re\left\{\frac{e^{(ik_{B_y}+k_{B_y})L}-1}{(ik_{B_y}+k_{B_y})L}\right\} + \\ \Re\{(w^+)(w_e^-)^*\} \Re\left\{\frac{e^{(ik_{B_y}-k_{B_y})L}-1}{(ik_{B_y}-k_{B_y})L}\right\} + \\ \Re\{(w^-)(w^+)^*\} \Re\left\{e^{ik_{B_y}L}\right\} \Re\left\{\frac{1-e^{-2ik_{B_y}L}}{2ik_{B_y}L}\right\} + \\ \Re\{(w^-)(w_e^+)^*\} \left\{e^{-k_{B_y}L}\right\} \Re\left\{e^{ik_{B_y}L}\right\} \Re\left\{\frac{e^{(k_{B_y}-ik_{B_y})L}-1}{(k_{B_y}-ik_{B_y})L}\right\} + \\ \Re\{(w^-)(w_e^-)^*\} \Re\left\{e^{ik_{B_y}L}\right\} \Re\left\{\frac{e^{-(ik_{B_y}+k_{B_y})L}-1}{-(ik_{B_y}+k_{B_y})L}\right\} + \\ \Re\{(w_e^+)(w^+)^*\} \left\{e^{-k_{B_y}L}\right\} \Re\left\{\frac{e^{(k_{B_y}-ik_{B_y})L}-1}{(k_{B_y}-ik_{B_y})L}\right\} + \\ \Re\{(w_e^+)(w^-)^*\} \left\{e^{-k_{B_y}L}\right\} \Re\left\{e^{-ik_{B_y}L}\right\} \Re\left\{\frac{e^{(k_{B_y}+ik_{B_y})L}-1}{(ik_{B_y}+k_{B_y})L}\right\} + \\ \Re\{(w_e^+)(w_e^-)^*\} \left\{e^{-k_{B_y}L}\right\} + \\ \Re\{(w_e^-)(w^+)^*\} \Re\left\{\frac{e^{-(ik_{B_y}+k_{B_y})L}-1}{-(ik_{B_y}+k_{B_y})L}\right\} + \\ \Re\{(w_e^-)(w^-)^*\} \Re\left\{e^{-ik_{B_y}L}\right\} \Re\left\{\frac{e^{(ik_{B_y}-k_{B_y})L}-1}{(ik_{B_y}-k_{B_y})L}\right\} + \\ \Re\{(w_e^-)(w_e^+)^*\} \left\{e^{-k_{B_y}L}\right\} \end{array} \right]. \tag{2.43}$$

The highest order terms are those which have multipliers of the form

$$\Re\left\{\frac{e^{(ik_{B_y}-k_{B_y})L}-1}{(ik_{B_y}-k_{B_y})L}\right\}. \tag{2.44}$$

Clearly, the numerator is always of order 1 or less. The denominator is of the order of $k_{B_y}L$ which has been shown to be a large value compared to unity.

For these reasons, the cross-terms will be neglected and only the terms in brackets in equation (2.39) will be used in the spatial averaging, or

$$\langle\overline{\dot{w}^2}\rangle = \frac{\omega^2}{2L}\int_0^L \left\{|w^+|^2+|w^-|^2+|w_e^+|^2e^{2k_{B_y}(x-L)}+|w_e^-|^2e^{-2k_{B_y}x}\right\}dx. \tag{2.45}$$

The temporally averaged mean square velocity is broken into harmonic and evanescent components

$$\langle\overline{\dot{w}(x,t)^2}\rangle_{Harmonic} = \frac{\omega^2}{2L}\int_0^L \left\{|w^+|^2+|w^-|^2\right\}dx \tag{2.46}$$

and

$$\langle\overline{\dot{w}(x,t)^2}\rangle_{Evanescent} = \frac{\omega^2}{2L}\int_0^L \left\{|w_e^+|^2e^{2k_{B_y}(x-L)}+|w_e^-|^2e^{-2k_{B_y}x}\right\}dx. \tag{2.47}$$

The spatial integration yields

$$\langle\overline{\dot{w}(x,t)^2}\rangle_{Harmonic} = \frac{\omega^2\left(|w^+|^2+|w^-|^2\right)}{2}, \tag{2.48}$$

and

$$\langle\overline{\dot{w}(x,t)^2}\rangle_{Evanescent} = \frac{\omega^2\left(|w_e^+|^2+|w_e^-|^2\right)}{2}\left\{\frac{1-e^{-2k_{B_y}L}}{2k_{B_y}L}\right\}. \tag{2.49}$$

Finally the radiated power equations (equation 2.24) are

$$\Pi_{RAD\,Harmonic} = \rho_a C_a S\sigma_{RAD}\frac{\omega^2}{2}\left(|w^+|^2+|w^-|^2\right) \tag{2.50}$$

and

$$\Pi_{RAD\,Evanescent} = \rho_a C_a S \sigma_{RAD} \omega^2 \left(|w_e^+|^2 + |w_e^-|^2 \right) \left\{ \frac{1 - e^{-2k_{B_y} L}}{4 k_{B_y} L} \right\}. \qquad (2.51)$$

These equations have been deliberately expressed in terms of the displacement amplitudes of the beam. In the next chapter the Direct Global Stiffness Matrix will be introduced and it will be seen that the output of the method is the displacement amplitudes of the beams in flexural vibration. It should be noted at this point that the above equations represent only $\frac{1}{2}$ of the radiated sound power. The beams will undergo flexural vibration in both the z and y directions. The only difference in the above equations is in the choice of the bending wave number k_{B_y} or k_{B_z} and the radius of gyration κ_y or κ_z. Fortunately, the cylindrical geometry means that the radii of gyrations and bending wavenumbers are the same for both the x and z direction flexural vibration.

C: The Radiated Noise From the Plates

The plates are more efficient radiators of sound and they also are highly directive. The sound radiation from the plates, however, is highly dependent on the amount of vibrational energy which is transferred to them from the beams and thus the coupling between the beams and plates is of crucial importance to the amount of sound radiated.

The plates were attached to the truss struts using a visco-elastic epoxy glue. The glue was placed on the struts for the entire length that the plate was in contact with the struts, making a continous joint. The placement of the plates was on the bottom of the pyramidal structures as shown in figure 2-5 below. The coupling between the struts and plates is a largely unknown quantity. It it expected that the epoxy, because of it's inherent visco-elasticity, will not allow strong coupling between the plates and the struts, but a quantitative relationship is not available.

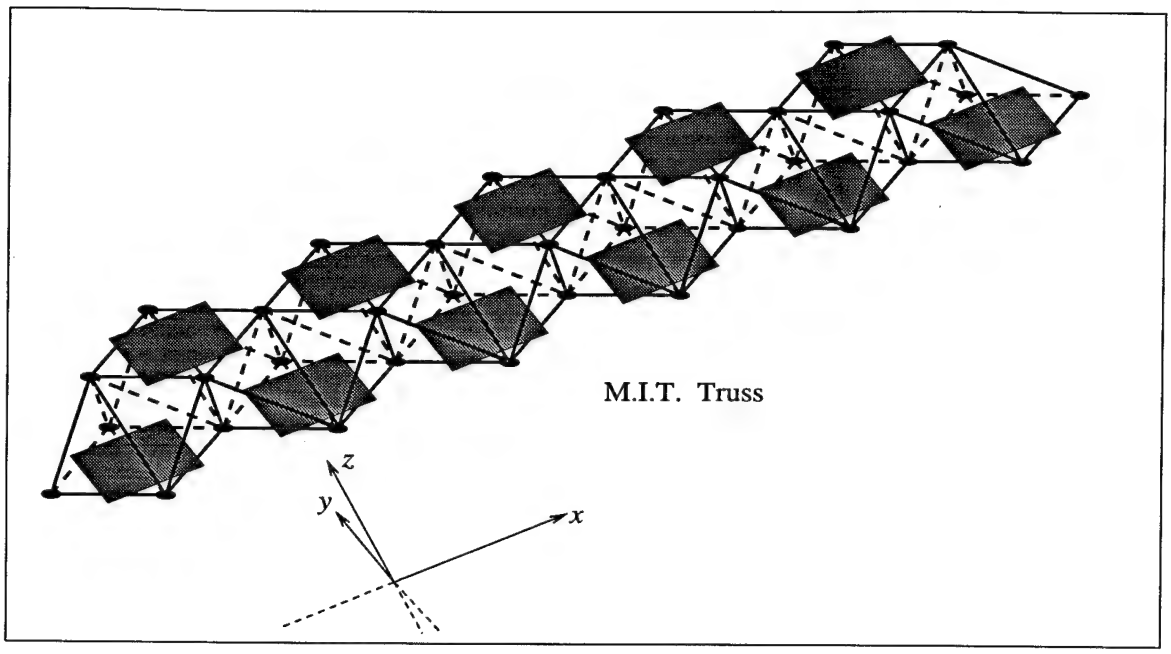

Figure 2-5: Placement of aluminum plates on truss.

As a worst case, first order, estimate, the plate strut combination will be modeled as a continuous welded line. Since bending waves are considered the main type of energy being transferred, and the two elements are strongly coupled, an equipartition between the modal energies of the beam and plate can be assumed [4]. This means

$$\frac{E_B}{n_B(\omega)} = \frac{E_P}{n_P(\omega)} = \frac{M_B\overline{\langle v_B^2 \rangle}}{n_B(\omega)} = \frac{M_P\overline{\langle v_P^2 \rangle}}{n_P(\omega)}, \tag{2.52}$$

where E represents the spatially and temporally averaged mean square vibrational energy, $n(\omega)$ represents the modal density, M is the mass, and the subscripts B and P represent the beam and plate respectively. So the temporally and spatially averaged mean square velocity of the plate can be found by

$$\overline{\langle v_P^2 \rangle} = \frac{M_B n_P(\omega)\overline{\langle v_B^2 \rangle}}{M_P n_B(\omega)}. \tag{2.53}$$

The masses of the beam and plate are known and the mean square velocity of the beam was found in equations (2.48) and (2.49), using the outputs of the DGSM program. Using the output of the DGSM program will introduce some

errors. In the development of the DGSM program, the vibrational energy of each strut is calculated assuming there is no coupling with adjacent systems other than the struts which are directly connected. Such an assumption is reasonable for the bare struts; it is not expected that there will be coupling with the acoustic space of the room. However, the addition of these plates to the truss, under the assumption of strong coupling with the struts, would affect the vibrational energies in the struts. For the present, these errors will be neglected, pending further investigation in chapter 5.

The modal densities of the beam and plate are

$$n_B(\omega) = \frac{L}{3.38\sqrt{C_{LB} d\omega}}, \tag{2.54}$$

where L is the length of the beam, C_{LB} is the longitudinal wave speed in the beam, and d is the diameter of the beam, and

$$n_P(\omega) = \frac{S}{3.6 C_{LP} t}, \tag{2.55}$$

where S is the surface area of the plate, C_{LP} is the longitudinal wave speed of the plate and t is the thickness of the plate.

In order to apply equation (2.24) to the plates, all that is needed is an expression for the radiation efficiency. Fortunately, Cremer [6] provides the following radiation efficiency for point excited, weakly damped two-dimensional plates

$$\sigma_{RAD} \approx \begin{cases} \frac{U\lambda_c}{\pi^2 S}\sqrt{\frac{f}{f_c}} & \text{for } f \ll f_c \\ 0.45\sqrt{\frac{U}{\lambda_c}} & \text{for } f = f_c \\ 1 & \text{for } f \gg f_c \end{cases}, \tag{2.56}$$

where U is the perimeter of the plate, λ_c is the critical wavelength of the plate (that wavelength where the bending wavespeed of the plate equals the speed of sound in air), S is the surface area of the plate and f_c is the critical frequency.

The critical frequency of the plate is when

$$C_a = C_B = \sqrt{\omega \kappa C_L}, \tag{2.57}$$

or,

$$f_c = \frac{C_a^2}{tC_L \frac{2\pi}{\sqrt{12}}} = 6006\ Hz. \tag{2.58}$$

The radiation efficiency of equation (2.56) is not defined as a smooth function of f, and is therefore not the optimal input for the DGSM program. In order to smooth the above values, they were fitted with a 13^{th} order polynomial fit. The upper limit of the frequency defined as $f \ll f_c$ was taken to be $\frac{1}{6}$ of the critical freqeuncy or 1000 Hz. The lower limit of the frequency defined as $f \gg f_c$ was taken as 15000 Hz. The curve is plotted below as figure 2-6.

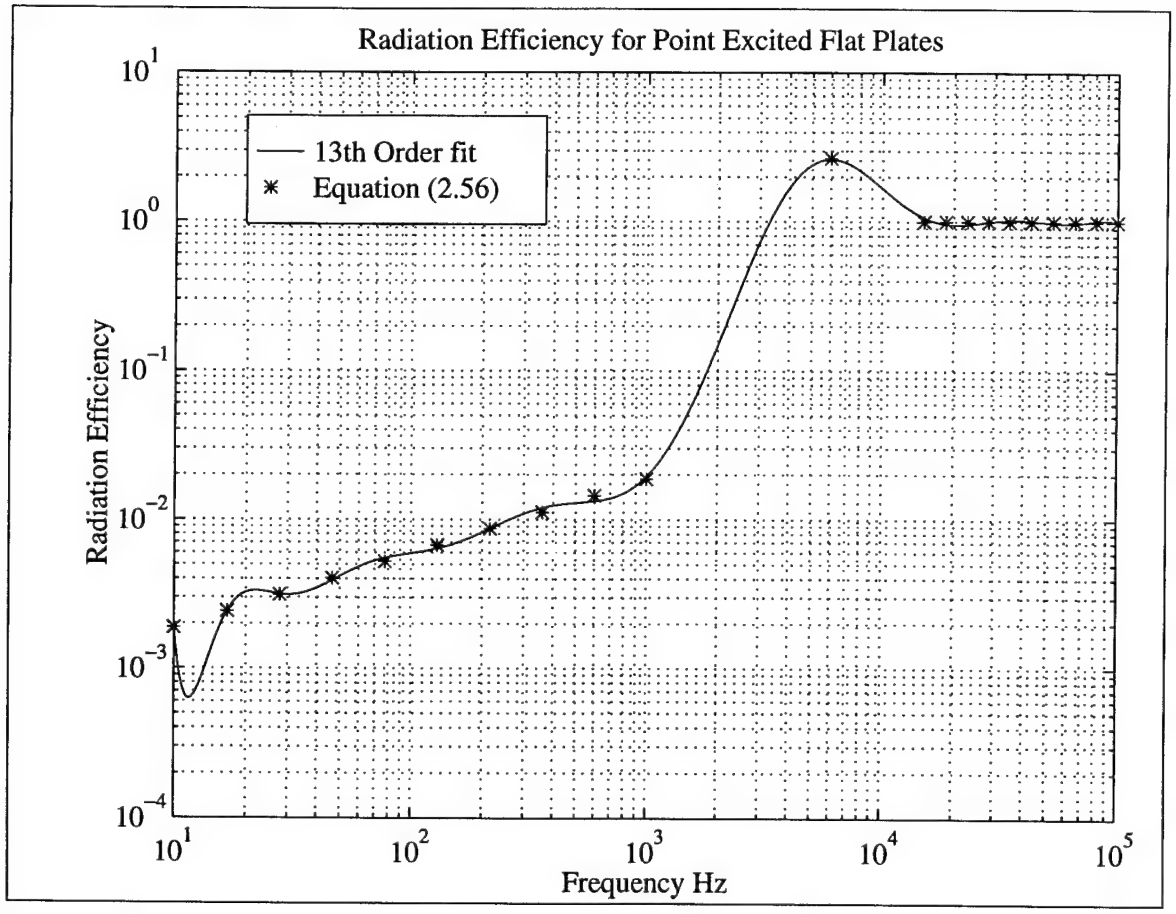

Figure 2-6: Radiation efficiency of the plates

D: Limits of the Analysis

For the radiated power equations (2.50) and (2.51) to hold there must be at least one flexural wavelength along the beam. So that the flexural wavelength must be less than the length of the beam or,

$$\lambda_B < \frac{C_B}{f} = \sqrt{\frac{2\pi f \kappa C_L}{f^2}} = \sqrt{\frac{2\pi\kappa C_L}{f}} = \sqrt{\frac{125.37}{f}} \text{ meters.} \tag{2.59}$$

Therefore, the theory will apply when,

$$f \;>\; \tfrac{125.37}{L^2} Hz \;=\; \left\{ \begin{array}{ll} 535.2\,Hz, & L = .484 \text{ meters} \\ 255.9\,Hz, & L = .700 \text{ meters} \\ 191.1\,Hz, & L = .810 \text{ meters} \end{array} \right\} \tag{2.60}$$

This limitation places no real restrictions on the analysis since it is also known that for an infinite beam to be an efficient radiator of energy, the flexural wave speed must be greater than the speed of sound in the surrounding fluid. The frequency of flexural vibration where the flexural wave speed equals the acoustic wave speed is known as the coincidence frequency. For the struts of the truss under consideration, the flexural frequency must therefore be

$$f > \frac{C_a^2}{2\pi\kappa C_L} \Longrightarrow f > 923Hz, \tag{2.61}$$

which is well above the limits placed on the analysis from the condition in equation (2.60). Another consideration that comes into effect later is that the background noise in the laboratory was high in the low frequency bands. The experimental measurements of chapter 4 will show that the region below 1 kHz was unusable due to this high background noise.

CHAPTER 3: An Analytical Model for the Vibration of the Truss

A: The Direct Global Stiffness Matrix Method

The Direct Global Stiffness Matrix (DGSM) Method is developed by Fricke and Hayner [11]. The DGSM method models the joints of the truss as separate elements having six degrees of freedom. The struts of the truss are modeled as being welded at the joints. By analyzing the wave types present in the struts themselves, a so-called Global Stiffness Matrix is developed and then inverted. The fact that the matrix is sparse and the that the matrix need be inverted only once for any possible forcing combination leads to a great savings in computation time. There is, however, one Global Stiffness Matrix for each frequency to be studied, which leads to a large number of iterations of the program to provide sufficient frequency coverage. For the purpose of completeness of later anaylsis, the derivation conducted by Fricke and Hayner is summarized here.

The following analysis considers all equations to be in the local coordinates of the struts. The x direction consists of the direction along the strut axis while the y and z directions are perpendicular to the x axis and are mutually orthogonal. Therefore u, v, and w are the displacements in the x, y, and z directions corresponding to the localized geometry and ϕ_x, ϕ_y, and ϕ_z are the corresponding rotations.

The compressional waves are first studied. The governing equation for the compressional waves is

$$\frac{\partial^2 u}{\partial t^2} = C_L^2 \frac{\partial^2 u}{\partial x^2}, \tag{3.1}$$

where C_L is the longitudinal wave speed and is equal to $\sqrt{\frac{E}{\rho}}$. The solution is

composed of a right and left going wave and may be written as

$$u = \{u^+ e^{ik_L x} + u^- e^{-ik_L(x-L)}\} e^{i\omega t}. \tag{3.2}$$

The total force in the beam in the longitudinal direction is computed from the stress

$$f_x = EA\frac{\partial u}{\partial x}. \tag{3.3}$$

From the above equations, a 2x2 system of equations is written in local coordinates, which relates the beam amplitudes u^+ and u^- to the force f_x and the beam displacement u

$$\begin{bmatrix} e^{ik_L x} & e^{-ik_L(x-L)} \\ iEAk_L e^{ik_L x} & -iEAk_L e^{-ik_L(x-L)} \end{bmatrix} \begin{bmatrix} u^+ \\ u^- \end{bmatrix} = \begin{bmatrix} u \\ f_x \end{bmatrix}. \tag{3.4}$$

In a similar way the governing equation of motion for the torsional waves is

$$\frac{\partial^2 \phi_x}{\partial t^2} = C_T^2 \frac{\partial^2 \phi_x}{\partial x^2}, \tag{3.5}$$

where C_T is the torsional wave speed of $\sqrt{\frac{G}{\rho}}$. This equation leads to solutions

$$\phi_x = \{\phi_x{}^+ e^{ik_T x} + \phi_x{}^- e^{-ik_T(x-L)}\} e^{i\omega t}. \tag{3.6}$$

The moment acting on the beam is now given by $m_x = GJ\frac{\partial \phi_x}{\partial x}$, which leads to another 2x2 matrix for the torsional excitation in the beam relating the torsional wave amplitudes to the rotation in the x direction and the moment about the x axis

$$\begin{bmatrix} e^{ik_T x} & e^{-ik_T(x-L)} \\ iGJk_T e^{ik_T x} & -iGJk_T e^{-ik_T(x-L)} \end{bmatrix} \begin{bmatrix} \phi_x{}^+ \\ \phi_x{}^- \end{bmatrix} = \begin{bmatrix} \phi_x \\ m_x \end{bmatrix}. \tag{3.7}$$

The last major wave type of interest in the beam are the flexural waves. As was previously postulated, these waves produce the majority of the sound

power being radiated and they will be assumed to be the *only* source of sound power being radiated. For the flexural waves, the governing equation is

$$\frac{EI_y}{\rho A}\frac{\partial^4 w}{\partial x^4} = -\frac{\partial^2 w}{\partial t^2}. \tag{3.8}$$

This leads to the solution,

$$w = \{w^+ e^{ik_{B_y}x} + w^- e^{ik_{B_y}(x-L)} + w_e^+ e^{k_{B_y}(x-L)} + w_e^- e^{-k_{B_y}x}\}e^{i\omega t}. \tag{3.9}$$

The first two terms are seen to be harmonic wave solutions to the equation. The last two terms represent waves which exist at the boundaries of the struts and then quickly dissipate. These so-called evanescent waves exist because the struts have finite length. It will be shown later that they do contribute to the root mean square velocity of the struts in flexure. The same progression as used before is utilized with the flexural waves to find the rotation, bending moments and shear forces associated with the wave amplitude in the z direction

$$\phi_y = -\frac{\partial w}{\partial x}, \tag{3.10}$$

$$m_y = -EI_y\frac{\partial^2 w}{\partial x^2}, \tag{3.11}$$

$$f_z = -EI_y\frac{\partial^3 w}{\partial x^3}. \tag{3.12}$$

These equations are used to produce a 4x4 matrix which relates the wave amplitudes w^+, w^-, w_e^+ and w_e^- to the displacement, rotation, shear force and bending moment

$$\begin{bmatrix} e^{ik_{B_y}x} & e^{k_{B_y}(x-L)} & e^{-ik_{B_y}(x-L)} & e^{-k_{B_y}x} \\ -ik_{B_y}e^{ik_{B_y}x} & -k_{B_y}e^{k_{B_y}(x-L)} & ik_{B_y}e^{-ik_{B_y}(x-L)} & k_{B_y}e^{-k_{B_y}x} \\ iEI_y{k_{B_y}}^3 e^{ik_{B_y}x} & -EI_y{k_{B_y}}^3 e^{k_{B_y}(x-L)} & -iEI_y{k_{B_y}}^3 e^{-ik_{B_y}(x-L)} & EI_y{k_{B_y}}^3 e^{-k_{B_y}x} \\ EI_y{k_{B_y}}^2 e^{ik_{B_y}x} & -EI_y{k_{B_y}}^2 e^{k_{B_y}(x-L)} & EI_y{k_{B_y}}^2 e^{-ik_{B_y}(x-L)} & -EI_y{k_{B_y}}^2 e^{-k_{B_y}x} \end{bmatrix} \begin{bmatrix} w^+ \\ w_e^+ \\ w^- \\ w_e^- \end{bmatrix} = \begin{bmatrix} w \\ \phi_y \\ f_z \\ m_y \end{bmatrix}. \tag{3.13}$$

In a similar way the equations for the bending about the z axis can also be obtained. The only real difference in the equations is in the moment of inertia and the wave number

$$\begin{bmatrix} e^{ik_{B_z}x} & e^{k_{B_z}(x-L)} & e^{-ik_{B_z}(x-L)} & e^{-k_{B_y}z} \\ -ik_{B_z}e^{ik_{B_z}x} & -k_{B_y}e^{k_{B_z}(x-L)} & ik_{B_z}e^{-ik_{B_z}(x-L)} & k_{B_z}e^{-k_{B_z}x} \\ iEI_z{k_{B_z}}^3e^{ik_{B_z}x} & -EI_z{k_{B_z}}^3e^{k_{B_z}(x-L)} & -iEI_z{k_{B_z}}^3e^{-ik_{B_z}(x-L)} & EI_z{k_{B_z}}^3e^{-k_{B_z}x} \\ EI_z{k_{B_z}}^2e^{ik_{B_z}x} & -EI_z{k_{B_z}}^2e^{k_{B_z}(x-L)} & EI_z{k_{B_z}}^2e^{-ik_{B_z}(x-L)} & -EI_z{k_{B_z}}^2e^{-k_{B_z}x} \end{bmatrix} \begin{bmatrix} v^+ \\ v_e^+ \\ v^- \\ v_e^- \end{bmatrix} = \begin{bmatrix} v \\ \phi_z \\ f_y \\ m_z \end{bmatrix}. \tag{3.14}$$

Combining equations (3-4), (3-7),(3- 13), and (3-14) will yield a complete set of matrix equations. For simplicity, the vector of wave amplitudes $\vec{W}$ is designated as

$$\vec{W}^T = [w^+, w^-, w_e^+, w_e^-, v^+, v^-, v_e^+, v_e^-, u^+, u^-, \phi_x^+, \phi_x^-]. \tag{3.15}$$

The coefficients of the wave amplitude vector are evaluated at $x = 0$ and $x = L$. The coefficients corresponding to the displacements and rotations is a 6x12 matrix and is designated as **D**. The matrix of force and moment coeffiecients is designated **C**. The displacements at the endpoints of the struts form a 6x1 matrix, which is designated $\vec{U}$

$$\vec{U}^T = [u, v, w, \phi_x, \phi_y, \phi_z]|_{x=0,L}. \tag{3.16}$$

Likewise the forces and moments at the endpoints of the struts also form a 6x1 matrix, which is designated $\vec{F}$

$$\vec{F}^T = [f_x, f_y, f_z, m_x, m_y, m_z]|_{x=0,L}. \tag{3.17}$$

Finally we can write two matrix equations which relate the displacements

rotations, forces, and moments at the strut endpoints to the wave amplitudes

$$\begin{bmatrix} \mathbf{D^0} \\ \mathbf{D^L} \end{bmatrix} \vec{W} = \begin{bmatrix} \vec{U}^0 \\ \vec{U}^L \end{bmatrix}, \tag{3.18}$$

or,

$$\mathbf{D}\vec{W} = \vec{U}, \tag{3.19}$$

and,

$$\begin{bmatrix} -\mathbf{C^0} \\ \mathbf{C^L} \end{bmatrix} \vec{W} = \begin{bmatrix} \vec{F}^0 \\ \vec{F}^L \end{bmatrix}, \tag{3.20}$$

or,

$$\mathbf{C}\vec{W} = \vec{F}. \tag{3.21}$$

These equations can be manipulated to form the equation

$$\mathbf{C}\mathbf{D}^{-1}\vec{U} \equiv \mathbf{K}\vec{U} = \vec{F}. \tag{3.22}$$

The matrix **K** is called the local stiffness matrix as it expresses the relationship between the applied forces and the displacements. The local stiffness matrix must be converted into global coordinates so that the contributions from each beam can be added together. This transformation is accomplished by using the two endpoints of each beam and one other point to define a local plane. If $\vec{g_1}$, $\vec{g_2}$, and $\vec{g_3}$ are the global coordinates of the three points chosen to define the local axes, the local $\vec{x}$ axis unit vector can be found by

$$\vec{x} = \frac{(\vec{g_2} - \vec{g_1})}{|(\vec{g_2} - \vec{g_1})|}, \tag{3.23}$$

the two vectors $(\vec{g_2} - \vec{g_1})$ and $(\vec{g_3} - \vec{g_1})$ define the plane in which all three points lie. Therefore, the local $\vec{z}$ axis unit vector is found by taking the cross product of these two vectors

$$\vec{z} = \frac{(\vec{g_2} - \vec{g_1}) \times (\vec{g_3} - \vec{g_1})}{|(\vec{g_2} - \vec{g_1}) \times (\vec{g_3} - \vec{g_1})|}. \tag{3.24}$$

The $\vec{y}$ axis unit vector follows from the cross product of $\vec{z}$ with $\vec{x}$

$$\vec{y} = \frac{\vec{z} \times \vec{x}}{|\vec{z} \times \vec{x}|}. \tag{3.25}$$

For each beam element a transformation matrix is constructed with column vectors, which are the local unit vectors $\vec{x}$, $\vec{y}$, and $\vec{z}$

$$T = [\vec{x}\ \vec{y}\ \vec{z}], \tag{3.26}$$

and a 12×12 matrix is built to transform the local displacements, forces moments and rotations into global coordinates

$$\mathcal{T} = \begin{bmatrix} T & 0 & 0 & 0 \\ 0 & T & 0 & 0 \\ 0 & 0 & T & 0 \\ 0 & 0 & 0 & T \end{bmatrix}. \tag{3.27}$$

Note that since the transformation matrix is made up of the individual unit vectors and due to the inherent orthogonality of the transformation vectors

$$\mathcal{T}^{-1} = \mathcal{T}^T, \quad \text{and} \quad \mathcal{T}\mathcal{T}^T = \mathcal{T}\mathcal{T}^{-1} = I. \tag{3.28}$$

The stiffness matrix for the i^{th} beam can be written in global coordinates

$$\mathcal{T}_i \mathrm{C}_i \mathrm{D}_i^{-1} \mathcal{T}_i^T \mathcal{T}_i \vec{U}_i \equiv \underbrace{\mathcal{T}_i \mathrm{K}_i \mathcal{T}_i^T}_{\mathcal{K}_i} \underbrace{\mathcal{T}_i \vec{U}_i}_{\vec{u}_i} = \underbrace{\mathcal{T}_i \vec{F}_i}_{\vec{\mathcal{F}}_i}, \tag{3.29}$$

thus the global stiffness for the i^{th} beam is defined. All that remains is to compile the Global Stiffness Matrix for all elements in the truss, which is done by matching the boundary conditions on each strut. The joints are considered to be welded joints, and the boundary condition is that the displacement of all the joints which terminate at one element must be equal. Likewise, the sum of the forces and moments at each joint due to the beams that terminate at that

joint must equal the applied forces and moments at that joint

$$\sum_{i=1}^{M_j} \vec{\mathcal{F}}_i = \vec{\mathcal{F}}^j_{ext}, \tag{3.30}$$

where M_j is the number of struts that terminate at the j^{th} joint and $\vec{\mathcal{F}}^j_{ext}$ is the applied external force to the j^{th} joint. Fortunately, since the joint displacements for all beam ends are equal, summing the stiffnesses works as well as summing the forces. The Global Stiffness Matrix is thus assembled and then inverted to solve for the joint displacements for any given applied force or moment combination. From the joint displacements, the amplitudes of the waves on any strut can be recovered using

$$\vec{W} = \mathrm{D}^{-1}\vec{U} = \mathrm{D}^{-1}\mathcal{T}^{-1}\vec{\mathcal{U}}. \tag{3.31}$$

B: Evaluation of the Mean Square Velocity

A Matlab© routine developed by Fricke and Hayner[8] is utilized as the basis for the numerical analysis that follows. The routine begins with a given set of frequencies under consideration and a specified input force. The force used in the prediction was chosen to be a force applied at one end of the truss, on the centerline and in the $+z$ direction. This force was chosen to match the actual applied force during the experimentation. An iterative loop is set up to utilize the above analysis by constructing the Global Stiffness Matrix for each of the given frequencies. This matrix is inverted and the displacements of the nodes of the truss are determined for the specified input force. The vector of wave amplitudes $\vec{W}$ is also determined. As discussed in chapter 2, the wave amplitude vector provides a more readily usable output for the purpose of computing the mean square velocity.

After the DGSM program is complete, post-processing is used to calculate

the radiated power from each strut using the calculated wave amplitude vector $\vec{W}$. Recalling equation (2-50) and (2-51):

$$\Pi_{RAD\,Harmonic} = \rho_a C_a S \sigma_{RAD} \frac{\omega^2}{2} \left(|w^+|^2 + |w^-|^2 \right) \tag{3.32}$$

and,

$$\Pi_{RAD\,Evanescent} = \rho_a C_a S \sigma_{RAD} \omega^2 \left(|w_e^+|^2 + |w_e^-|^2 \right) \left\{ \frac{1 - e^{-2k_{B_y} L}}{4 k_{B_y} L} \right\} \tag{3.33}$$

The resulting radiated power is normalized by the input power:

$$\Pi_{in} = \frac{1}{2} \Re \{ \mathrm{f} v^* \}, \tag{3.34}$$

where f is the input force and v is the velocity of the input node in the direction of the applied force.

C: Numerical Prediction of Radiated Sound Power for the Bare Truss

In the formulation of the DGSM analytics, no mention was made of internal losses in the structure, and the problem was formulated strictly by applying known wave propagation solutions. Now the structural loss will be added by making the wave number complex. Namely,

$$E = \rho C_L^2 (1 + i\eta_L), \tag{3.35}$$

where,

$$C_L = \sqrt{\frac{E}{\rho}} \quad \text{(complex)}, \tag{3.36}$$

and therefore,

$$k_{By} = \sqrt{\frac{\omega}{\kappa_y C_L}} \quad \text{(complex)}. \tag{3.37}$$

The normalized radiated sound power output from the DGSM prediction is plotted as figure 3-1 for a nominal structural damping value of $\eta_s = 1 \times 10^{-3}$.

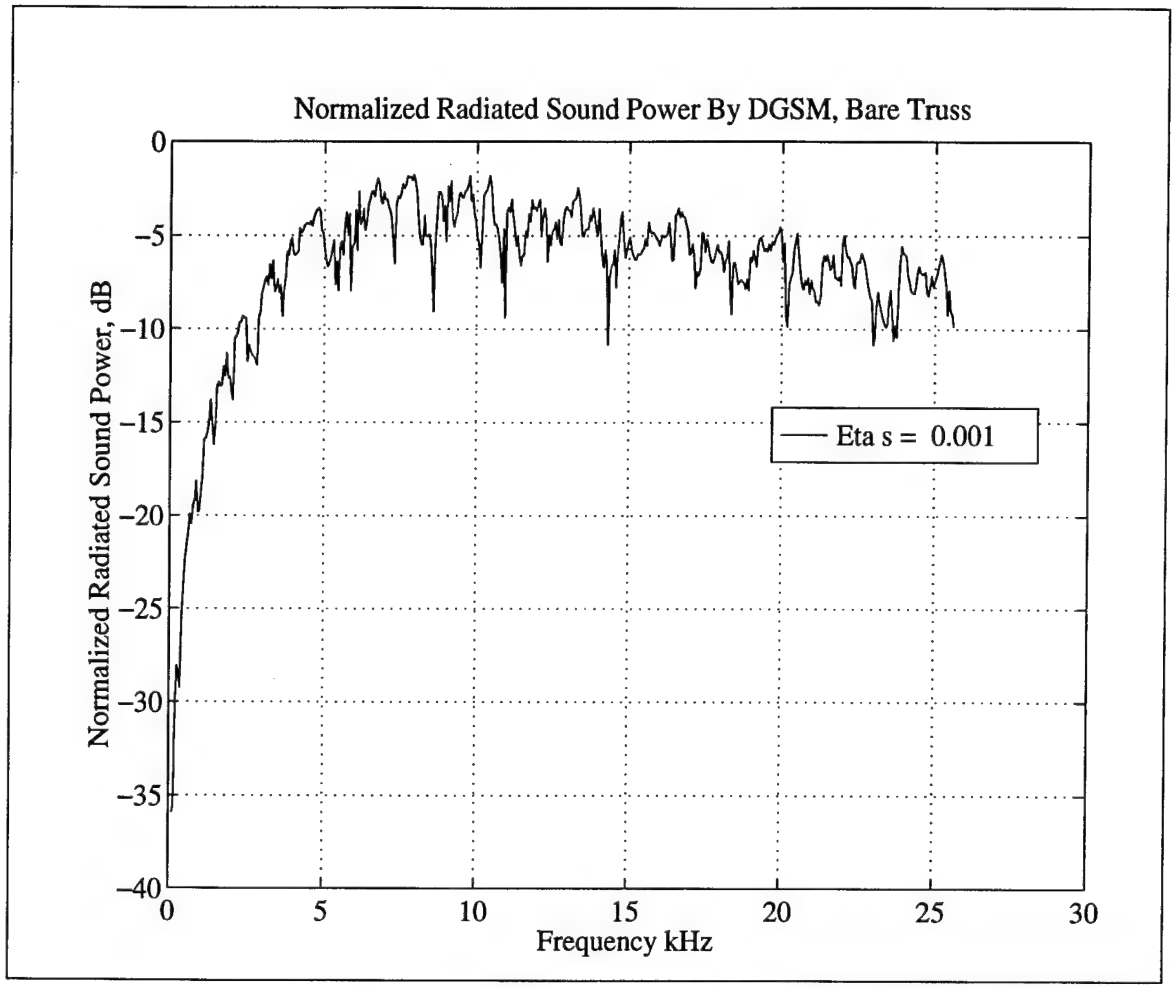

Figure 3-1: Prediction of radiated sound power from DGSM method for frequency range of 100 Hz - 25600 Hz. Structural damping, η_s, = 1 x 10^{-3} and 500 frequency points are included.

The value for the structural damping factor η_s was estimated to be 1 x 10^{-3} by Heath [1]. This is a factor of 10 higher than the estimates found in the literature. However, the truss was assembled using a two-part epoxy in the joints so it is not unreasonable that there could be a factor of 10 difference between the accepted values of η_s and the actual truss values. This parameter plays an important role in determining the amount of sound being radiated; the vibrational energy dissipated in the structure cannot contribute to the radiated

sound field. For this structure, it is expected that the loss due to radiation of sound will be much less than the loss due to strutural damping.

A parametric study was conducted to determine the effect of the structural loss factor on the sound radiated by the truss. Values for η_s were chosen as .01, .001 and .0001, to bracket the value proposed by Heath . The DGSM model was run for all three cases with 500 frequency points linearly spaced between 100 Hz and 25600 Hz. The upper limit of 25600 Hz was chosen based on the upper frequency limit of the data analysis equipment. The raw results are plotted as figure 3-2. These results were then averaged over $\frac{1}{3}$ octave bands, and are plotted as figure 3-3. All results are plotted on a decibel scale, specifically

$$\text{Normalized Radiated Sound Power}\{\text{db}\} = 10 \log_{10} \frac{\Pi_{rad}}{\Pi_{in}}. \qquad (3.38)$$

It is interesting to note that the curves appear to have the same basic shape. As the structural damping decreases, the amount of steady-state vibrational energy in the truss members increases. Increased vibrational levels lead directly to increased sound radiation. What is most interesting is that the curves shift up by an amount which is directly proportional to the change in the loss factor. However the fact that the radiated sound power exceeds the input power for η_s = .0001 points out a major failing of the DGSM prediction. Since the DGSM program computes steady state vibration levels in the struts and assumes that the structural losses are independent of the sound being radiated, the actual physics of the problem are not always accurately modeled. If the structural losses *were* as low as .0001, or lower, the increased radiated sound power would take vibrational energy away from the struts and cause the mean square velocity of the struts to be lower than predicted by DGSM. Radiation losses could no longer be considered as de-coupled from structural losses. The reduced mean square velocity would give a radiated power lower than that predicted by DGSM, and in fact a normalized power ratio of greater than unity would never be achieved. So the relationship between these curves follows the assumptions

used in formulating the DGSM prediction; however, since the structural loss factor plays such an important role in determining the radiated sound power levels, it is crucial that this parameter be accurately determined before entering the DGSM program. The structural loss factor should also be expected to have some dependence on frequency. Unfortunately, the literature provides few clues as to the frequency dependence of the loss factor. The tabulated values for aluminum are usually given as $1x10^{-4}$. Heath [1] finds that for the given truss the value is more on the order of $1x10^{-3}$, the difference being due to the joint losses in the truss. As a first order estimate, the structural loss factor used will be $\eta_s = 1x10^{-3}$. Later chapters will compare this prediction with the actual measured sound power and some refinements in the choice of η_s will be suggested.

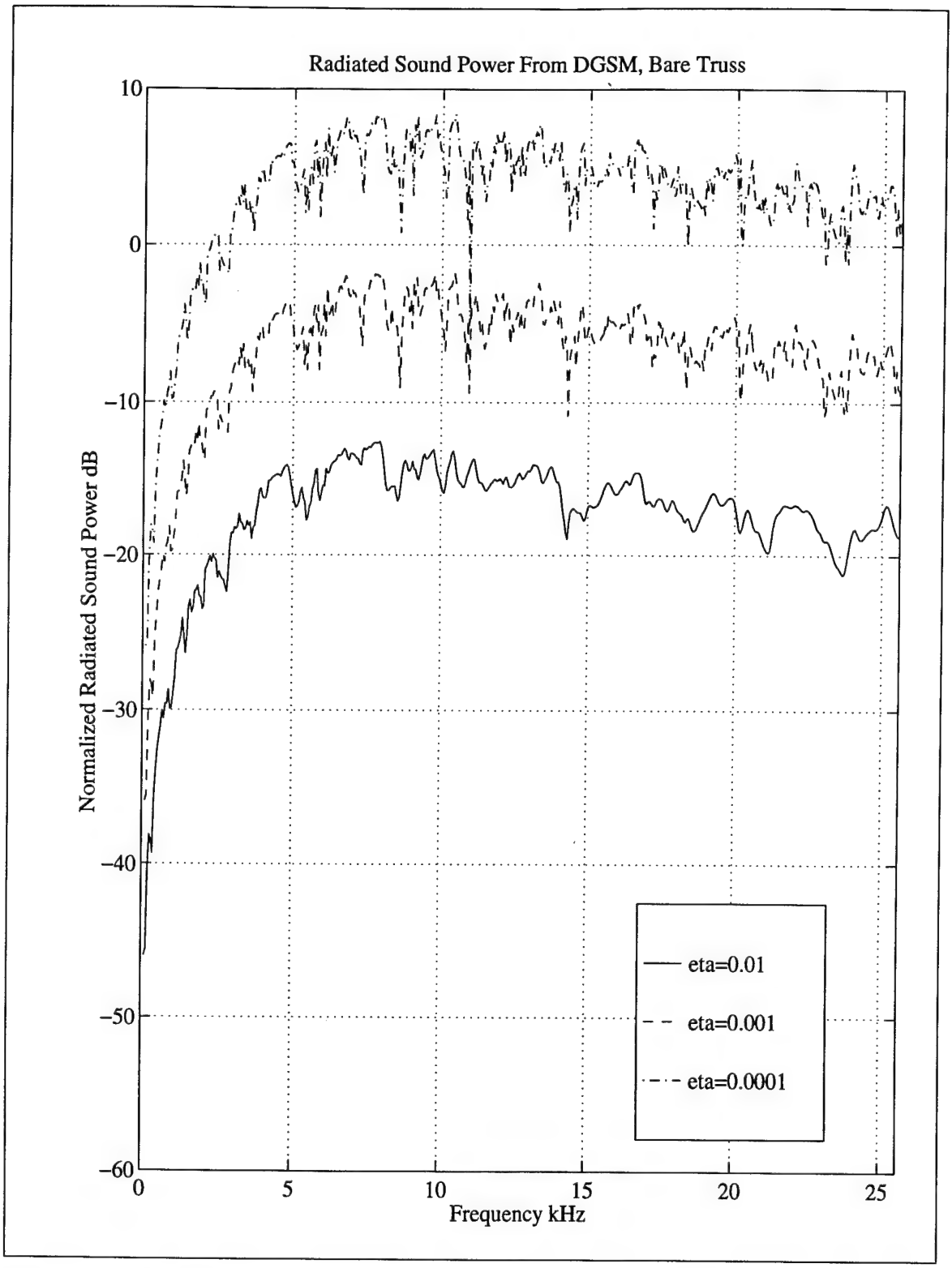

Figure 3-2: Prediction of radiated sound power from DGSM method for bare truss and structural damping, η_s = .0001, .001, and .01. Frequency range is 100-25600 Hz and 500 frequency points are selected.

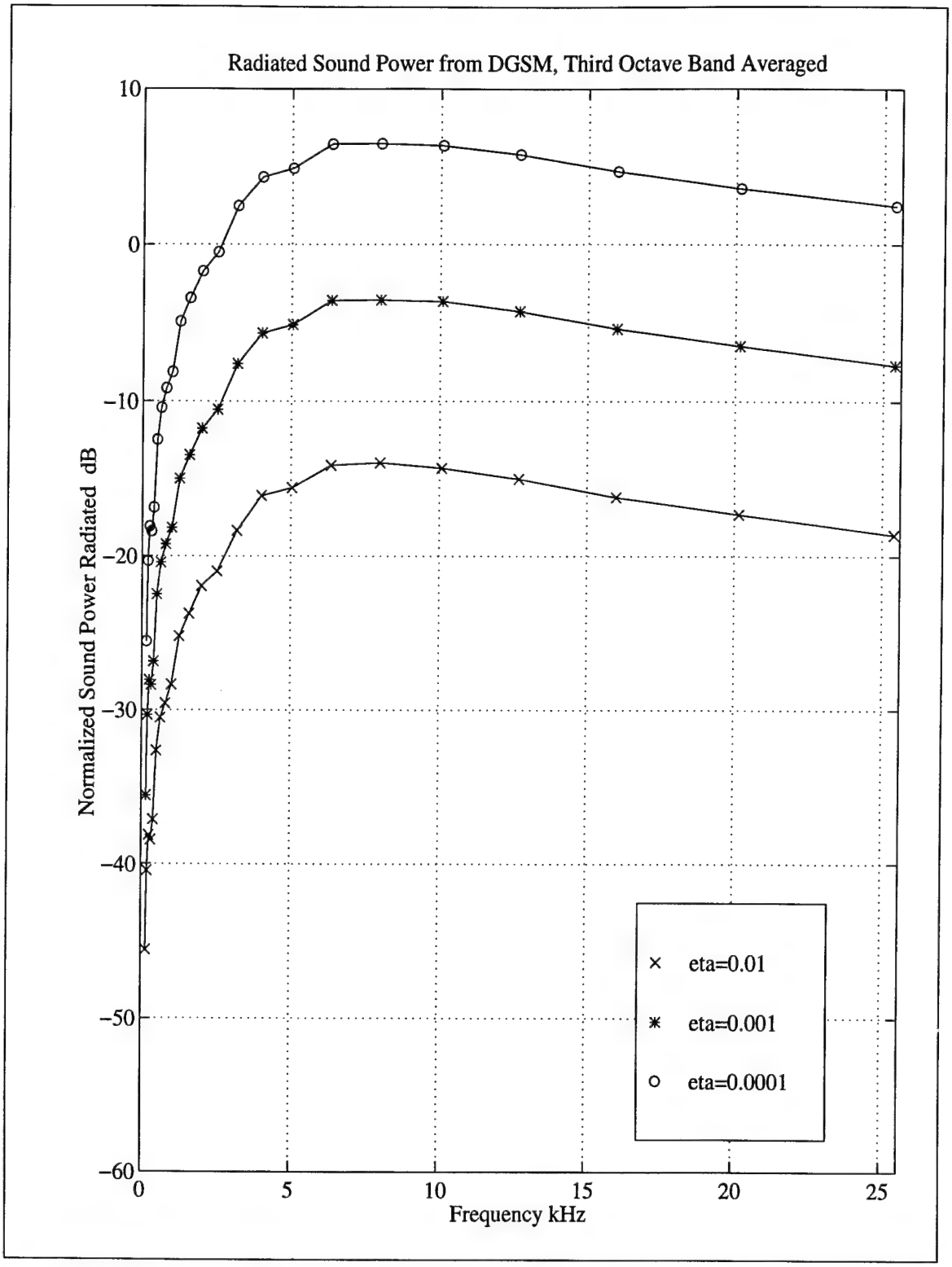

Figure 3-3: Prediction of radiated sound power from DGSM method for bare truss and structural damping, η_s = .0001, .001, and .01. Frequency range is 100-25600 Hz and 500 frequency points are selected. Results are averaged in $\frac{1}{3}$ octave bands.

D: Numerical Prediction of Radiated Sound Power for the Truss With Plates

The DGSM program with plate radiation added was run for the same values of η_s as the bare truss. However the frequencies chosen consisted of only 250 points between 100 Hz and 25600 Hz, since it was felt that this would provide sufficient frequency resolution and reduce computation time. The raw results are plotted as figure 3-4. These results were then averaged over $\frac{1}{3}$ octave bands, and are plotted as figure 3-5.

Again, an immediate problem is noticed. If figure 3-5 were true, the radiated power would be 1000 times the input power, which is clearly ludicrous. Again the DGSM prediction fails to model the physics. If the coupling between the struts and the plates were as strong as postulated in formulating the DGSM prediction, the majority of the vibrational energy in the truss would be transferred to the plates and then radiated most efficiently into the air, again lowering the mean square velocity of the struts. In actuality the vibrational energy of the truss is not significantly altered by the addition of plates, which will be shown in chapter 6. This suggests that the assumption of strong coupling is incorrect, which is discussed in chapter 5, part B.

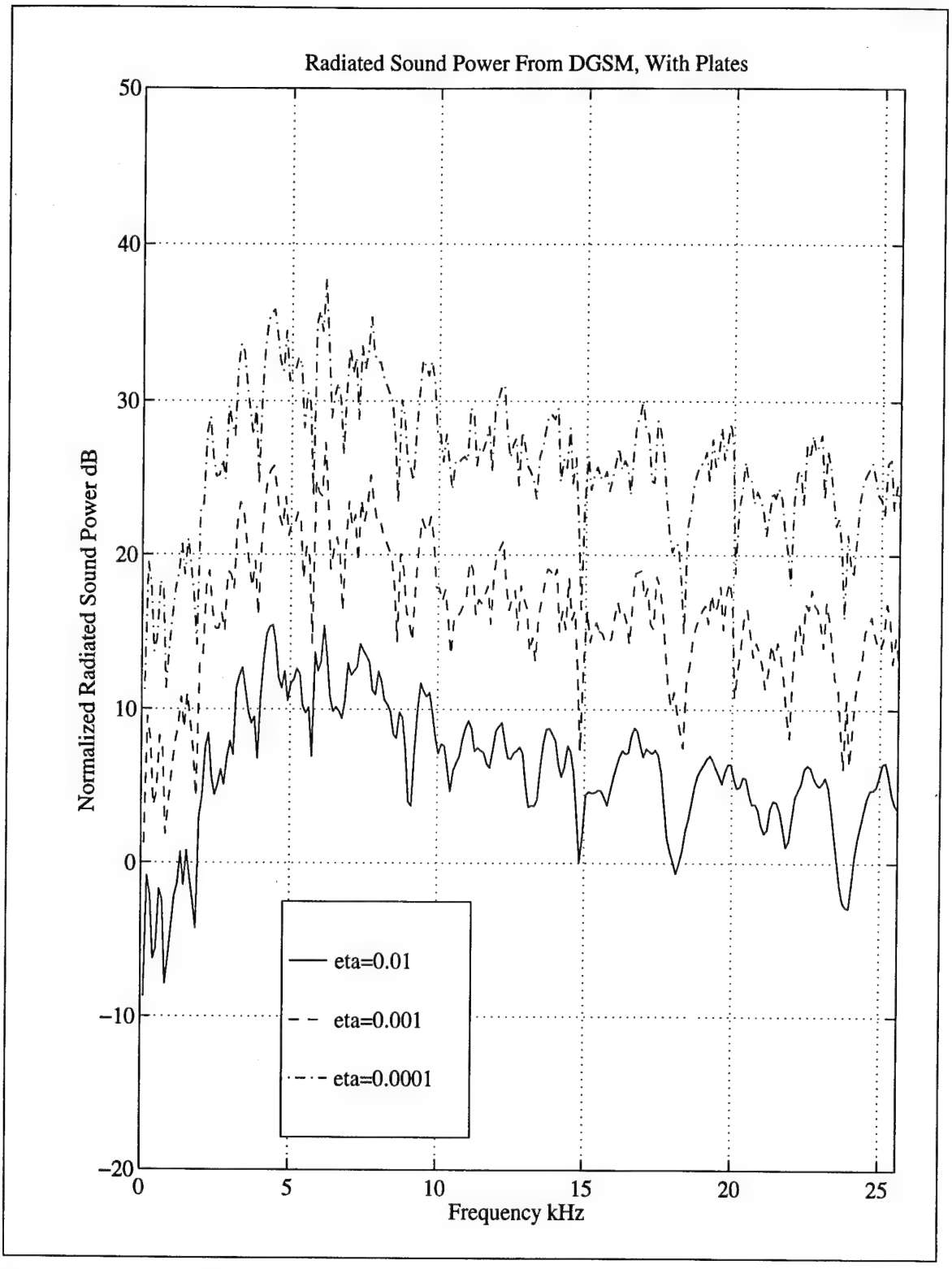

Figure 3-4: Prediction of radiated sound power from DGSM method for truss with plates and structural damping, η_s = .0001, .001, and .01. Frequency range is 100-25600 Hz and 250 frequency points are selected.

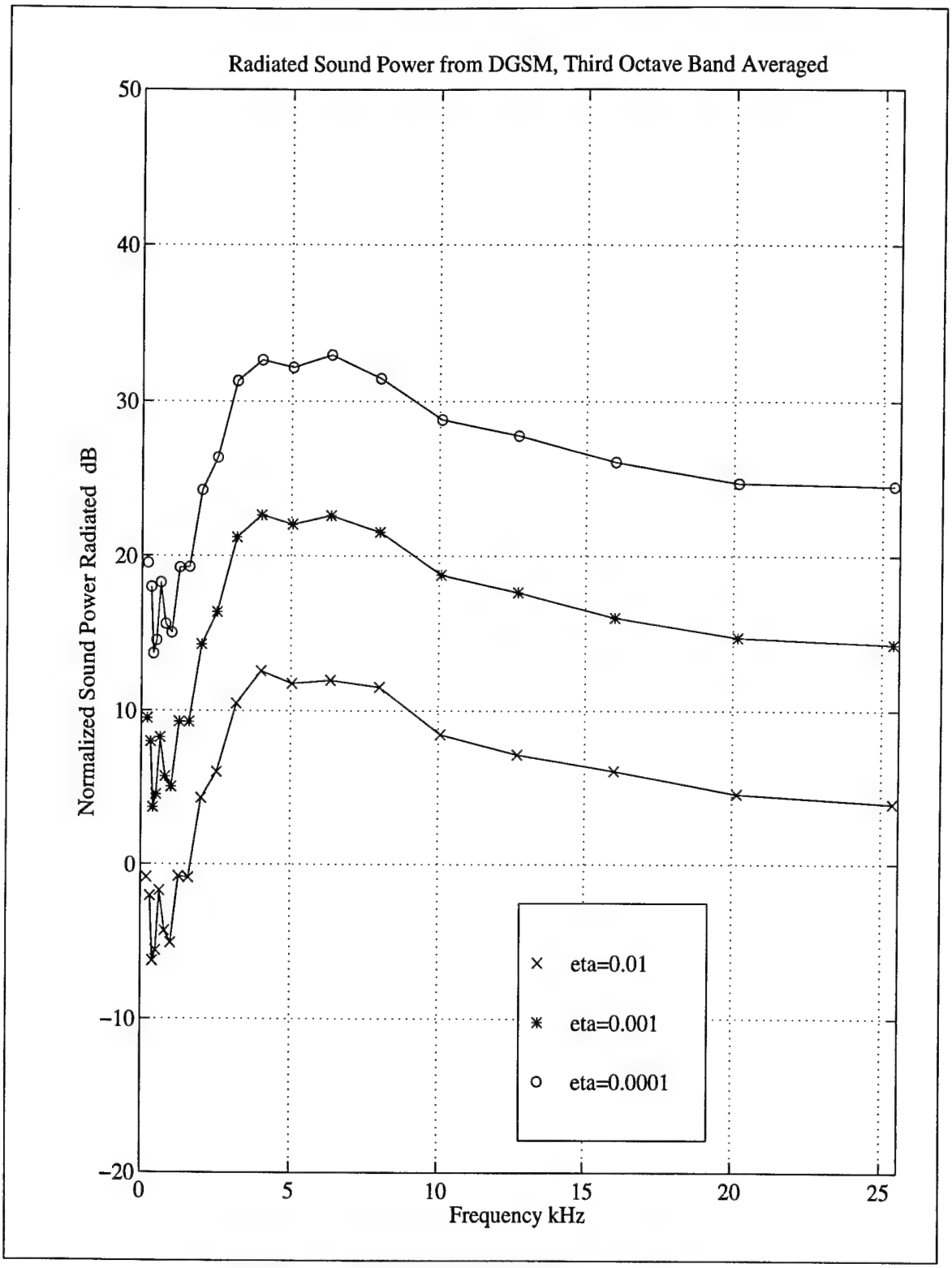

Figure 3-5: Prediction of radiated sound power by DGSM method for truss with plates and structural damping, η_s = .0001, .001, and .01. Frequency range is 100-25600 Hz and 250 frequency points are selected. Results are averaged in $\frac{1}{3}$ octave bands.

CHAPTER 4: Experimental Procedures

A: Description of Intensity Probe Experiments

The experimentation was conducted with a Brüel and Kjær intensity probe using $\frac{1}{2}$ inch microphones and an 8 mm spacer. It was necesary to use an intensity probe since the truss was located in a semi-reverberant room. The intensity probe allows measurement of radiated sound power in a reverberant environment since it detects sound power radiated per unit area from a specific direction. A diagram of the intensity probe is shown below as figure 4-1.

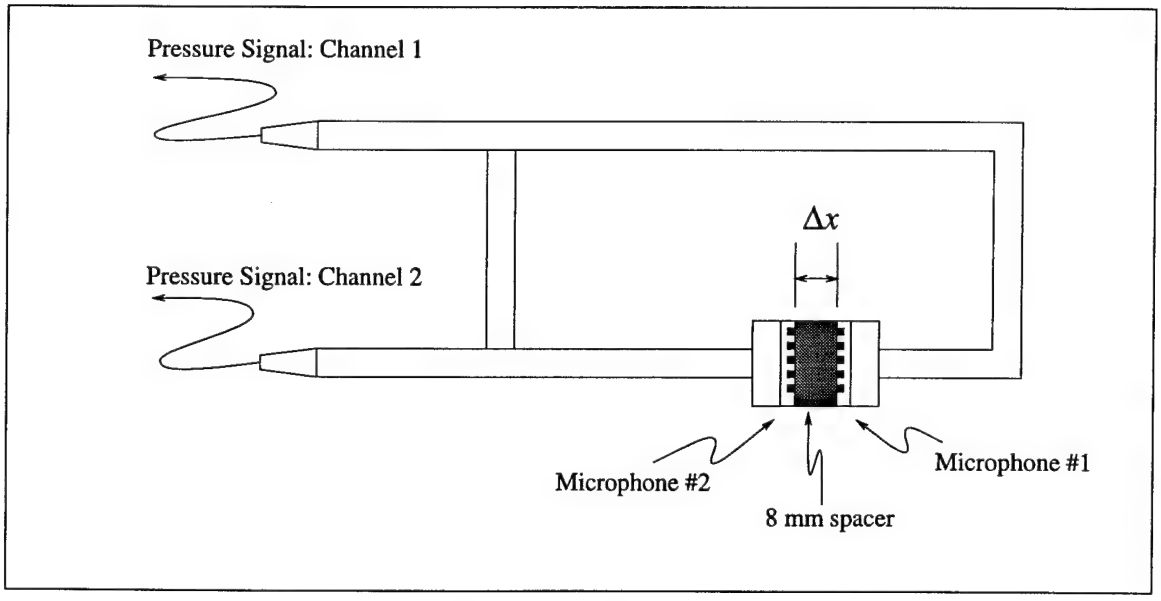

Figure 4-1: Diagram of Intensity Probe

The sound intensity is the time averaged product of the pressure and the particle velocity

$$\vec{I} = \frac{1}{T}\int_0^T \mathrm{p}(\vec{x},t)\vec{\mathrm{u}}(\vec{x},t)dt. \tag{4.1}$$

The pressure can be readily measured with only one microphone. However, two microphones are needed to measure the particle velocity. The linearized and inviscid Euler equation is used to relate the pressure gradient to the particle

velocity

$$\frac{\partial \vec{u}}{\partial t} = -\frac{1}{\rho}\vec{\nabla} p. \tag{4.2}$$

The vector notation can be neglected if only plane waves are being measured. The experiment is designed so that all measurements will be taken in a direction pointing radially inward towards the centerline of the truss; the only waves of importance are plane waves radiating in the outward radial direction. The experiment has also been designed so that all measurements are taken in the far-field, as described in equation (2.13). So in one dimension (chosen as the radial direction) the intensity equation becomes

$$I_r = \frac{1}{T}\int_0^T p(r,t)u_r(r,t)dt. \tag{4.3}$$

Likewise the one dimensional inviscid and linearized Euler equation becomes

$$\frac{\partial u_r}{\partial t} = -\frac{1}{\rho}\frac{\partial p}{\partial r}. \tag{4.4}$$

Integrating to find velocity leads to the expression

$$u_r(t) = -\int_0^t \frac{1}{\rho}\frac{\partial p}{\partial r}d\tau, \tag{4.5}$$

where the partial differentiation can be replaced by a finite difference

$$\frac{\partial p}{\partial r} = \frac{(p_2 - p_1)}{\rho_a \Delta r}, \tag{4.6}$$

and Δr is the distance between the microphones. Therefore the instantaneous velocity becomes

$$u_r(t) = -\int_0^t \frac{(p_2 - p_1)}{\rho_a \Delta r}d\tau. \tag{4.7}$$

This approximation will only be valid when the spacing of the two microphones

is small compared with the wavelength of the frequencies of interest

$$\Delta x \ll \frac{C_a}{f}. \tag{4.8}$$

For a nominal speed of sound in air of 340 $\frac{\text{meters}}{\text{second}}$ and a microphone spacing of 8 mm, the maximum usable frequency is on the order of 10000 Hz.

The instantaneous fluctuating acoustic pressure is

$$\mathrm{p} \approx \frac{(\mathrm{p}_1 + \mathrm{p}_2)}{2}. \tag{4.9}$$

Substituting the instantaneous values of pressure and velocity into equation (4-1) yields

$$\vec{I} = -\frac{1}{T}\int_0^T \left\{ \frac{(\mathrm{p}_1 + \mathrm{p}_2)}{2} \int_0^t \frac{(\mathrm{p}_2 - \mathrm{p}_1)}{\rho_a \Delta r} d\tau \right\} dt. \tag{4.10}$$

In practical use the pressure signal from the microphone is put through a Fast Fourier Transform (FFT) analyser to obtain the spectrum of the signal. The Fourier transform of the pressure and velocity become (respectively)

$$\mathrm{P}(f) = \frac{\{\mathrm{P}_1(f) + \mathrm{P}_2(f)\}}{2} \tag{4.11}$$

and

$$\mathrm{U_r}(f) = -\frac{1}{i\omega\rho_a\Delta r}\{\mathrm{P}_2(f) - \mathrm{P}_1(f)\}. \tag{4.12}$$

By substitution the intensity can be expressed in terms of the imaginary part of the cross spectra between microphones 1 and 2 [16]

$$I_r = -\frac{1}{2\pi f \rho_a \Delta r}\Im\left[\mathrm{P_{12}}(f)\right], \tag{4.13}$$

where $\mathrm{P_{12}}(f)$ is the cross-spectra between channels 1 and 2 of the intensity probe.

B: Calibration of Microphones and Background Noise Determination

The microphones which were installed in the intensity probe were Brüel and Kjær $\frac{1}{2}$ inch microphones which had been phase matched specifically for use in an intensity probe. These microphones had been purchased two months prior to the conduct of the experiments and were accompanied by factory calibration certificates. However, to ensure the correct calibration, prior to conducting the experimental run, the two microphones were individually calibrated using a Brüel and Kjær type 4228 pistonphone. The pistonphone output was nominally +124.10 dB re 20μPa at 250 Hz, and corrections were supplied with the pistonphone for actual pressure and amplification by the power supply. With the total corrections the expected output level measured by the microphone was +123.70 dB re 20μPa, at 250 Hz. After each microphone was tested the data acquisition computer calculated a correction factor relating the voltage supplied by the microphone to the sound pressure. This factor was automatically used by the data acquisition equipment and the output of all subsequent sound pressure measurements was given in mean square pressure in Pa^2. All experiments utilized a frequency range of 0-25600 Hz with 3201 frequency lines, for a frequency resolution of 8 Hz. The data acquisition equipment selected a sampling frequency so as to avoid aliasing effects. Figure 4-2 shows the calibration results for microphone #1 (channel #3 of the data acquisition equipment corresponded to microphone #1) and figure 4-3 shows the calibration results for microphone #2 (channel #2 of the data acquisition equipment corresponded to microphone #2).

Also, prior to making the sound measurements a background noise level was measured at the midpoint of the truss in the $-y$ direction. With the vibration source secured, the sound pressure level was measured for both channels of the intensity probe. The sound pressure level was also measured with the vibration source activated. The Sound Pressure Level (SPL) is calculated from the output

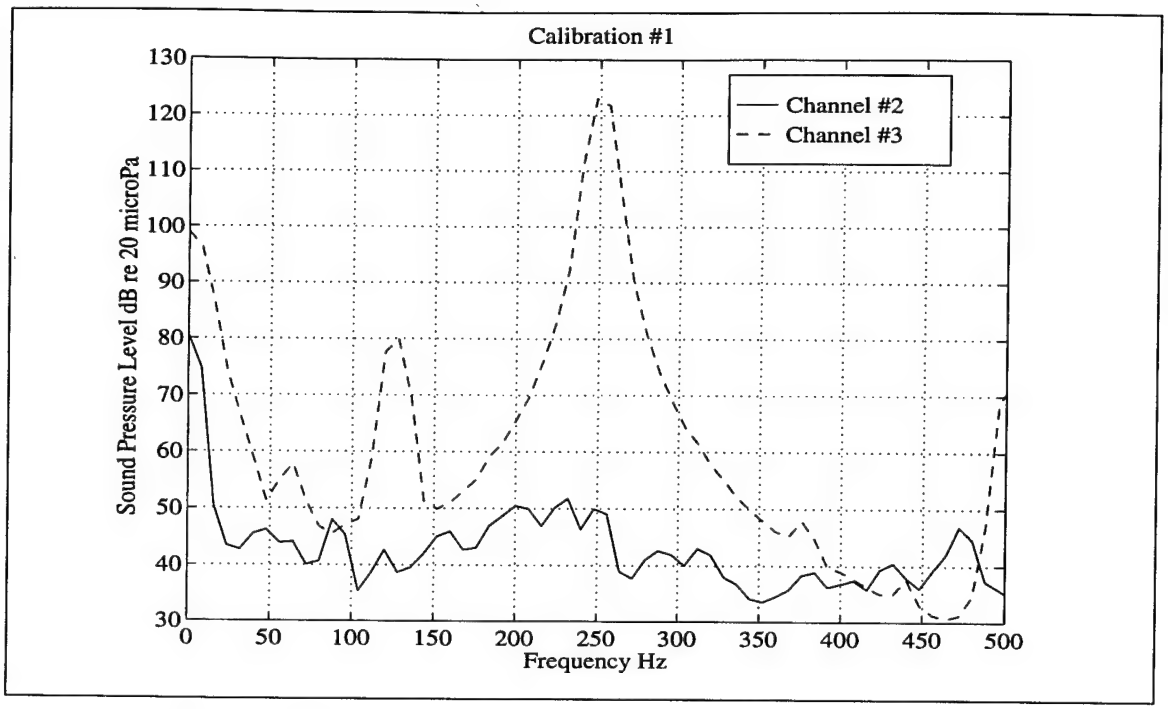

Figure 4-2: Calibration of microphone channel #1, which corresponds to data acquisition channel # 3.

mean square pressure using

$$\mathrm{SPL} = 10 \log_{10} \left\{ \frac{\langle P^2 \rangle}{(20 \mu Pa)^2} \right\}. \tag{4.14}$$

Figure 4-4 shows the SPL from the background noise and compares it to channels # 2 and #3 of the data acquisition system, which corresponds to channels # 2 and # 1 of the intensity probe. At very low frequencies there is poor quality of signal to noise ratio (SNR). The data acquisition equipment was located near the truss and its internal cooling fan probably caused this low frequency noise. In any event, data below 1000 Hz should not be given too much weight.

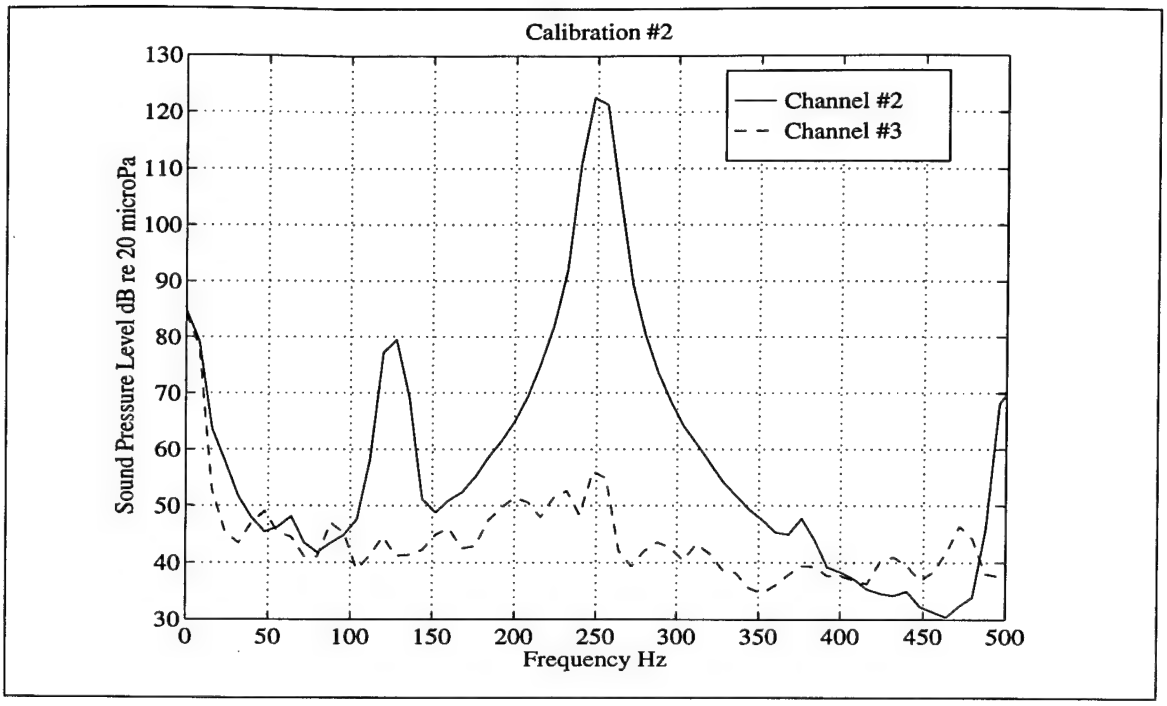

Figure 4-3: Calibration of microphone channel #2 which corresponds to data acquisition channel # 2.

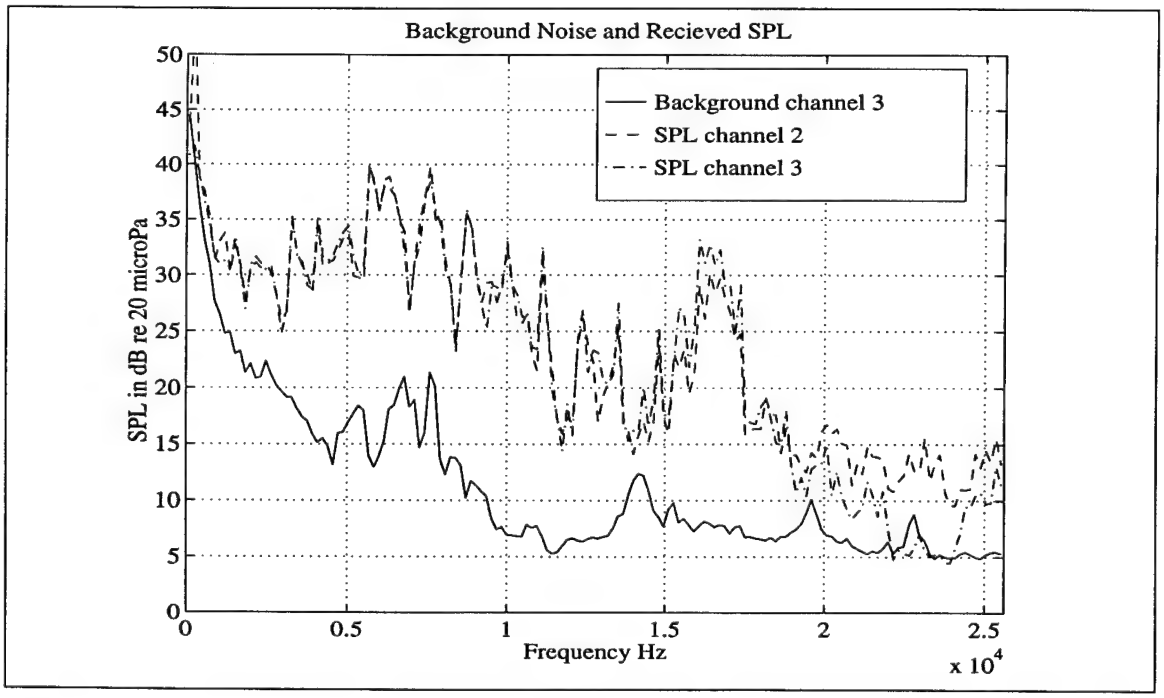

Figure 4-4: Background noise level as compared to sound pressure level from intensity probe microphones. Channel # 2 refers to microphone # 2, Channel #3 refers to microphone channel # 1.

C: Measurement of Sound Intensity

For the intensity experiments a cylindrical surface was used as the measurement surface. The volume extended out 1 meter from the centerline of the truss and measurements were taken at $\frac{1}{2}$ meter increments, in the x direction, at y values of - 1 meter and + 1 meter. There were therefore 11 data runs on each side of the truss and one at each end of the truss. The experimental configuration for one side of the truss is shown as figure 4-5. For all data runs, the microphone pointed towards the center of the truss. For runs 0 -10 the microphone was pointed in the $-y$ direction, for runs 11 through 20, the $+y$ direction, for run 22 the $+x$ direction and for run 23 the $-x$ direction. When the plates were added, intensity probe measurements were also taken at 1 meter from the truss directly above and below the centerline of the truss ($y = 0$), at $\frac{1}{2}$ meter increments in x. Extra readings were taken with the plates to ensure that the directional variation of the sound power radiated was adequately sampled.

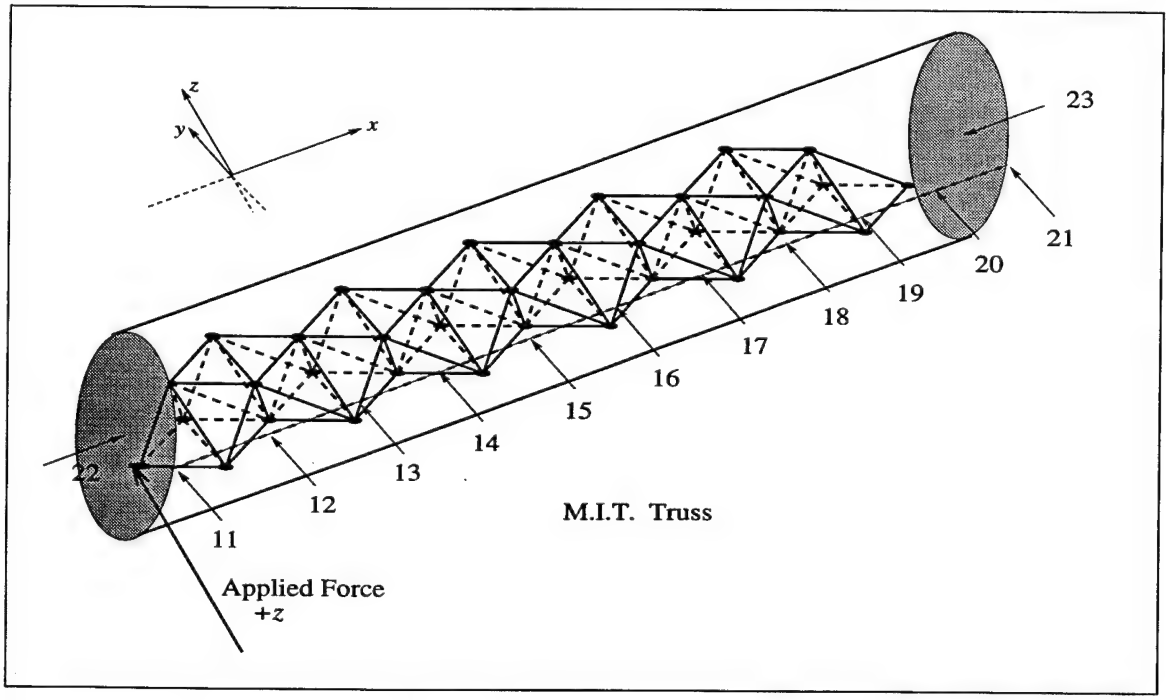

Figure 4-5: Measurement of sound intensity on one side of the truss; numbers indicate data run number. The opposite side was also measured with data runs 0 through 10; run number 10 was at the end where the force was applied.

D: Measured Sound Power

The experiments consisted of exciting the truss at joint B1 using a 1 Newton, Brüel and Kjær type 4810 shaker which was excited by broadband white noise in the frequency range of 0 - 25 kHz. The shaker had an internal impedance head mounted between the shaker and the truss which was also manufactured by Brüel and Kjær. The truss was excited in two configurations, in the as-built condition and with $\frac{1}{2}$ meter square aluminum plates of thickness .002 meters attached in the center of each pyramidal assembly. Figure 4-6 shows the configuration for the bare truss and figure 4-7 shows the configuration for the truss with plates.

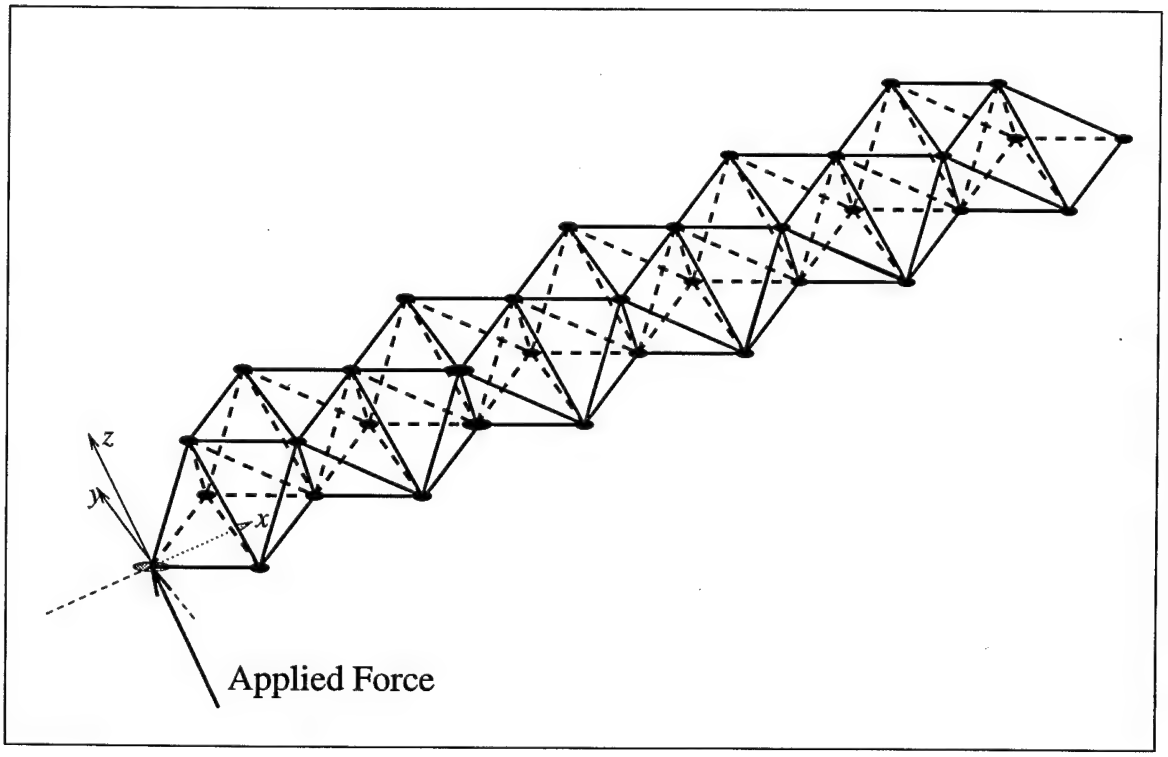

Figure 4-6: Configuration of radiated sound power experiment for bare truss experiment. Force was applied at joint B1, as shown.

The data acquisition system had 48 channels available for these experiemnts. Only 4 were needed and they were assigned as listed in table 4-1 below. The output consisted of a [9x3201] matrix which contained the auto-spectra and cross-spectra of the measured signals versus frequqncy. These matrices

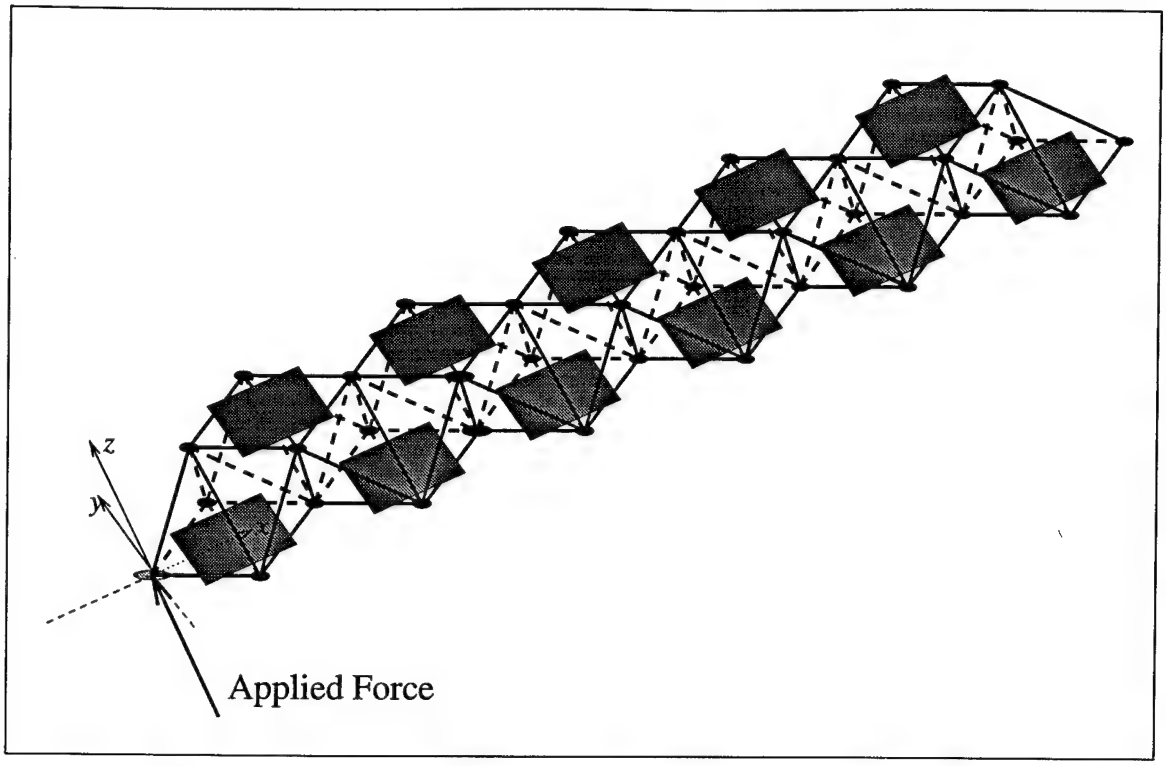

Figure 4-7: Configuration of radiated sound power experiment for experiment with plates. Force was applied at joint B1, as shown.

were saved to a file and then read into Matlab©, for processing. The column assignment for the output is listed in table 4-2 below.

After the data was taken, the sound intensity was obtained using column 8 of the output and equation (4.13). The results for all 23 measurements (45 with plates) were multiplied by their effective area and the resulting sound power radiated with and without plates is presented as figure 4-9 and figure 4-8, respectively. The graphs shown are of normalized radiated power. They are normalized by the power which is input to the truss as measured by the mounted impedance head and calculated by

$$\text{Input Power} = \frac{1}{2}\Re\{\mathbf{F}\mathbf{V}^*\} = \frac{1}{2}\Re\{\mathbf{S_{fa}}\}. \tag{4.15}$$

The result is plotted in a deciBel scale

$$\text{Normalized Power} = 10 \log_{10} \left\{ \frac{\Pi_{RAD}}{\Pi_{in}} \right\}. \tag{4.16}$$

Finally, the results for the bare truss and the truss with plates were also averaged in standard one third octave bands and are shown together in figure 4-10. The shape of the curves is essentially the same. The big difference is that the radiated noise with plates is approximately 4 dB higher than the bare truss.

Channel 1:	Input force transducer
Channel 2:	Pressure channel # 2
Channel 3:	Pressure channel # 1
Channel 4:	Input acceleration transducer

Table 4-1: Data acquisition channel assignment

Column 1:	Auto-spectra of input force $\mathbf{S}_{ff}$
Column 2:	Auto-spectra of pressure channel 2 $\mathbf{S}_{22}$
Column 3:	Auto-spectra of pressure channel 1 $\mathbf{S}_{11}$
Column 4:	Auto-spectra of input accleration $\mathbf{S}_{aa}$
Column 5:	Cross-spectra $\mathbf{S}_{f2}$
Column 6:	Cross-spectra $\mathbf{S}_{f1}$
Column 7:	Cross-spectra $\mathbf{S}_{fa}$
Column 8:	Cross-spectra $\mathbf{S}_{21}$
Column 9:	Cross-spectra $\mathbf{S}_{2a}$

Table 4-2: Output data location in output matrix

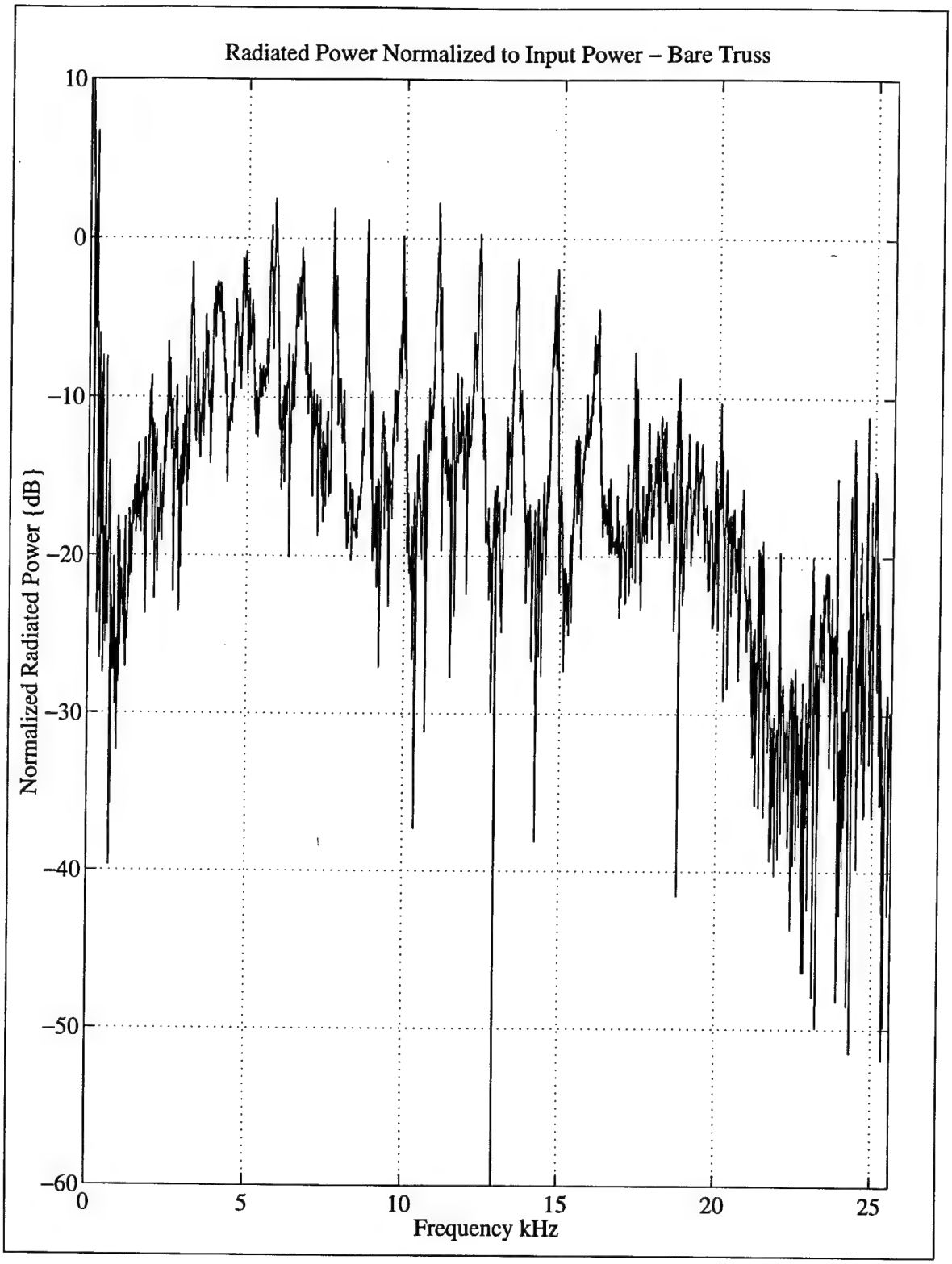

Figure 4-8: Radiated sound power for bare truss

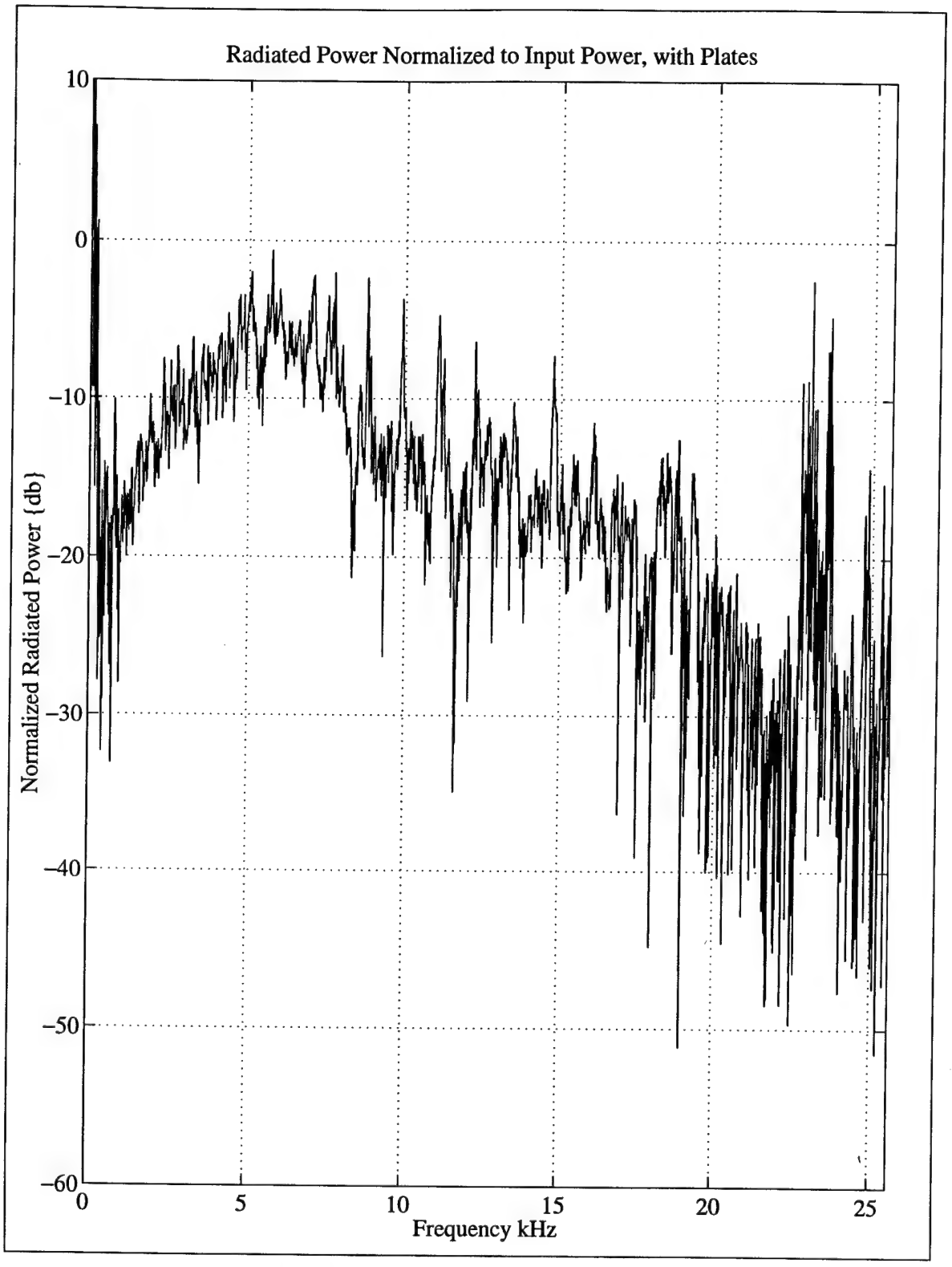

Figure 4-9: Radiated sound power with plates

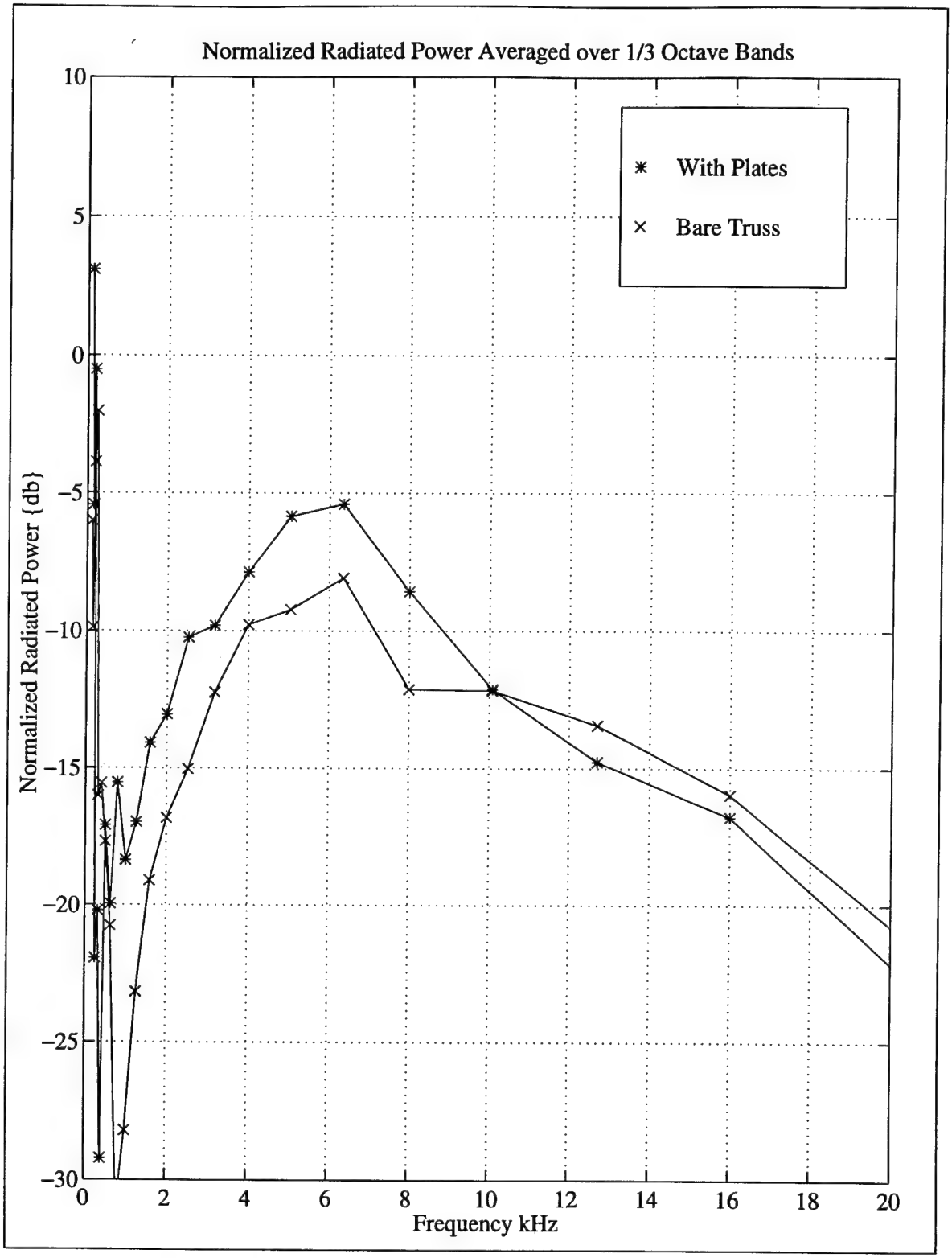

Figure 4-10: Comparison between radiated sound power with and without plates, averaged over $\frac{1}{3}$ octave bands.

CHAPTER 5: Comparison of Results With Initial Prediction

A: Comparison Between Predicted and Measured Results for the Bare Truss

The measured sound power for the bare truss case, with the results averaged in one third octave bands, is plotted with the predicted sound power from the DGSM program using a constant loss factor of η_s of $1x10^{-4}$, $1x10^{-3}$, and $1x10^{-2}$ as figure 5-1.

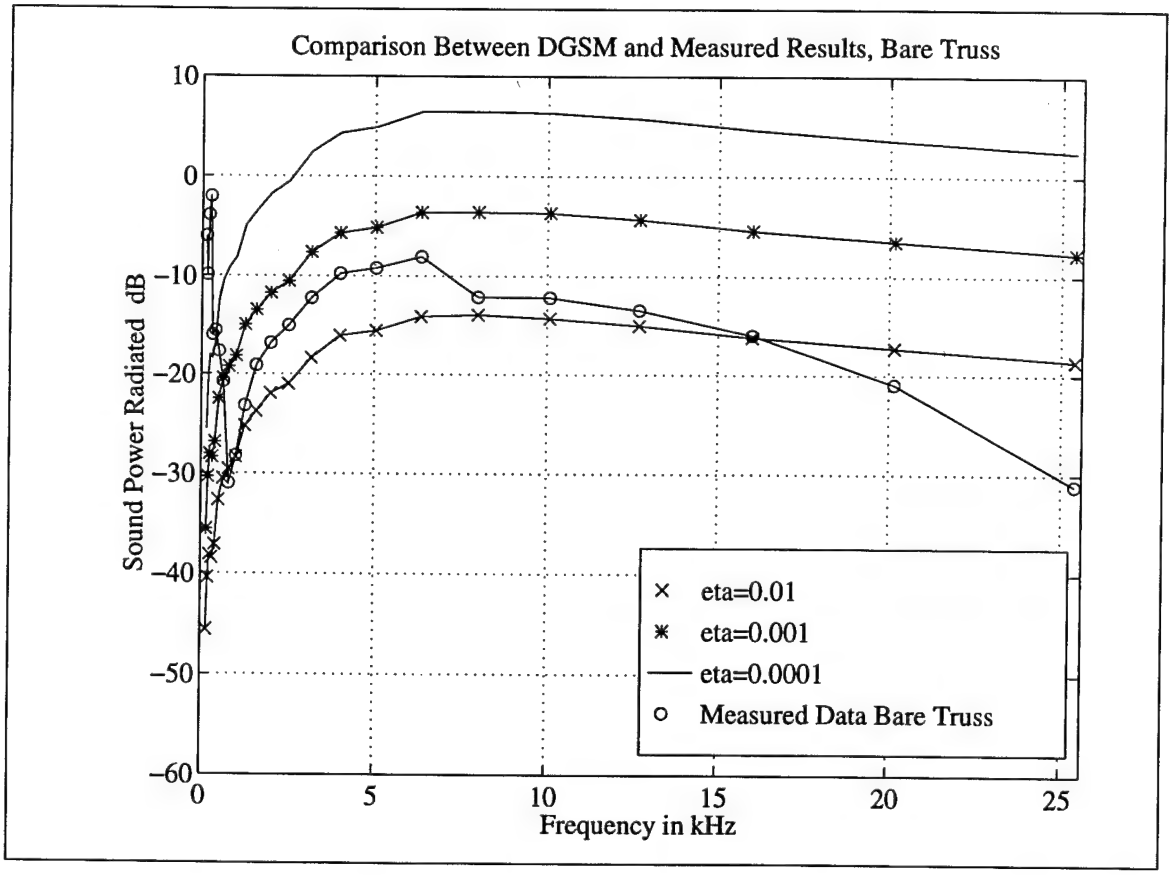

Figure 5-1: Comparison between measured radiated sound power and predicted radiated sound power using the DGSM program for the bare truss case. Structural loss factor, η_s = $1x10^{-2}$, $1x10^{-3}$, and $1x10^{-4}$.

The values of the structural loss factor η_s chosen as inputs for the DGSM program in the bare truss case have predicted a radiated sound power that falls on either side of the measured radiated sound power. The intial postulation that η_s is higher than that predicted by Heath ($1x10^{-3}$), appears to be correct. Also, since the apparent value of η_s is so much higher than the intrinsic value for aluminum ($1x10^{-4}$), it is obvious that the joints exhibit considerable loss. There are some inconsistancies which can be seen, however. At very low frequencies, the measured values have a very high peak. As discussed in the previous chapter, this can be attributed to the high levels of background noise which were present in the low frequency bands. The measured data contains a prominent peak at approximately 6 kHz, which the DGSM prediction doesn't support. Also, the slope of the curve after the peak is much steeper for the actual data. The possibility raised earlier of there being a frequency dependence to the structural loss factor appears to have been borne out.

When this data was obtained, these differences were a source of concern. The data collection methodology and data analysis was checked and verified to be correct. In addition, the data obtained using the intensity probe was compared to data which had previously been obtained using a single microphone and the assumption that the room was non-reverberant. The previous results agreed with the intensity probe experiments in that the shape of the response was correct. The single microphone response was 5 dB higher in the magnitude. This difference was attributed to the fact that the single microphone was including some reverberent field contributions which the intensity probe was able to filter out. So the measured data was determined to be correct. The difference had to be attributed to the DGSM prediction technique.

The analytical development of the DGSM technique and the formulae for the radiated sound power are fairly straightforward and therefore not suspect. However, as was mentioned before, one of the most uncertain inputs to the DSGM program was the structural loss factor. As a first order estimate it was assumed to be constant but that estimate now appears to be too simplistic. A

refinement of the DGSM structural loss factor is required and discussion of that refinement is contained in the next chapter.

B: Comparison Between Predicted and Measured Results for the Truss with Plates

The measured sound power for the truss with plates, with the results averaged in one third octave bands, is plotted with the predicted sound power from the DGSM program using a constant loss factor of η_s of $1x10^{-4}$, $1x10^{-3}$, and $1x10^{-2}$ as figure 5-2.

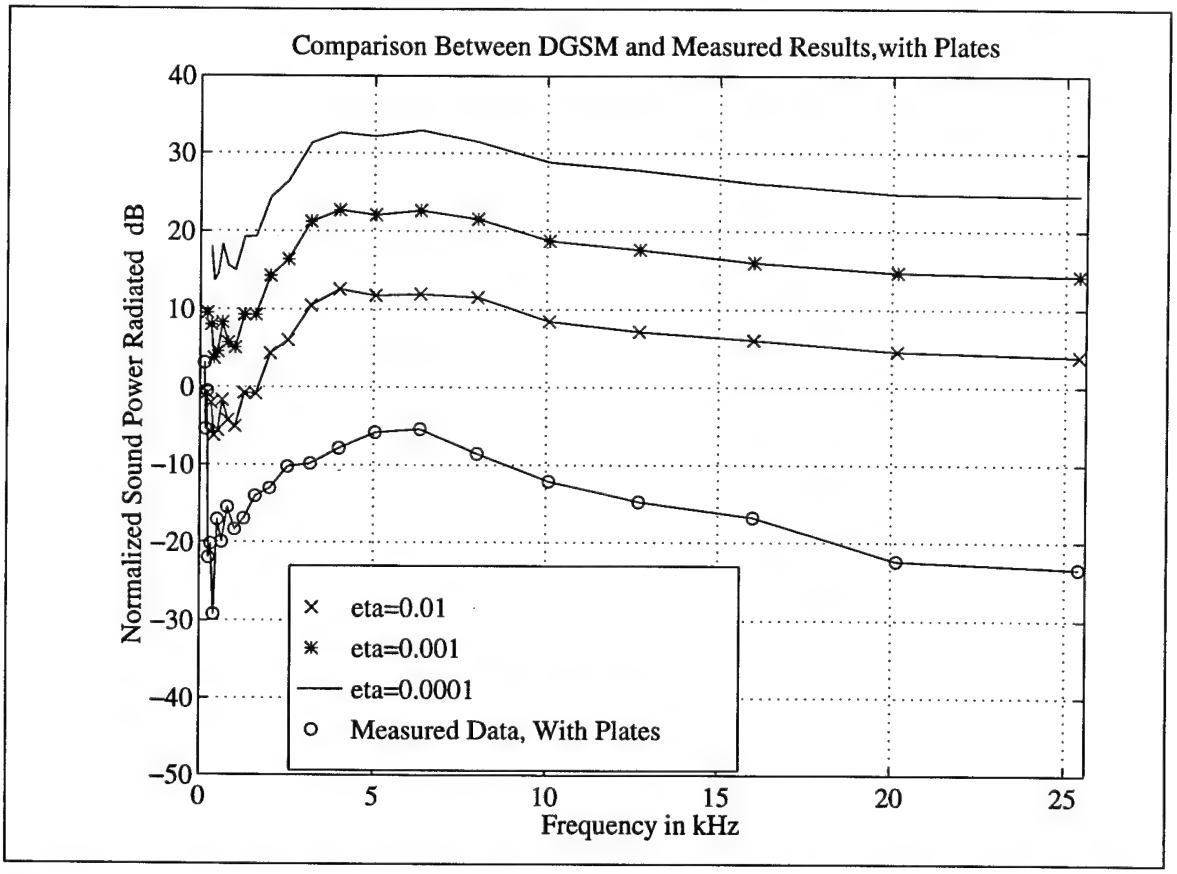

Figure 5-2: Comparison between measured radiated sound power and predicted sound power using the DGSM program for the truss with plates. Structural loss factor, η_s = $1x10^{-4}$, $1x10^{-3}$, and $1x10^{-2}$.

Clearly the DGSM prediction grossly overestimates the amount of sound

power radiated by the plates. The data in figure (4-10) shows approximately 4 dB difference between the case where the truss was bare and the case where the plates were attached. This agrees with experimental observation. The ambient noise levels in the laboratory were not significantly higher during the runs with the plates attached.

As discussed earlier, the assumption of strong coupling between the struts and the truss in the DGSM prediction is the source of the error; there is not strong coupling. Experiments conducted in chapter 6, part f will show that the vibrational energy of the truss with plates was not significantly higher than without plates. So the DGSM prediction, in this case, should correctly calculate the mean square velocity of the struts. Therefore, the fault must lie in the method of computing the mean square velocity of the plates from the mean square velocity of the struts. Clearly equation (2.53) must be revisited. Consider a simple two element Statistical Energy Analysis (SEA) model as shown below in figure 5-3.

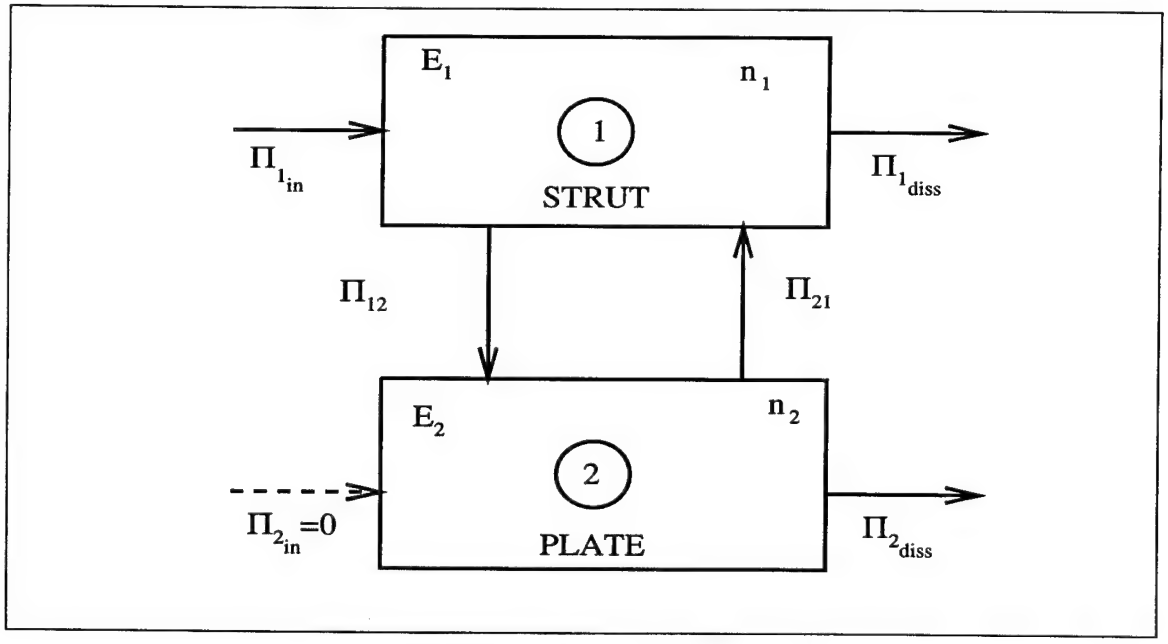

Figure 5-3: Two element SEA model

The terms in the diagram are defined as [17]

$$\Pi_{in} = \text{Input Power}, \tag{5.1}$$

$$E = \text{Energy}, \tag{5.2}$$

$$n = \text{Modal Density}, \tag{5.3}$$

$$\Pi_{1diss} = \text{Dissipated Power of Element 1} = \omega E_1 \eta_1, \tag{5.4}$$

and

$$\Pi_{12} = \text{Power transmitted from element 1 to element 2} = \omega E_1 \eta_{12}, \tag{5.5}$$

where the subscripts refer to element 1 or 2, loss factors of the form η_1 refer to the internal loss factor of element 1, and the loss factors of the form η_{12} are known as coupling loss factors. Energy balance equations can be written as

$$\Pi_{1in} = \omega E_1 \eta_1 + \omega E_1 \eta_{12} - \omega E_2 \eta_{21} \tag{5.6}$$

and

$$0 = \omega E_2 \eta_2 + \omega E_2 \eta_{21} - \omega E_1 \eta_{12}. \tag{5.7}$$

The energy of element 2 can be calculated from the energy of element 1 using equation (5.7)

$$\frac{E_2}{E_1} = \frac{E_P}{E_B} = \frac{M_P \overline{\langle v_P^2 \rangle}}{M_B \overline{\langle v_B^2 \rangle}} = \frac{\eta_{12}}{\eta_2 + \eta_{21}}. \tag{5.8}$$

Using a known SEA relation [17]

$$n_1 \eta_{12} = n_2 \eta_{21}, \tag{5.9}$$

equation (5.8) can be transformed to

$$\frac{M_P\overline{\langle v_P^2\rangle}}{M_B\overline{\langle v_B^2\rangle}} = \frac{1}{\frac{\eta_2}{\eta_{12}} + \frac{n_1}{n_2}}, \tag{5.10}$$

or,

$$\overline{\langle v_P^2\rangle} = \overline{\langle v_B^2\rangle}\frac{M_B}{M_P}\frac{1}{\frac{\eta_P}{\eta_{BP}} + \frac{n_B}{n_P}}. \tag{5.11}$$

The ratio of modal densities can be calculated from equations (2.54) and (2.55) as

$$\frac{n_B(\omega)}{n_P(\omega)} = \frac{(5.692)L}{\sqrt{\omega}}. \tag{5.12}$$

For frequencies on the order of 10000 Hz, and strut lengths on the order of 1 meter, this term is on the order of .01.

Before, it was assumed the coupling was strong (i.e. very large coupling loss factor), or that $\eta_P \ll \eta_{BP}$. Equation (5.11) reduces to equation (2.53) when $\frac{\eta_P}{\eta_{BP}} \ll .01$

$$\overline{\langle v_P^2\rangle} = \overline{\langle v_B^2\rangle}\frac{M_B}{M_P}\frac{n_P}{n_B} \approx \overline{\langle v_B^2\rangle}\frac{M_B}{M_P}(100). \tag{5.13}$$

If the coupling is weak, or if $\eta_{BP} \approx \eta_P$ then equation (5.11) will reduce to

$$\overline{\langle v_P^2\rangle} = \overline{\langle v_B^2\rangle}\frac{M_B}{M_P}\frac{\eta_{BP}}{\eta_P} \approx \overline{\langle v_B^2\rangle}\frac{M_B}{M_P}. \tag{5.14}$$

So if the coupling is weak, where DGSM assumes it is strong, then the mean square velocity of the plate will be predicted as 20 dB higher than it should be. It will be shown in chapter 6 that there is evidence of weak coupling. The difference between the DGSM prediction and the measured sound power is due to the coupling being weaker than assumed by DGSM.

CHAPTER 6: Refinement of DGSM Prediction for the Bare Truss

A: Measurement of Total Loss Factor

In the last chapter, the differences between the predicted and measured sound power was discussed. The assumption of the loss factor being a constant value is too simplistic. There are methods to measure the total loss factor experimentally, and these methods will be exploited on the truss structure. The truss is vibrated at a given point and the input force and acceleration are measured using an impedance head mounted on the shaker. The analysis equipment takes this signal and computes the cross-spectra between the force and acceleration. The power being input to the truss is then computed with

$$\Pi_{in} = \frac{1}{2}\Re\{\mathbf{F}\mathbf{V}^*\}. \tag{6.1}$$

The spatially averaged energy of vibration of the truss is also determined by placing accelerometers at many points on the truss. The signal from the accelerometers is also processed as a Fast Fourier Transform and the resulting output is the auto-spectra of the mean square velocity. These autospectra are averaged and multiplied by the total mass of the truss to obtain the energy of the truss

$$E = M\langle\overline{v^2}\rangle = \frac{1}{2N}M\sum_1^N \mathbf{V}\mathbf{V}^* = \frac{1}{2N\omega^2}M\sum_1^N \mathbf{A}\mathbf{A}^*, \tag{6.2}$$

where **A** and **V** are the Fourier tranforms of the acceleration and velocity, N is the total number of measurement points, a factor of ω^2 is inserted to convert from acceleration to velocity, and the factor M is the total mass of the truss, which is 16 kg.

Using the above measured input power and the total vibrational energy of the truss, the total loss factor η_{TOT} is calculated from

$$\eta_{TOT} = \frac{\Pi_{in}}{\omega E}. \tag{6.3}$$

Note that the total loss factor is specified because this measurement cannot distinguish between the structural loss factor and the radiation loss factor. The generally accepted formula for the total loss factor from a Statistical Energy Analysis (SEA) viewpoint is the following [4]

$$\eta_{TOT}(f) = \eta_s(f) + \eta_{RAD}(f) + \eta_{joints}(f) + \underbrace{\frac{\frac{n_2(f)}{n_1(f)}\eta_2(f)\eta_{21}(f)}{\eta_2(f) + \eta_{21}(f)}}_{\text{Coupling}}, \tag{6.4}$$

where n_1, and n_2 are the modal densities of the strut and the room respectively, η_2 is the loss factor of the room, and η_{21} is the coupling loss factor between the strut and the room. The connections between the joints are rigid and it is reasonable to assume that the joints losses can be included in the structural loss factor. The coupling losses can be neglected since they only become significant if there is significant coupling from the room to the struts, and since the struts of the truss are not thin-walled, it is not expected that the room modes will couple well with them [4]. The equation reduces to:

$$\eta_{TOT}(f) = \eta_s(f) + \eta_{RAD}(f). \tag{6.5}$$

The amount of radiated sound power can be obtained from the input power from the following:

$$\Pi_{RAD} = \Pi_{in}\frac{\eta_{RAD}}{\eta_{RAD} + \eta_s} = \Pi_{in}\frac{\eta_{RAD}}{\eta_{TOT}}. \tag{6.6}$$

B: Experimental Measurement

The MIT truss was excited at joints B1, B5, and D5, in the x, y, and z directions, for a total of nine data runs, as shown in figure 6-1. For each run, the input force and input accelerations were measured using a Brüel and Kjær type 4962 impedance head. The vibration measurements were taken for each data

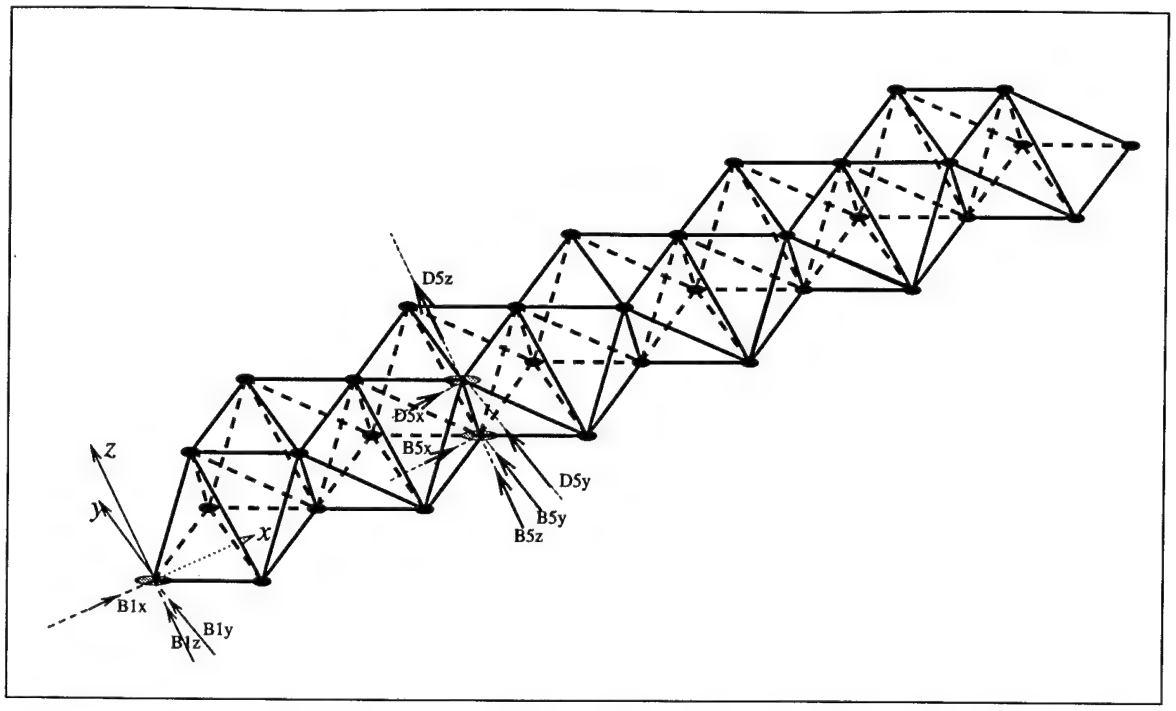

Figure 6-1: Configuration of total loss factor, η_{TOT}, experiment for bare truss. Force was applied at joints B1, B5, and D5, as shown.

run by applying .5 gram accelerometers on all 13 centerline joints of the truss in the x, y, and z directions, for a total of 39 velocity measurements. The total energy of the truss was a result of averaging those 39 mean square velocities, in effect performing a spatial average; the temporal averaging was computed by the data acquisition system's FFT algorithm. This mean square velocity was used in equation (6.3) along with the input power from the impedance head, the total mass of the truss M, and equation (6.1) to calculate the total loss factor η_{TOT}. Lastly, the nine separate data run results were averaged to provide the resulting value of η_{TOT}. The averaging methodology provides a good estimate of the spatially averaged energy of the truss. Since the impedance head provides an accurate measurement of the input power, an accurate measurement of η_{TOT} is the result. The results of the input power, average energy and resultant total loss factor are presented as figure 6-2. The dashed lined surrounding the values of input power, energy and η_{TOT} represent the standard deviation of the nine separate measurements. All values are in deciBel format.

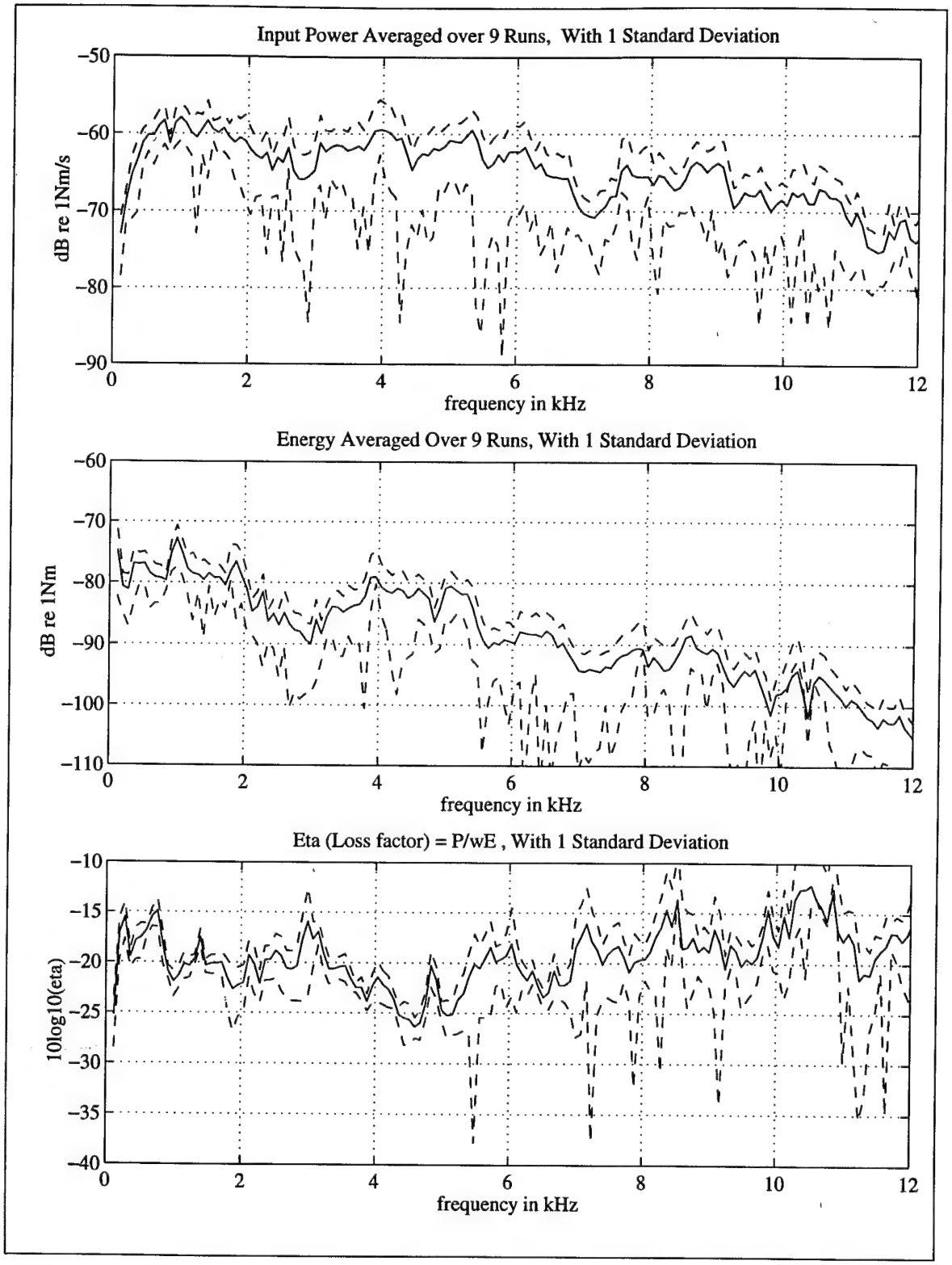

Figure 6-2: Measured values of total input power, spatially averaged energy in the truss, and total loss factor, η_{TOT}.

C: Comparison of Experimental Total Loss Factor To Predicted Total Loss Factor

The output of the DGSM program provides a method of computing the total loss factor, in the same manner as was just described for the experimental procedure. The DGSM program computes the displacement amplitudes of each joint of the truss. The input force is a given quantity and the velocity at the input point is calculated by the program. These outputs can be used to perform the same calculation as was just measured. In effect, the total *effective* loss factor can be obtained. In other words, even though the DGSM program starts with a constant structural loss factor, which has been postulated to contain the internal losses and the joint losses, the method it uses to compute the velocities of the joints and struts *implicitly* accounts for the multiple energy flowpaths and the partitioning of energy. So the true loss factor is different from the intrinsic material loss factor.

The DGSM predicted loss factor $\eta_{TOT\,DGSM}$ was calculated for an input structural loss factor η_s = .003. This value was chosen because the comparison between measured sound power and predicted sound power (figure 4.10) fell almost midway between the predictions for $\eta_s = 1\text{x}10^{-3}$ and $\eta_s = 1\text{x}10^{-2}$. Figure 6-3 shows the result for the two values $\eta_{TOT\,DGSM}$ and $\eta_{TOT\,MEAS}$. In Figure 6-4, the same data is averaged in $\frac{1}{3}$ octave bands. It is interesting to note that even though the structural loss factor which was input to the DGSM program was set at $3\text{x}10^{-3}$, or a value of

$$\eta_s = 10\log_{10}(.003) = -25 \text{ dB}, \tag{6.7}$$

the output calculation shows a value of -21 dB. This means that the multi-path losses add approximately $2\frac{1}{2}$ times the losses due to internal losses alone. The calculated values of $\eta_{TOT\,DGSM}$ and $\eta_{TOT\,MEAS}$ show good agreement.

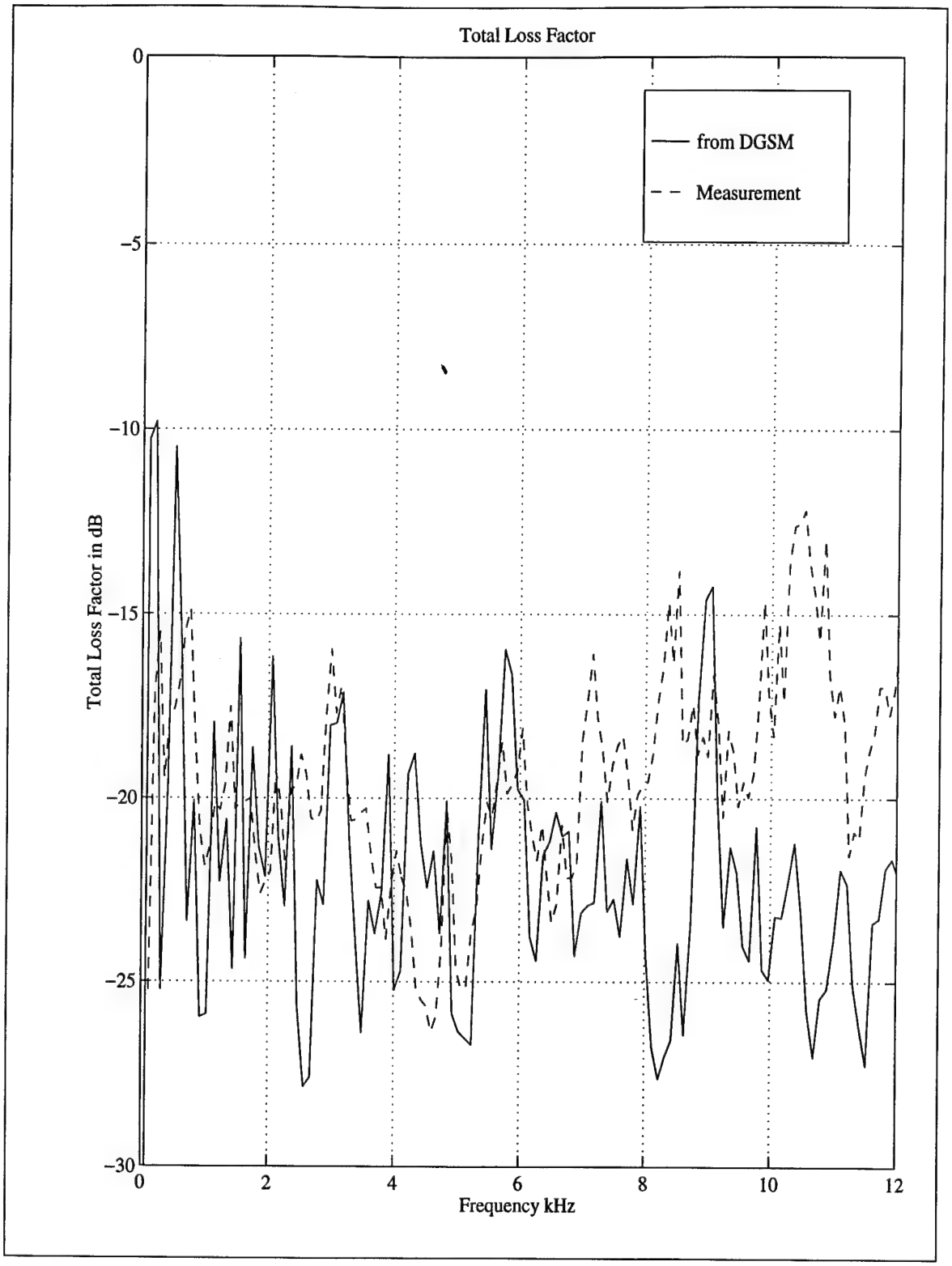

Figure 6-3: Total loss factor as measured $\eta_{TOT\,MEAS}$, and from the DGSM prediction, $\eta_{TOT\,DGSM}$.

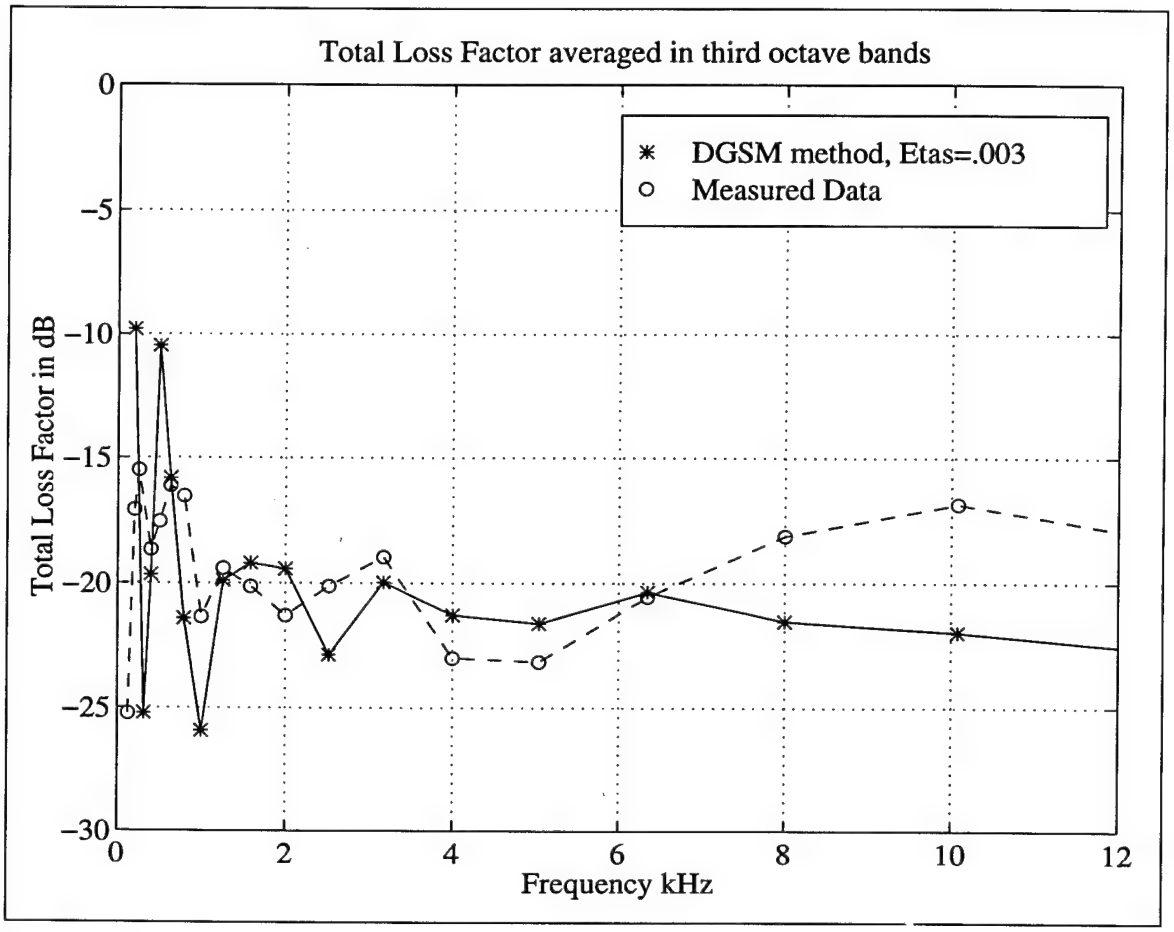

Figure 6-4: Total loss factor as measured $\eta_{TOT\,MEAS}$ and from the DGSM prediction,$\eta_{TOT\,DGSM}$, averaged in $\frac{1}{3}$ octave bands

D: Comparison of Structural Loss Factor to Radiation Loss Factor

The results of the experimentally determined total loss factor $\eta_{TOTMEAS}$ and the results of the normalized radiated power can be used with equations (6.6) and (6.5) to find the radiation loss and structural loss factors as follows:

$$\eta_{RAD} = \eta_{TOTMEAS} \frac{\Pi_{RAD}}{\Pi_{in}} \tag{6.8}$$

and

$$\eta_s = \eta_{TOTMEAS} - \eta_{RAD}. \tag{6.9}$$

Figure 6-5 shows the results from this calculation.

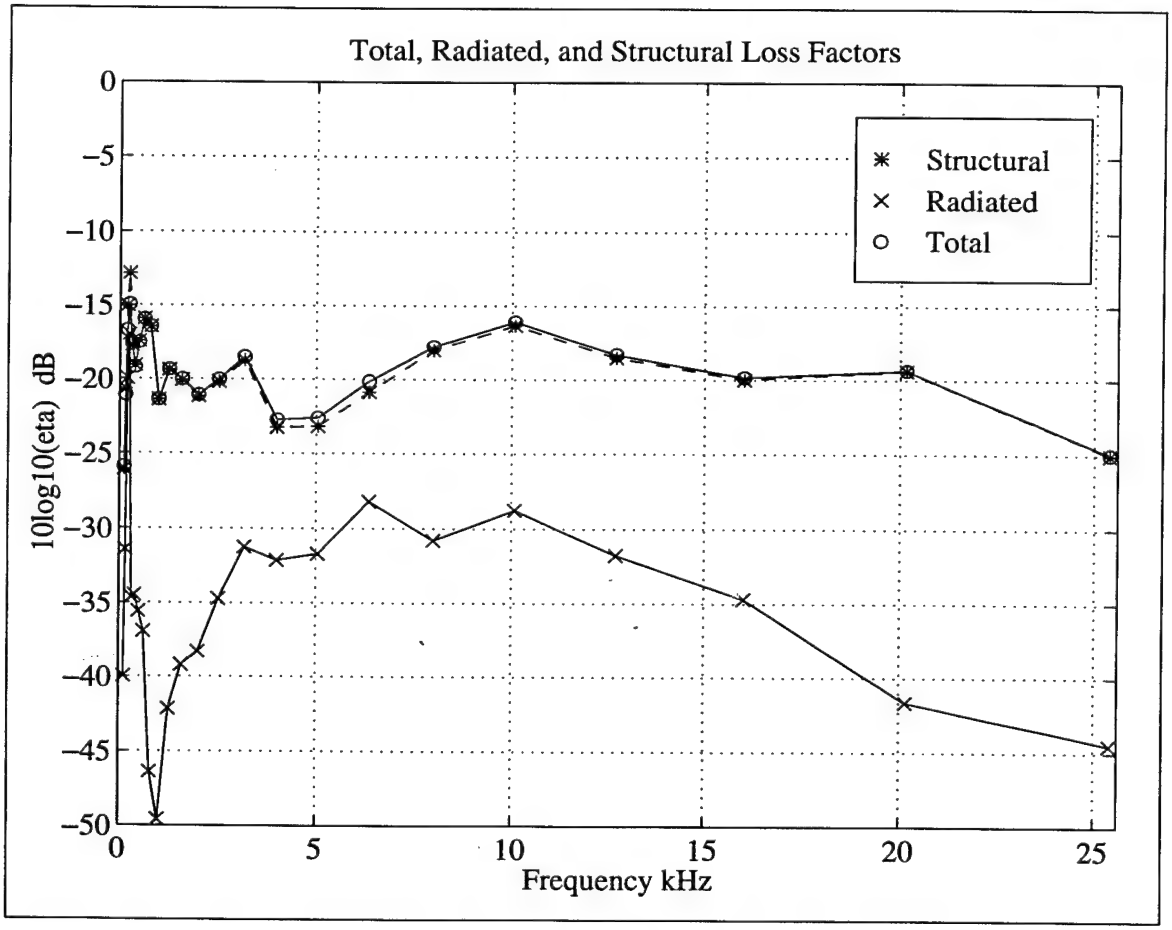

Figure 6-5: Total, structural, and radiated loss factors averaged in $\frac{1}{3}$ octave bands.

As was mentioned before, the radiation loss factor is significantly lower than the structural loss factor for the bare truss.

E: Recomputation of the DGSM Estimate using Updated Structural Loss Factor and Comparison to Experimental Data

The measured value of the total loss factor, $\eta_{TOTMEAS}$, will be compared to the predicted value of the total loss factor, $\eta_{TOTDGSM}$, to compute a *correction* to the structural loss factor which is input to the DGSM program. To obtain $\eta_{TOTDGSM}$, the input structural loss factor was set to be a constant equal to .003. The total loss factor which that constant value produced is known. This computed loss factor can be compared to the measured total loss factor, $\eta_{TOTMEAS}$, to compute a correction factor to the DGSM program structural loss factor input,

$$\text{Correction Factor} = \frac{\eta_{TOTMEAS}}{\eta_{TOTDGSM}}. \tag{6.10}$$

First the measured and predicted total loss factors were averaged in $\frac{1}{3}$ octave bands as above in figure 6-4. The third octave averaged results were then smoothed with a third order polynomial fit using MATLAB©'s polyfit routine. The Correction Factor was then calculated and is plotted in deciBel format in figure 6-7.

Finally the DGSM prediction was re-run using an input structural loss factor of

$$\eta_s = \text{Correction Factor}(.003). \tag{6.11}$$

The result of this corrected DGSM prediction and the measured sound power is presented in figure 6-8. The corrected DGSM estimate gives a greatly improved prediction of the radiated sound power.

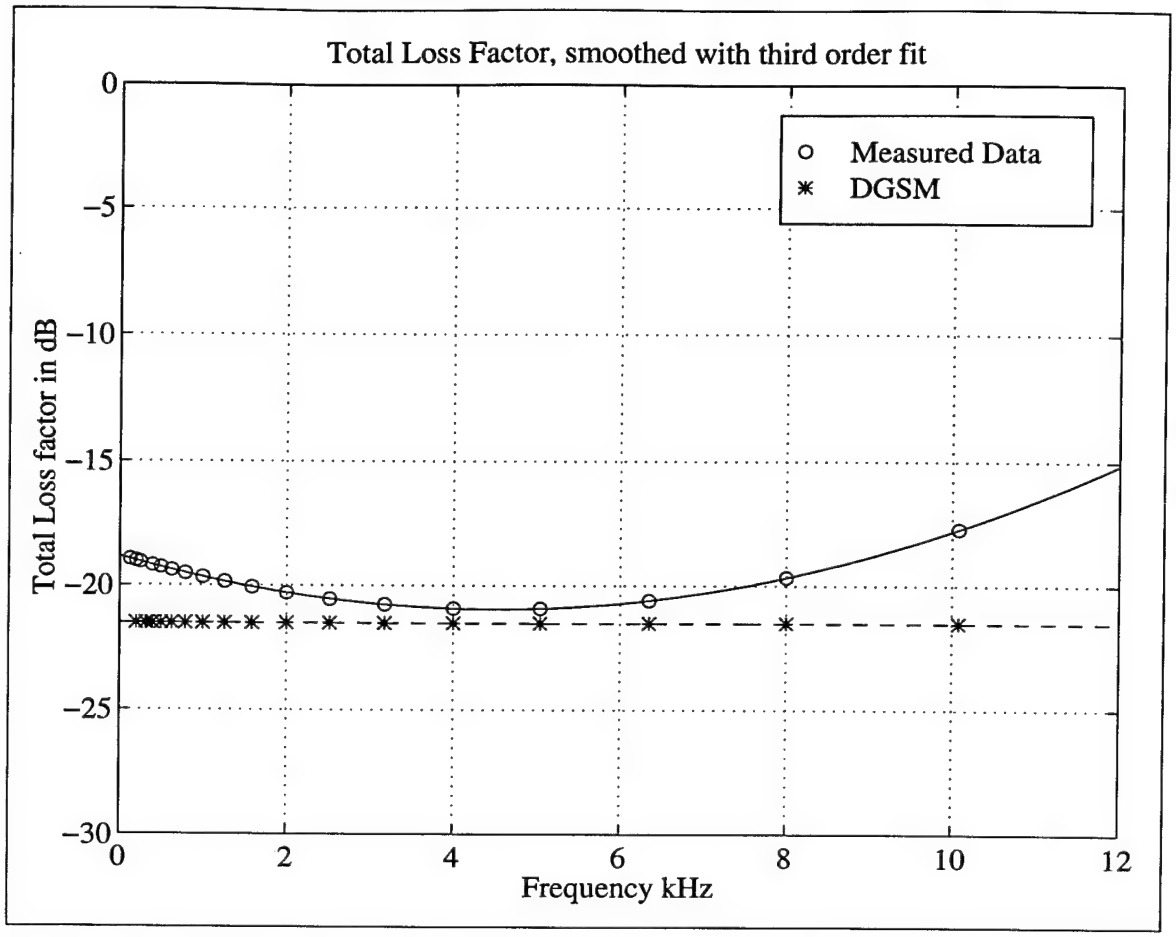

Figure 6-6: Third order polynomial fit of the measured, $\eta_{TOTMEAS}$, and predicted, $\eta_{TOTDGSM}$, total loss factors.

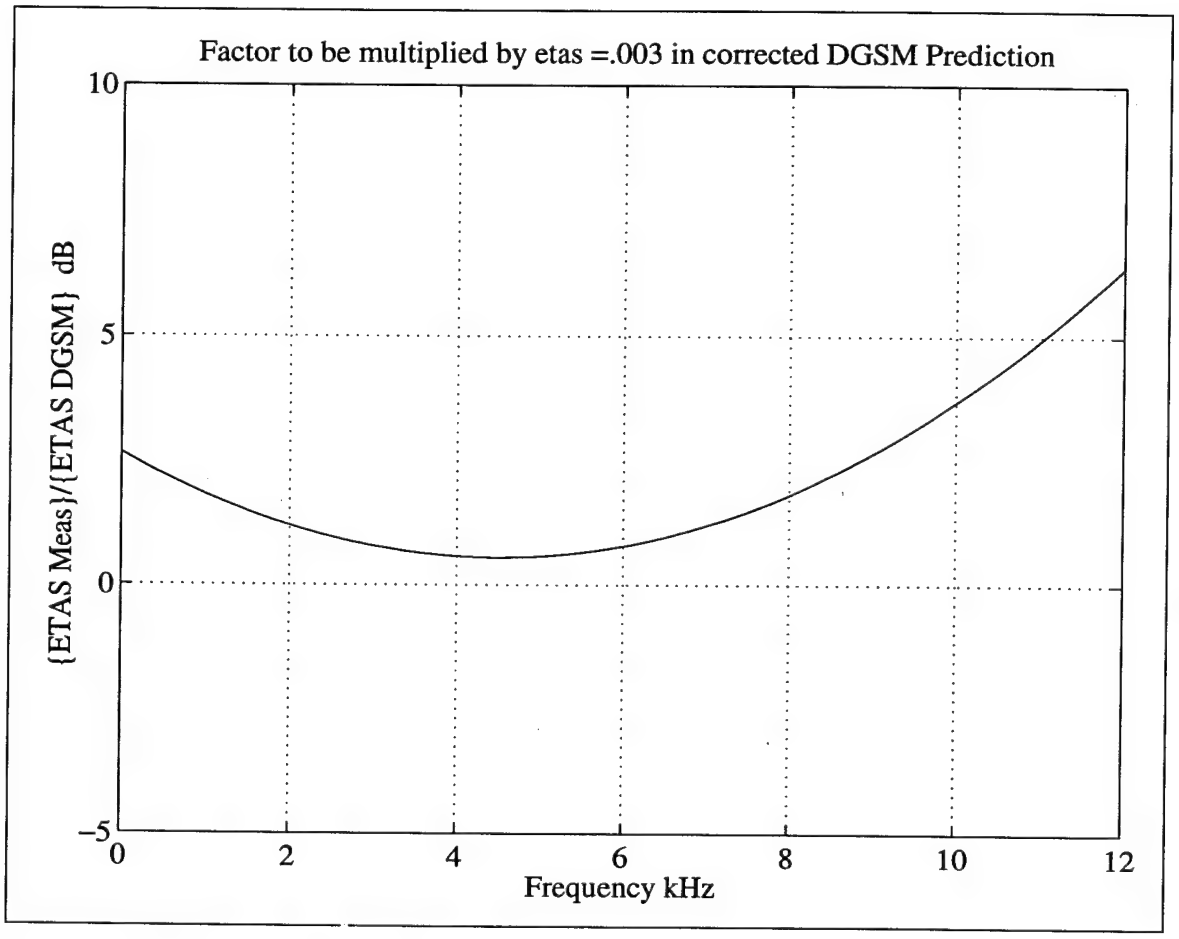

Figure 6-7: Factor to be multiplied by the constant value of $\eta_{Structural}$ to correct the input to the DGSM program.

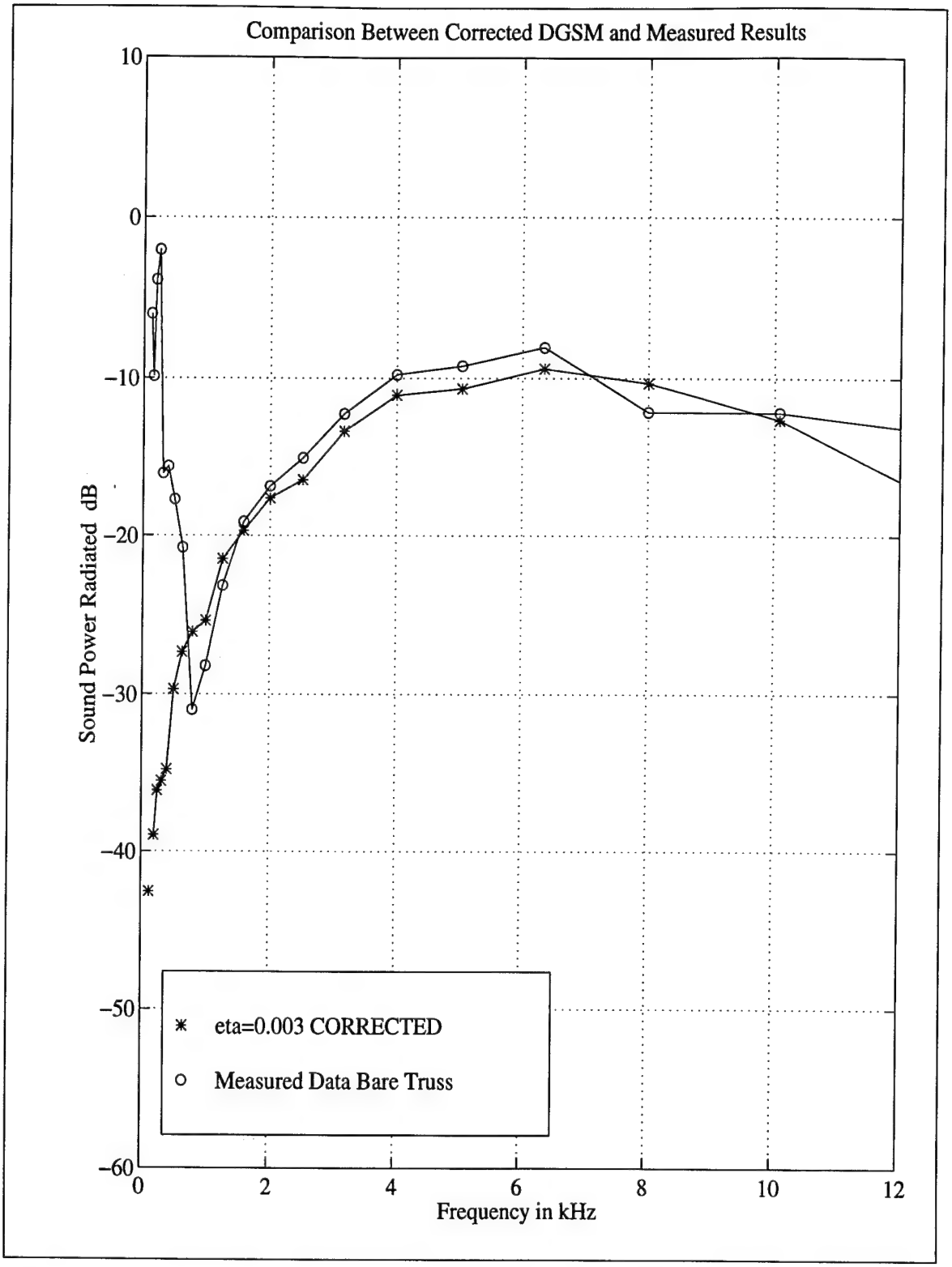

Figure 6-8: Normalized radiated sound power from DGSM corrected prediction and measured data.

F: Comparison of Vibrational Energy of the Bare Truss and the Truss with Plates

For the bare truss and truss with plates experiments above, the vibrational energy of the truss is calculated according to equation (6.2). The result for the bare truss and the truss with plates is plotted as figure 6-9. The issue of coupling between the plates and the truss has been discussed several times. If there were strong coupling between the plates and the truss, the vibrational energy of the struts should be much lower with the plates attached, which is clearly not observed.

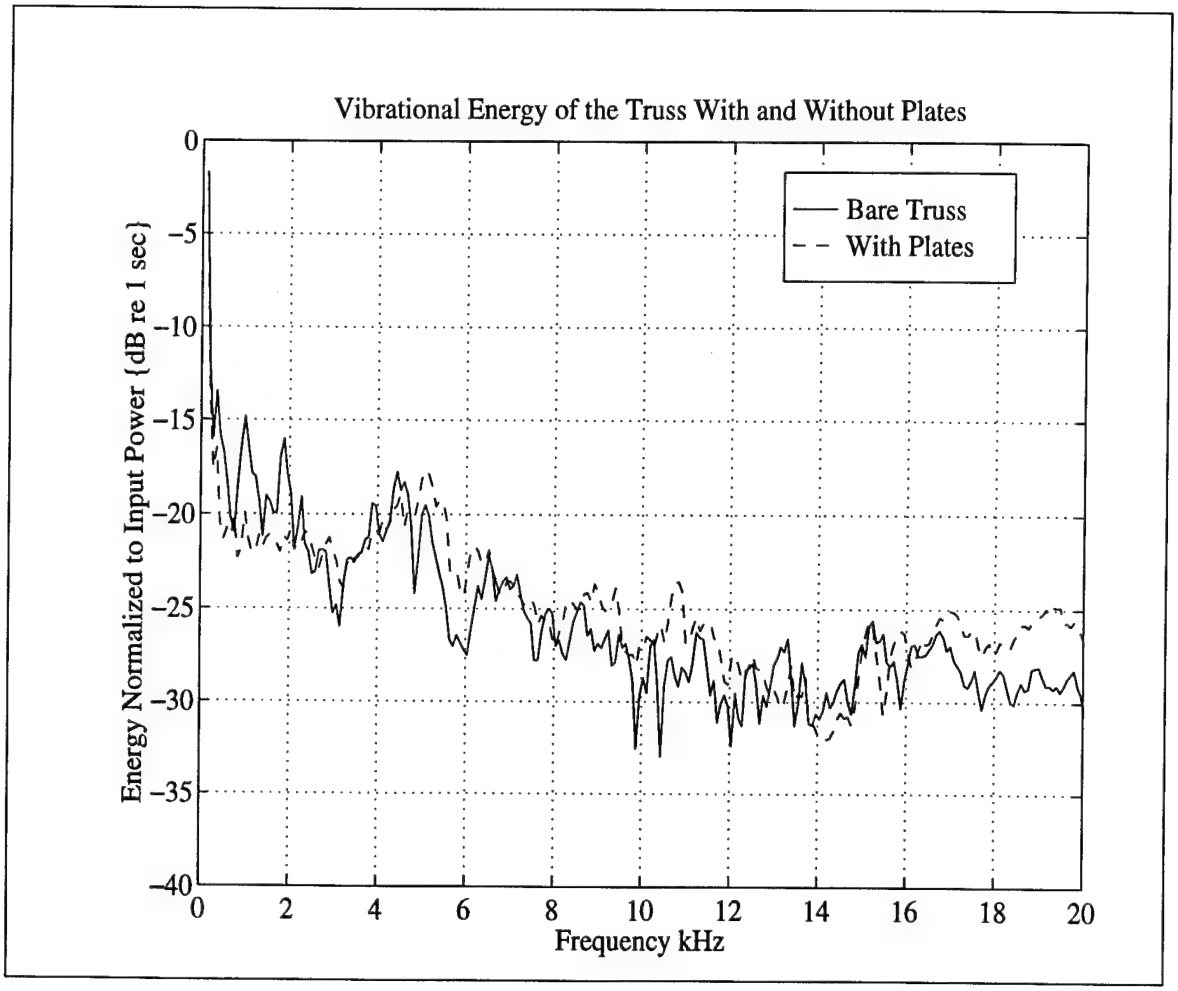

Figure 6-9: Vibrational energy of the truss, with and without plates

CHAPTER 7: Conclusions

A method has been developed to determine the radiated sound power from a three dimensional truss. The method builds upon the development of the Direct Global Stiffness Matrix (DGSM) method and uses analytically derived formulae for radiation efficiency, modeling the struts as vibrating wires. The DGSM method determines the vibrational energy of the members of the truss and then the radiated sound power is independently calculated. This approach may not have worked except for the fact that the structural loss factor, η_s, is much higher than the radiation loss factor, η_{RAD}, as shown in figure 6-5. This difference in size means that the structural energy loss is effectively *decoupled* from the radiation energy loss, and so the DGSM approach is validated. In any feasible truss which would support heavy machinery, the struts would have to be relatively thick-walled to support the weight. It is therefore conceivable that therefore the structural loss will always outweigh the radiation loss in a practical truss.

The DGSM method does not allow *apriori* estimation of the radiated sound power. The structural loss factor, η_s, which is input to the DGSM program determines the radiated sound power almost exclusively. The method described in chapter 6 for determining the structural loss factor to be used as an entering argument to the DGSM program is universally applicable to any given truss, is reasonable easy to implement, and provides significant refinement to the DGSM estimate.

An attempt was made to determine the radiated sound power from the plates attached to the truss, with little success. The coupling between the struts and plates will determine the amount of vibrational energy that the plates have, and thus will determine their radiated sound power. An assumption was made of rigid coupling between the two, which grossly overestimated the radiated sound power. Analysis and experimentation shows that for the mounting method

chosen, there is not strong coupling. Again, in a real truss, the deckplates would be insulated with rubber to prevent the transmission of vibrational energy from the struts to the plates, making this a valid model of the real truss behavior.

BIBLIOGRAPHY

1. DYNAMIC BEHAVIOR OF A THREE DIMENSIONAL ALUMINUM TRUSS IN FREE SPACE., Marcus R. A Heath, Master's Thesis, © May 1994, Massachusetts Institute of Technology.

2. ACOUSTICS., Leo L. Beranek, ©1954, 1986, The Acoustical Society of America.

3. SOUND AND STRUCTURAL VIBRATION., Preston W. Smith and Richard H. Lyon, NASA Contractor report CR-160.

4. FUNDAMENTALS OF NOISE AND VIBRATION ANALYSIS FOR ENGINEERS, M.P. Norton, © 1989, Cambridge University Press.

5. VIBRATION AND SOUND, P.M. Morse, ©1948 McGraw Hill Company, New York, NY.

6. STRUCTURE-BORNE SOUND, Cremer, Heckl and Ungar, second edition, ©1973 Springer-Verlag, New York.

7. SOUND, STRUCTURES AND THEIR INTERACTION, 2nd edition M.C. Junger and D. Feit, © 1986 M.I.T., Cambridge MA.

8. FUNDAMENTALS OF UNDERWATER ACOUSTICS., CLASS NOTES, © Professor Ira Dyer, Massachusetts Institute of Technology.

9. FORMULAS FOR NATURAL FREQUENCY AND MODE SHAPE., Robert D. Blevins, ©1979 Van Nostrand Reinhold Company, Inc.

10. THE BUCKLING AND FREQUENCY OF FLEXURAL VIBRATION OF RECTANGULAR ISOTROPIC AND ORTHOTROPIC PLATES USING RAYLEIGH'S METHOD., S.M. Dickinson, ©1978 Journal of Sound and Vibration, **61**, 1-8.

11. DIRECT GLOBAL STIFFNESS MATRIX METHOD FOR 3-D TRUSS DYNAMICS. J. Robert Fricke and Mark A. Hayner, ASME 15th Biennial Conference on Mechanical Vibration and Noise, September 17-21, 1995.

12. FREE VIBRATION ANALYSIS OF THE COMPLETELY FREE RECTANGULAR PLATE BY THE METHOD OF SUPERPOSITION., D.J.Gorman, ©1978 Journal of Sound and Vibration, **57**(3), 437-447.

13. VIBRATIONS OF FREE SQUARE PLATES, PART I: NORMAL VIBRATING MODES, Mary D. Waller, ©1939 Proceedings of the Physics Society, London, **51**, 831-844.

14. THE FREE VIBRATION OF RECTANGULAR PLATES, A.W. Leissa, ©1973 Journal of Sound and Vibration, **31**(3), 257-293.

15. RADIATION EFFICIENCIES OF BEAMS IN FLEXURAL VIBRATION, R.K. Jeyapalan and E. J. Richards, ©1979 Journal of Sound and Vibration, **67**(1), 55-67.

16. INTENSITY-IT'S MEASUREMENT AND USES, Gunnar Rasmussen, ©1989 Sound and Vibration.

17. STATISTICAL ENERGY ANALYSIS OF DYNAMICAL SYSTEMS, THEORY AND APPLICATIONS, R.H.Lyon, ©1975 M.I.T. Press.

APPENDIX A: MATLAB© Code

```
% ------------------------------------------------
% NEWETA11.m  17 April 1995
% ADAPTED from original program by M. Hayner to remove
% portions dealing with Energy analysis and ability to
% change strut charactaristics in attempt to speed up
% analysis.  ALSO, I added a portion to compute radiated sound
% power directly.  Calculation of wave amplitudes on truss
% is still the original work of Hayner.
%------------------------------------------------

clear all

f= linspace(100,25600,500);
etaL=.001;              % Longitudunal Loss Factor
etas=.001;              % Shear Loss Factor
kjmag=i*4737;           % Joint Stiffness (not used)
mjmag=.120;             % Joint Mass
%------------------------------------------------
load trusscon.dat       % Connectivity Data
load trussgrd.dat       % Grid Point Data
conn=trusscon;          % Connectivity Matrix
node=trussgrd;          % Truss Nodes Matrix
clear trusscon trussgrd

rho=2700;
E=rho*5051^2*(1+i*etaL);
G=rho*3100^2*(1+i*etas);
cL=sqrt(E/rho);
cs=sqrt(G/rho);
Axs=5.728e-5;
Ky=3.95e-3;             % Radius of Gyration
Kz=Ky;
```

```
Kx=sqrt(Ky^2+Kz^2);

norm =0;

ndpt=1;                    % drive point node number
dofdpt=3;                  % drive point dof
Fa=rho(1)*cL(1)^2*Axs;     % applied force amplitude
force=zeros(1,7);                                          40
force([1,1+dofdpt])=[ndpt,Fa];
dpt=6*(ndpt-1)+dofdpt;

Nelem=max(size(conn(:,1)));
Nnode=max([conn(:,3);conn(:,4)]);
Nfreq = max(size(f));

% ---------------Calculate Sigma RAD-----------------

rhoc = 415                                                 50
ca = 340.15;
ka = (2..*pi.*f)./ca;
a = .00635;
x = ka.*a;
ha = -besselj(2,x)-i*bessely(2,x);
hb = (1../x).*(besselj(1,x)+i*bessely(1,x));
dhank = ha+hb;
dhank2 = 1../(dhank .*conj(dhank));
sigrad=(2../(pi*x)).*dhank2;
loglog(f,sigrad)                                           60
figure

global  lchar tchar mchar Gxfm conn norm
global  spwr udp ndpt Nnode Nelem dofdpt Nfreq
global  kL kt ky kz EA EIy EIz GJ L rhoc
global  A UUj VVa VVb VVj C B velrms
global  constr redux test sigrad PRAD PRADn
global  iter_sec total_sec
```

```
tgms10(node,force,rho,cL,cs,Kx,Ky,Kz,Axs,f);

                                                                    70

semilogx(f,10..*log10(abs(PRADn)))
grid
xlabel('Frequency in Hz')
ylabel('Sound Power radiated  dB')
title (['Sound Power Radiated Normalized to Input Power  with  '.....
     num2str(length(f)) '  points'])

save neweta11

                                                                    80

c = date
leo = fix(clock);
time  = leo(4:5)

timperiter= total_sec/Nfreq

                                                                    90

                                                                   100
```

```
%-----------------------------------------------------
% REVISION of the original TGMS10.m (done by Mark Hayner)
%  Modifications are made to eliminate the portions which are
%  not needed for our relatively simple truss so that program
%  efficiency can be speeded up.  Basic program structure remains
%  as the same work done by Hayner.
%-----------------------------------------------------
%          DESCRIPTION of various parameters
%
% INPUTS:                                                          10
%   1.  Nelem  =  # of elements in the truss
%   2.  Nnode  =  # of nodes in the truss
%   3.  conn(Nelem x 5) = (elemnum,pid,G1,G2,G3)
%         * pid is property ID and allows for later on changing
%           the properties of individual struts.
%         * G1, G2 are the nodal endpoints of each strut
%         * G3 is a reference point to allow the shift from
%           local to global coordinates. G3 is the same for each
%           strut. G3 is at the reference nodes.
%   4.  node = ((Nnode +Nrefnode) X 4) = nodenum, x,y,z             20
%         * x,y,z are in global coordinates
%         * Nrefnode = the number of reference nodes used for the
%           transformation to the local coordinate system.

% OUTPUTS:
%   1.  A(1 X 12*Nnodes) = Wave amplitudes in the local beam
%       coordinate system.
%   2.  UUj(6*Nnodes x Nfreq) = Joint Displacements in Global coordinates
%   3.  VVj(6*Nnodes x Nfreq) = Joint Displacements in Local coordinates
%   4.  VVb(12*Nnodes x Nfreq) = Beam Displacements in Local coordinates  30
%
%-----------------------------------------------------
function[]=tgms(node,force,rho,cL,cs,Kx,Ky,Kz,Axs,f)

global  lchar tchar mchar Gxfm conn norm
```

```
global  etot pwr udp ndpt dofdpt spwr
global  ndpt Nnode Nelem Nfreq rhoc
global  kL kt ky kz EA EIy EIz GJ L
global  A UUj VVa VVb VVj C B PRAD PRADn
global  constr redux test sigrad velrms                                    40
global  iter_sec total_sec

time1=clock;
%-------------- Non-dimensionalize --------%
  tchar=1;
  lchar=1;
  mchar=1;
  kmb=[ones(Nelem,12),zeros(Nelem,12)];
  kmj=zeros(Nnode,12);
  kbc=1e20*ones(Nelem,12);          % USES Welded bc                       50


%-------------- Precalculations ---------------%
  z6=zeros(6);
  w=2*pi*f;
  kL=(1)./cL.'*w;
  kt=(1)./cs.'*w;
  ky=( (1)./(Ky.*cL).' *w).^.5;
  kz=( (1)./(Kz.*cL).' *w).^.5;
  EA=rho.*Axs.*cL.^2;                                                      60
  EIy=rho.*Axs.*cL.^2 .*Ky.^2;
  EIz=rho.*Axs.*cL.^2 .*Kz.^2;
  GJ=rho.*Axs.*cs.^2 .*Kx.^2;

%-------- Size large matricies and vectors---------%
 PRADn=zeros(Nfreq,1);
 PRAD=zeros(Nfreq,1);
 velrms = zeros(Nfreq,1);
 Gxfm=zeros(12,12*Nelem);
 A=zeros(12*Nelem,1);                                                      70
 B=zeros(1,6*Nnode);
```

```
if Nnode<50
  C=zeros(6*Nnode);
else
  C=sparse(zeros(6*Nnode));
end

Za=zeros(Nelem,12);
Zj=zeros(Nnode,6);
Zbc = kbc;

ZZ=zeros(12,12*Nelem);
DDinv=zeros(12,12*Nelem);

UUj=zeros(6*Nnode,1);
VVj=zeros(12*Nelem,1);
VVb=zeros(12*Nelem,1);
VVa=zeros(12*Nelem,1);

udp=zeros(max(size(ndpt)),Nfreq);
redux=ones(1,Nnode*6);
if constr~=[];
  redux(constr)=zeros(size(constr));
end

%-------- Calculate transform. matricies and load vector ------%
gp=node(:,2:4);
for k=1:Nelem
    g1=gp(conn(k,3),:);
    g2=gp(conn(k,4),:);
    g3=gp(conn(k,5),:);
    L(k)=sqrt(sum((g1-g2).^2));
    [gxfm]=xfrm1(g1,g2,g3);
    Gxfm(:,(k-1)*12+1:k*12)=gxfm;
end
for kk=1:max(size(force(:,1)));
  index=(force(kk,1)-1)*6+[1:6];
```

```
    B(index)=force(kk,2:7);
  end

%-------------- Iterate over frequency --------------%
  time2=clock;
  for n=1:Nfreq
    n_Nfreq=[n,Nfreq]
    C=0*C;
  time3=clock;

%-------------- Assemble global matrix, C ------------%
    for k=1:Nelem
      m=conn(k,2);  % property card
      [Z,D]=imp1(EA(m),EIy(m),EIz(m),GJ(m),L(k),...
            kL(m,n),kt(m,n),ky(m,n),kz(m,n));
      DDinv(:,(k-1)*12+[1:12])=inv(D);
      for kk=1:12;  % Zb-->Zba
        Z(kk,kk)=Z(kk,kk)+Za(k,kk);
      end % for kk
      Z=inv(Z);  % let Z=Y temporarily
      Yba=Z;    % need later
      for kk=1:12   % Yba-->Ybabc
        Z(kk,kk)=Z(kk,kk)+(1)./Zbc(k,kk);
      end % for kk
      Z=inv(Z);  % Ybabc-->Z=Zbabc
      ZZ(:,(k-1)*12+[1:12])=Yba*Z;

      G=Gxfm(:,(k-1)*12+1:k*12);
      Z=G*Z*G.';
      mm=(conn(k,3)-1)*6+[1:6];
      nn=(conn(k,4)-1)*6+[1:6];
      C(mm,mm)=C(mm,mm)+Z(1:6,1:6);
      C(mm,nn)=C(mm,nn)+Z(1:6,7:12);
      C(nn,mm)=C(nn,mm)+Z(7:12,1:6);
      C(nn,nn)=C(nn,nn)+Z(7:12,7:12);
    end
```

```
    time4=clock;
    rC=C(redux,redux);
    rB=B(redux);
    UUj(redux)=(rC\rB.');
    time5=clock;

%---------- Solve for beam displacements --------%                    150
    for k=1:Nelem  % care for coord sys
      mm=(conn(k,3)-1)*6+[1:6];
      nn=(conn(k,4)-1)*6+[1:6];
      G=Gxfm(:,(k-1)*12+1:k*12);
      Vj=G.'*UUj([mm,nn]);
      Vb=ZZ(:,(k-1)*12+[1:12])*Vj;
      Va=Vb.*(1-(Za(k,1:12)./kmb(k,1:12)).');
      VVj((k-1)*12+[1:12],1)=Vj;
      VVb((k-1)*12+[1:12],1)=Vb;
      VVa((k-1)*12+[1:12],1)=Va;                                       160
      A((k-1)*12+[1:12])=DDinv(:,(k-1)*12+[1:12])*Vj;
   end

  udp(n)=UUj(6*(ndpt-1)+dofdpt);
  iter = n;
  omeg = w(n);
  invel = udp(n);
  inforce = force(dofdpt+1);
  powrad(A,iter,omeg,inforce,invel,cL,Ky);

                                                                       170
  end              % End of Iteration over n=1:Nfreq

  time6=clock;


%---------- Elapsed times ---------------%

etime21=etime(time2,time1);
etime32=etime(time3,time2);etime43=etime(time4,time3);
```

```
etime54=etime(time5,time4);etime65=etime(time6,time5);
etime61=etime(time6,time1);

iter_sec=etime(time6,time2)
total_sec=etime61
```

```
% Subroutine POWRAD.M
%   Computes Radiated Sound Power, Given Radiation
%   Efficiency and Wave Amplitudes on each Strut.
%   The Power Radiated is Normalized by the Input
%   Power.
% ------------------------------------------------
function[]=power(A,n,w,force,vel,CL,KY)

global  lchar tchar mchar Gxfm conn norm
global  etot pwr udp dpt dofdpt spwr
global  ndpt dofdpt Nnode Nelem rhoc
global  kL kt ky kz EA EIy EIz GJ L
global  A UUj VVa VVb VVj C B velrms
global  constr redux test sigrad PRAD PRADn
global  iter_sec total_sec

A=A*lchar;

w = w*(1/tchar);
force = force*(tchar^2)/(mchar*lchar);
vel = vel*lchar;

i = sqrt(-1);

POWERIN = .5*real(force*conj(i*w*vel));
PRAD(n)=0;
velrms(n) =0;
ky1 = ky(n);
kz1 = kz(n);

for r = 0:108;
  l = 12*r+1;
  L1 = L(r+1);
vms = 0;
```

```
facty = .5;
factz = .5;
factey = (1 − exp(−2*ky1*L1))/(4*ky1*L1) ;
factez = (1 − exp(−2*kz1*L1))/(4*kz1*L1) ;                                    40
vms = facty* (A(l)*conj(A(l)) + A(l+1)*conj(A(l+1))+ ....
      A(l+4)*conj(A(l+4)) + A(l+5)*conj(A(l+5)) )+ .....
      (A(l+2)*conj(A(l+2)) + A(l+3)*conj(A(l+3)))*factey + .....
      (A(l+6)*conj(A(l+6)) + A(l+7)*conj(A(l+7)))*factez;

velrms(n)=velrms(n)+vms;
PRAD(n) = PRAD(n)+ real(rhoc*w^2*vms*sigrad(n)*pi*L(r+1)*.00635) ;
end;

PRADn(n) = PRAD(n)/POWERIN ;                                                  50

                                                                              60
```

```
% File TRUSSCON.DAT
% This file contains the endpoints for each strut,
%    and a third point which serves as a reference
%    point when the local x,y,z coordinate system
%    is generated.
% ------------------------------------------------------------
  1   1   1   2  38
  2   1   1   3  38
  3   1   1   4  37                                          10
  4   1   2   3  37
  5   1   2   4  37
  6   1   2   5  39
  7   1   2   6  36
  8   1   3   4  37
  9   1   3   5  39
 10   1   3   7  36
 11   1   4   5  37
 12   1   4   6  38
 13   1   4   7  38                                          20
 14   1   5   6  37
 15   1   5   7  37
 16   1   5   8  38
 17   1   5   9  38
 18   1   5  10  37
 19   1   6   7  37
 20   1   6   8  36
 21   1   6  10  39
 22   1   7   9  36
 23   1   7  10  39                                          30
 24   1   8   9  37
 25   1   8  10  37
 26   1   8  11  39
 27   1   8  12  36
 28   1   9  10  37
```

29	1	9	11	39
30	1	9	13	36
31	1	10	11	37
32	1	10	12	38
33	1	10	13	38
34	1	11	12	37
35	1	11	13	37
36	1	11	14	38
37	1	11	15	38
38	1	11	16	37
39	1	12	13	37
40	1	12	14	36
41	1	12	16	39
42	1	13	15	36
43	1	13	16	39
44	1	14	15	37
45	1	14	16	37
46	1	14	17	39
47	1	14	18	36
48	1	15	16	37
49	1	15	17	39
50	1	15	19	36
51	1	16	17	37
52	1	16	18	38
53	1	16	19	38
54	1	17	18	37
55	1	17	19	37
56	1	17	20	38
57	1	17	21	38
58	1	17	22	37
59	1	18	19	37
60	1	18	20	36
61	1	18	22	39
62	1	19	21	36
63	1	19	22	39
64	1	20	21	37

40

50

60

70

65	1	20	22	37
66	1	20	23	39
67	1	20	24	36
68	1	21	22	37
69	1	21	23	39
70	1	21	25	36
71	1	22	23	37
72	1	22	24	38
73	1	22	25	38
74	1	23	24	37
75	1	23	25	37
76	1	23	26	38
77	1	23	27	38
78	1	23	28	37
79	1	24	25	37
80	1	24	26	36
81	1	24	28	39
82	1	25	27	36
83	1	25	28	39
84	1	26	27	37
85	1	26	28	37
86	1	26	29	39
87	1	26	30	36
88	1	27	28	37
89	1	27	29	39
90	1	27	31	36
91	1	28	29	37
92	1	28	30	38
93	1	28	31	38
94	1	29	30	37
95	1	29	31	37
96	1	29	32	38
97	1	29	33	38
98	1	29	34	37
99	1	30	31	37
100	1	30	32	36

80

90

100

101	1	30	34	39
102	1	31	33	36
103	1	31	34	39
104	1	32	33	37
105	1	32	34	37
106	1	32	35	39
107	1	33	34	37
108	1	33	35	39
109	1	34	35	37

110

```
% File TRUSSGRD.DAT. This file Contains the
%    Locations of the Joints in Global x,y,z
%    Coordinates.
% ---------------------------------------

 1.0000      0       0       0
 2.0000   0.3800   0.3800      0
 3.0000   0.3800  -0.3800      0
 4.0000   0.3800      0   0.7600
 5.0000   0.7600      0       0
 6.0000   0.7600   0.3800   0.7600
 7.0000   0.7600  -0.3800   0.7600
 8.0000   1.1400   0.3800      0
 9.0000   1.1400  -0.3800      0
10.0000   1.1400      0   0.7600
11.0000   1.5200      0       0
12.0000   1.5200   0.3800   0.7600
13.0000   1.5200  -0.3800   0.7600
14.0000   1.9000   0.3800      0
15.0000   1.9000  -0.3800      0
16.0000   1.9000      0   0.7600
17.0000   2.2800      0       0
18.0000   2.2800   0.3800   0.7600
19.0000   2.2800  -0.3800   0.7600
20.0000   2.6600   0.3800      0
21.0000   2.6600  -0.3800      0
22.0000   2.6600      0   0.7600
23.0000   3.0400      0       0
24.0000   3.0400   0.3800   0.7600
25.0000   3.0400  -0.3800   0.7600
26.0000   3.4200   0.3800      0
27.0000   3.4200  -0.3800      0
28.0000   3.4200      0   0.7600
29.0000   3.8000      0       0
```

30.0000	3.8000	0.3800	0.7600
31.0000	3.8000	−0.3800	0.7600
32.0000	4.1800	0.3800	0
33.0000	4.1800	−0.3800	0
34.0000	4.1800	0	0.7600
35.0000	4.5600	0	0
36.0000	10	27	31
37.0000	10	27	31
38.0000	10	27	31
39.0000	10	27	31

40